RADIO ASTRONOMY

Journal of the Society of Amateur Radio Astronomers
September - October 2021

Dennis Farr
SARA President

Dr. Richard A. Russel
Editor

Whitham D. Reeve
Contributing Editor

Radio Astronomy is published bimonthly as the official journal of the Society of Amateur Radio Astronomers.

It is the mission of the Society of Amateur Radio Astronomers (SARA) to: Facilitate the flow of information pertinent to the field of Radio Astronomy among our members; Promote members to mentor newcomers to our hobby and share the excitement of radio astronomy with other interested persons and organizations; Promote individual and multi station observing programs; Encourage programs that enhance the technical abilities of our members to monitor cosmic radio signals, as well as to share and analyze such signals; Encourage educational programs within SARA and educational outreach initiatives. Founded in 1981, the Society of Amateur Radio Astronomers, Inc. is a membership supported, non-profit [501(c) (3)], educational and scientific corporation.

Cover Photo: Jack Lobinger

Contents

Radio Waves

President's Page

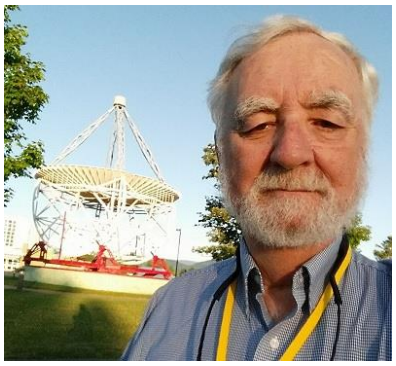

It's hard to imagine the amount of effort that went into building receiving systems when SARA was first created. If you haven't done so already, you should order the complete archive of the Journal and read some of the earliest issues.

The RTL-SDR and other modern receiving systems and band pass filters have truly modernized the detection of signals hitting the earth.

We hope that the Society provides you with assistance with your hobby. Lots going on on the email list on a multitude of topics. We are glad to support this as a way of sharing information between enthusiasts.

Please let me or any other board member know if you think there is anything SARA can do to enhance the radio astronomy experience for people at any and all levels of experience.

Keep your antennas pointed up!

Dennis

Editor's Notes

We are always looking for basic radio astronomy articles, radio astronomy tutorials, theoretical articles, application and construction articles, news pertinent to radio astronomy, profiles and interviews with amateur and professional radio astronomers, book reviews, puzzles (including word challenges, riddles, and crossword puzzles), anecdotes, expository on "bad astronomy," articles on radio astronomy observations, suggestions for reprint of articles from past journals, book reviews and other publications, and announcements of radio astronomy star parties, meetings, and outreach activities.

New Journal Feature – Observation Reports

We are now accepting 1-2 page observation reports. These reports should include the astronomical objects RA/DEC plus UTC of the observation. Also include the telescope configuration, process used to observe the object and results. Picture of the setup and plots of the observation are a plus to the report.

If you would like to write an article for Radio Astronomy, please follow **the newly updated Author's Guide** on the SARA web site:
http://www.radio-astronomy.org/publicat/RA-JSARA_Author's_Guide.pdf.

Let us know if you have questions; we are glad to assist authors with their articles and papers and will not hesitate to work with you. You may contact your editors any time via email here: edit@radio-astronomy.org.

The editor(s) will acknowledge that they have received your submission within two days. If they do not reply, assume they did not receive it and please try again.

Please consider submitting your radio astronomy observations for publication: any object, any wavelength. Strip charts, spectrograms, magnetograms, meteor scatter records, space radar records, photographs; examples of radio frequency interference (RFI) are also welcome.
Guidelines for submitting observations may be found here: http://www.radio-astronomy.org/publicat/RA-JSARA_Observation_Submission_Guide.pdf

Issue	Articles	Review	Distribution
2021			
Nov-Dec	December 12	December 22	December 31
2022			
Jan-Feb	February 12	February 21	February 28
Mar-Apr	April 12	April 25	April 30
May-Jun	Jun 12	Jun 20	Jun 28
Jul-Aug	Aug 12	Aug 22	Aug 31

SARA NOTES

SARA Student & Teacher Grant Program

All, SARA has a grant program that is, sad to say very underutilized. We will provide kits or money to students and teachers including college students to help them with a radio telescope project. SARA can supply any of the following kits:

- SuperSID
- Scope in a Box
- IBT (Itty Bitty Telescope)
- Radio Jove kit
- Inspire
- Sky Scan

We can also provide up to five hundred dollars ($500.00 USD) for an approved radio telescope project.

We have on occasion provided more money based on the merits of the project and the SARA Grant Committee approval.

More information on the grant program can be found at the URL below.
SARA Student and Teacher Project Grants | Society of Amateur Radio Astronomers (radio-astronomy.org)

All that is required is the SARA grant request form be filled out and sent in. If it needs more work for approval, we will work with the student to help ensure their success.

Please pass the word that SARA will fund any legitimate radio telescope project anywhere in the world.

If you have a question, contact me at crowleytj at hotmail dot com.

Tom Crowley
SARA Grant Program Administrator

Drake's Lounge

Join the SARA community as we discuss the latest astronomy and radio astronomy news. The lounge also provides a forum to share and get advice on your radio astronomy projects from very experienced amateur radio astronomers.

Drake's Lounge is every month on the 3rd Sunday at 2 pm Eastern time. ZOOM email notifications will be sent to all members.

See you there!

News: (Sep-Oct 2021)

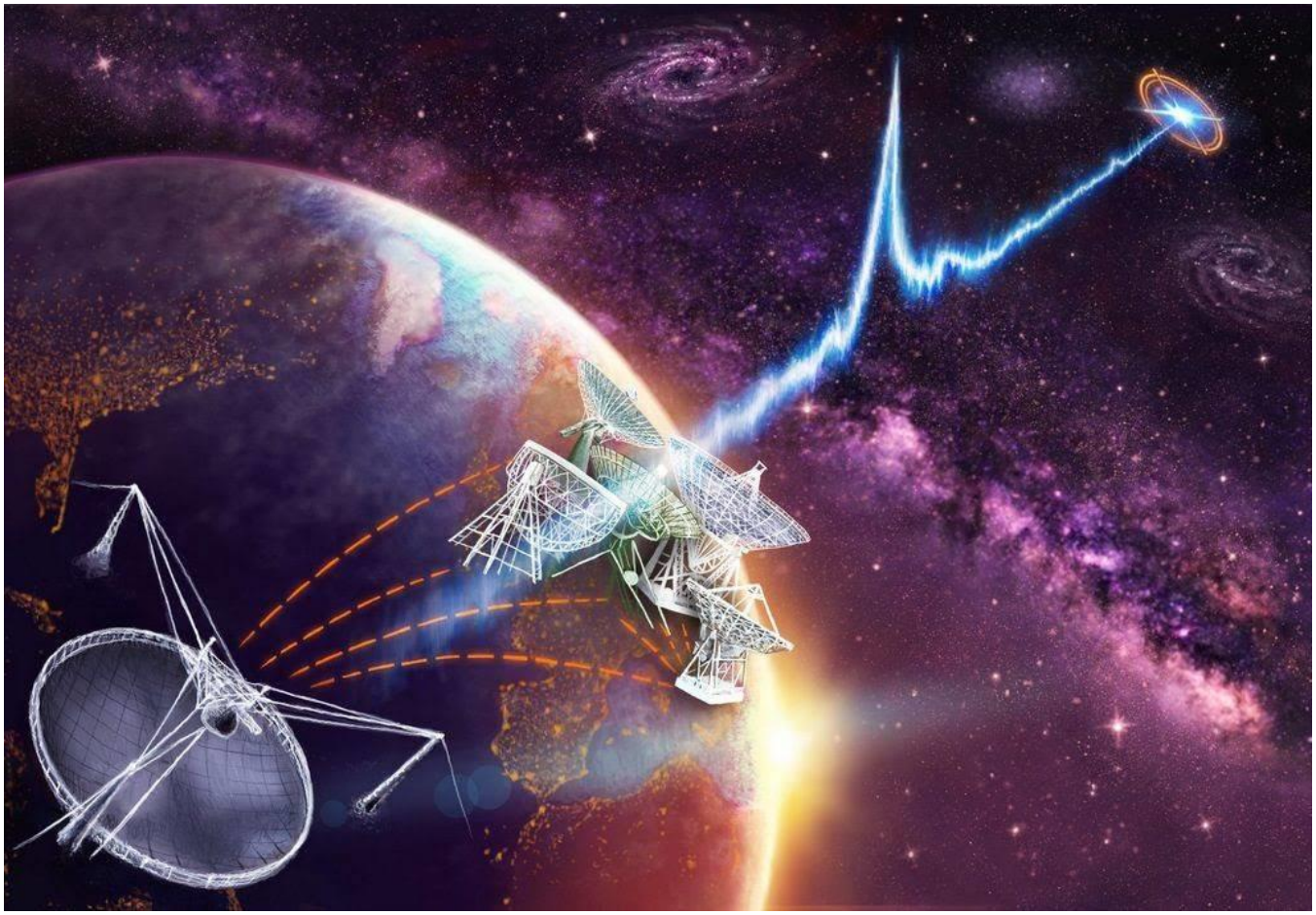

Hey, Mac, I guess what you've been sayin' all along is official now: Universe Today ~ *We'll Have to Wait About 3,000 Years for a Reply From Intelligent Civilizations*: https://www.universetoday.com/152112/well-have-to-wait-about-3000-years-for-a-reply-from-intelligent-civilizations/

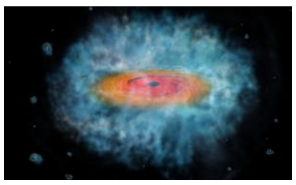

Universe Today ~ *If the First Black Holes Collapsed Directly, Could we Detect Radio Signals From Those Moments?*: https://www.universetoday.com/152192/if-the-first-black-holes-collapsed-directly-could-we-detect-radio-signals-from-those-moments/

Hey, Mac, what took them so long? American Astronomical Society ~ *AAS Journals Will Switch to Open Access*: https://aas.org/press/aas-journals-open-access

Jet Propulsion Laboratory ~ *NASA's Deep Space Network Looks to the Future*: https://www.jpl.nasa.gov/news/nasas-deep-space-network-looks-to-the-future

Tektronix ~ *XYZs of Oscilloscopes - Primer*: https://download.tek.com/document/03W_8605_6.pdf

Hey, Mac, get that bunker finished...!: LiveScience ~ *An 'Internet apocalypse' could ride to Earth with the next solar storm, new research warns*: https://www.livescience.com/solar-storm-internet-apocalypse

Research Notes of the American Astronomical Society (RNAAS) ~ *Solar Cycle 25 is Currently Very Similar to Solar Cycle 24*: https://iopscience.iop.org/article/10.3847/2515-5172/ac19a2

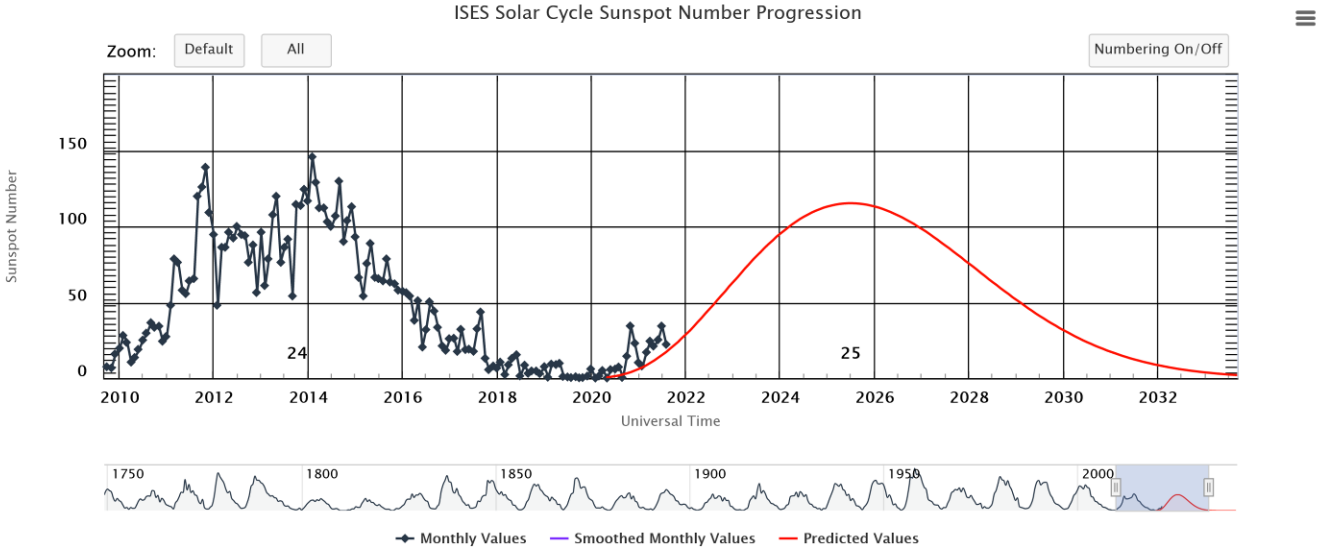

Space Weather Prediction Center

SpaceWeather.com ~ *Earth Can Make Its Own Auroras*: https://spaceweather.com/archive.php?view=1&day=01&month=10&year=2021

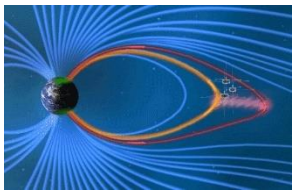

Jet Propulsion Laboratory ~ *Working Overtime: NASA's Deep Space Atomic Clock Completes Mission*: https://www.jpl.nasa.gov/news/working-overtime-nasas-deep-space-atomic-clock-completes-mission

Solar-Terrestrial Center for Excellence (STCE) ~ The largest solar flare: https://www.stce.be/newsletter/pdf/2021/STCEnews20211008.pdf

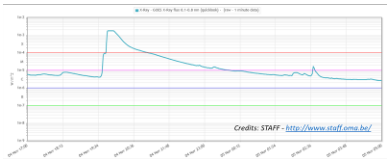

Technical Knowledge & Education: (Sep-Oct 2021)

HERA (Hydrogen Epoch of Reionization Array) ~ http://reionization.org/

International Space Science Institute (ISSI)

- *Game Changers Online Seminars, Ideas and Findings about the Solar System, the Universe and our Terrestrial Environment* (new series starting 16 September 2021): https://www.issibern.ch/issi-spotlight/online-seminars-game-changers/
- Game Changers Videos from 2020-2021: https://www.issibern.ch/issi-spotlight/recorded-game-changers-seminars/

Keysight Technologies ~ *Manuals for discontinued Keysight, Agilent and Hewlett-Packard test equipment*: https://edadocs.software.keysight.com/kkbopen/where-can-i-find-manuals-for-discontinued-keysight-agilent-and-hewlett-packard-test-equipment-577941709.html

Rohde & Schwarz ~

- *Fundamentals of an RF design - white paper*: https://www.rohde-schwarz.com/us/solutions/test-and-measurement/electronic-design/fundamentals-of-an-rf-design_253353.html
- *Everything Test – Webinar series, 5 tracks, 30 webinars on-demand*: https://www.rohde-schwarz.com/us/campaigns/rsa/icr/everything-test-webinar-series_254047.html

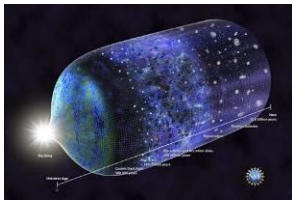

Cornell University ~ *A Multi-messenger view of Cosmic Dawn: Conquering the Final Frontier*: https://arxiv.org/abs/2109.00003

YouTube ~ *21cm (1420MHz) Amateur Radio Astronomy*: https://www.youtube.com/watch?v=vHxzKCaay0w&t=4153s

Community of European Solar Radio Astronomers (CESRA) ~ *Langmuir wave motion observed in the most intense radio sources in the sky*: https://www.astro.gla.ac.uk/users/eduard/cesra/?p=3028

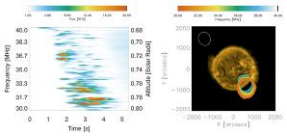

Whole Heliosphere and Planetary Interactions (WHPI) Workshop: https://app.virtualpostersession.org/e/5016ae2434452b0b747e3a63ef84b10b

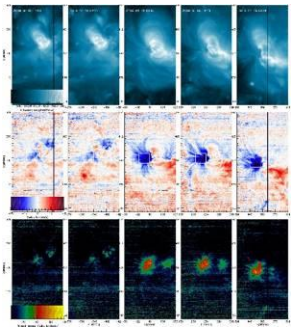

Community of European Solar Radio Astronomers (CESRA) ~ *The active region source of a type III radio storm observed by Parker Solar Probe during encounter 2*: https://www.astro.gla.ac.uk/users/eduard/cesra/?p=3058

Everything RF ~ *Top 10 Questions Engineers Ask About Software Defined Radios*: https://www.everythingrf.com/community/top-10-questions-engineers-ask-about-software-defined-radios

Community of European Solar Radio Astronomers (CESRA) ~ *Properties of High-Frequency Type II Radio Bursts and Their Relation to the Associated Coronal Mass Ejections*: https://www.astro.gla.ac.uk/users/eduard/cesra/?p=3067

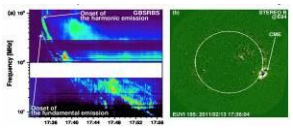

Carnegie Astronomy ~ YouTube video, *Pinpointing fast radio bursts in space and time, Prof. Jason Hessels (University of Amsterdam & ASTRON)*: https://www.youtube.com/watch?v=a_Cps29leS0

History of Geo- and Space Sciences ~ *History of EISCAT (European Incoherent Scatter Scientific Association):*

- *Part 1: On the early history of EISCAT with special reference to the Swedish part of it*: https://hgss.copernicus.org/articles/2/115/2011/
- *Part 2: The early history of EISCAT in Finland*: https://hgss.copernicus.org/articles/2/123/2011/
- *Part 3: The early history of EISCAT in Norway*: https://hgss.copernicus.org/articles/3/47/2012/
- *Part 4: On the German contribution to the early years of EISCAT*: https://hgss.copernicus.org/articles/7/67/2016/
- *Part 5: Operation and development of the system during the first two decades*: https://hgss.copernicus.org/preprints/hgss-2021-16/

For Your Radio Astronomy Bookshelf

(Prices in USD)

- **Radio Astronomy (Above and Beyond)** by Adele D. Richardson $4.79
- **Radio Astronomy;** F.Graham Smith; Pelican Books. 1962, $17.69
- **Astronomy for Dummies**; Stephen P. Maran; $20.49

SuperSID

Collaboration of Society of Amateur Radio Astronomers and Stanford Solar Center

- ✓ Stanford provides data hosting, database programming, and maintains the SuperSID website
- ✓ Society of Amateur Radio Astronomers (SARA) sells the SuperSID monitors for 48 USD to amateur radio astronomers and the funds are then used to support free distribution to students all over the world (image below as of Fall 2017)
- ✓
- ✓ Jonathan Pettingale at SARA is responsible for building and shipping the SuperSID monitor kits: SuperSID@radio-astronomy.org
- ✓ SuperSID kits may be ordered through the SARA SuperSID webpage: http://radio-astronomy.org/node/210
- ✓ Questions about the SuperSID project may be directed to Steve Berl at Stanford: steveberl@gmail.com
- ✓ Jaap Akkerhuis at Stanford is responsible for the SuperSID software and SARA has provided financial support for his efforts
- ✓ SuperSID website hosted by Stanford: http://solar-center.stanford.edu/SID/sidmonitor/
- ✓ SuperSID database: http://sid.stanford.edu/database-browser/
- ✓ The data is searchable by time, station, date, and multiple plots may be placed on the same graph for comparison.

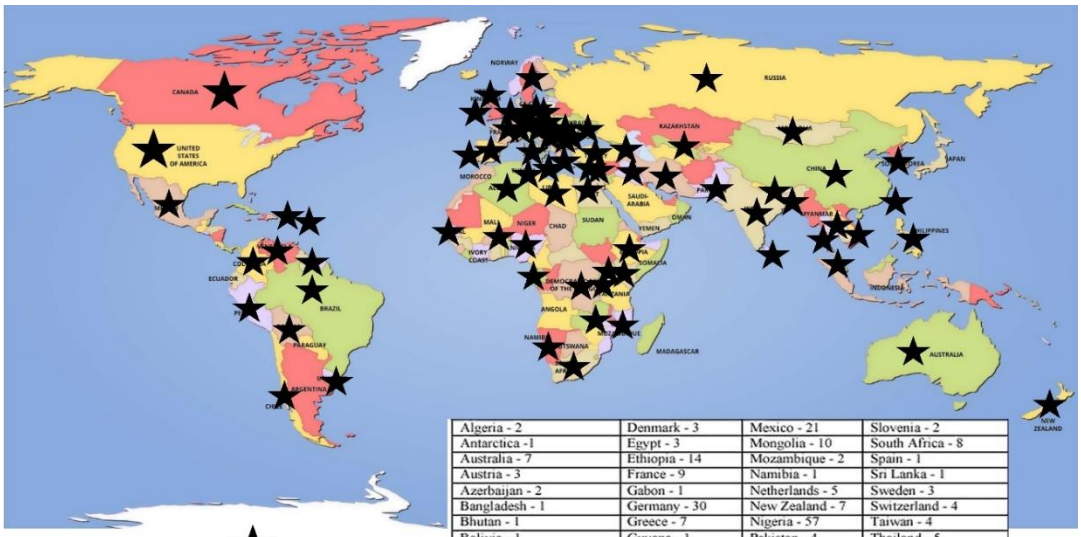

Algeria - 2	Denmark - 3	Mexico - 21	Slovenia - 2
Antarctica -1	Egypt - 3	Mongolia - 10	South Africa - 8
Australia - 7	Ethiopia - 14	Mozambique - 2	Spain - 1
Austria - 3	France - 9	Namibia - 1	Sri Lanka - 1
Azerbaijan - 2	Gabon - 1	Netherlands - 5	Sweden - 3
Bangladesh - 1	Germany - 30	New Zealand - 7	Switzerland - 4
Bhutan - 1	Greece - 7	Nigeria - 57	Taiwan - 4
Bolivia - 1	Guyana - 1	Pakistan - 4	Thailand - 5
Bosnia-Herzegovina - 2	Hungary - 1	Peru - 10	Tunisia - 9
Brazil - 11	India - 33	Philippines - 3	Turkey - 2
British Virgin Islands - 1	Indonesia - 2	Poland - 2	Uganda - 5
Bulgaria - 2	Iran - 4	Portugal - 3	UK - 32
Burkino Faso - 1	Iraq - 1	Rep of Congo - 3	Uruguay - 9
Canada - 33	Ireland - 9	Romania - 4	US Virgin Islands - 2
Chile - 1	Italy - 42	Russia - 3	USA - 491
China - 38	Kenya - 23	Rwanda - 1	Uzbekistan - 2
Columbia - 9	Korea (South) - 2	S Africa - 4	Venezuela - 2
Croatia - 7	Lebanon - 11	Senegal - 1	Vietnam - 1
Cypress - 1	Libya - 1	Serbia - 1	Zambia - 2
Czech Republic - 1	Malaysia - 19	Singapore - 3	
D Rep of Congo - 4	Malta - 1	Slovak Repub - 2	

For official use only
Monitor assigned: _____
Site name: _____
Country: _____

SuperSID Space Weather Monitor

Request Form

	Your information here		
Name of site/school *(if an institution)*:			
Choose a site name: *(3-6 characters) No Spaces*			
Primary contact person:			
Email:			
Phone(s):			
Primary Address:	Name School or Business Street Street City Country	 State/Province Postal Code	
Shipping address, if different:	Name School or Business Street Street City Country	 State/Province Postal Code	
Shipping phone number:			
Latitude & longitude of site:	Latitude: _____	Longitude: _____	

I understand that neither Stanford nor the Society of Amateur Radio Astronomers is responsible for accidents or injuries related to monitor use. I will assure that a surge protector and other lightning protection devices are installed if necessary.

Signature: _____ **Date:** _____

I will need:

What	*Cost*	*How many?*
SuperSID distribution USB Power	$48 (assembled)	
USB Sound card 96 kHz sample rate *(or provide this yourself)*	$40 *(optional)*	
Antenna wire (120 meters) *(or you can provide this yourself)*	$23 *(optional) with connectors attached and tested*	
RG 58 Coax Cable (9 meters) *(or provide this yourself)*	$14 *(optional) with connectors attached and tested*	
Shipping	US $12 Canada & Mexico $40 all other $60	
	TOTAL	$

____ **I have included a $**_____ **check** (payable to SARA)

____ **I will make payment thru** www.paypal.com to treas@radio-astronomy.org

or

____ If you are a Minority-serving institution, in a Developing or economically deprived nation, and/or you are using the monitor with students for educational purposes, you may qualify for obtaining a monitor at reduced or no cost. Check here if you wish to apply for this designation. Then tell us how you want to use the SuperSID monitor. Include type of site, number of students involved, whether public or private school, grade levels, etc. and describe your program. The goal of the SuperSID project is to provide as many students with systems as possible. If you are able to pay for a system, even if you qualify for a free one, please do so and help support our goal.

_____

_____

_____

For more details on the Space Weather Monitor project, see: **http://sid.stanford.edu**

To set up a SuperSID monitor you will need:

1. Access to power and an antenna location that is relatively free of electric interference (could be indoors or out)
2. A **PC**** with the following minimal specifications:
    - A sound card that can record (sample) up to 96 kHz, or a USB port to connect such a sound card (for North and South America)
        - All other countries can use AC97 sound card with 48 kHz record (sample) rate. Most computers made after 1997 will have AC97.
    - Windows 2000 or more recent operating system
    - 1 GHz Processer with 128 mb RAM
    - Ethernet connection & internet browser (desirable, but not required)
    - Standard keyboard, mouse, monitor, etc.
3. An inexpensive antenna that you build yourself. You'll need about 120 meters (400 feet) of **insulated** wire. Solid wire is easier to wind than stranded. Magnet wire will work but be more fragile. You can use anything from #18 to #26 size wire. The antenna frame can be made of wood, PVC pipe, or similar materials. We'll provide instructions. You can purchase the wire from us or obtain your own.
4. RG58 coax cable with a BNC connector at one end to run from the antenna to the SuperSID receiver. 9 meters is recommended, but the length will depend on where you place the antenna. You can purchase the coax from us or obtain your own.
5. Surge protector and other protection against a lightning strike

---

Return this form to: SuperSID@radio-astronomy.org
or mail to: SARA
Brian O'Rourke, SARA Treasurer
337 Meadow Ridge Rd,
Troy, VA 22974-3256

Founded in 1890

The British Astronomical Association

A company limited by guarantee Registered Charity No. 210769

Burlington House, Piccadilly, London, W1J 0DU

Telephone: 020 7734 4145 Fax No.: 020 7439 4629

Email: office@britastro.org Website: www.britastro.org

Please send all reports and observations to jacook@jacook.plus.com

John Cook's VLF Report

BAA Radio Astronomy Section **2021 July**

July started with a 'bang' as the first X-class flare of solar cycle 25 was recorded on the 3rd. Active region AR12838 was right on the North Western limb of the sun when the flare occurred, and was responsible for all of the activity that we recorded on the 3rd.

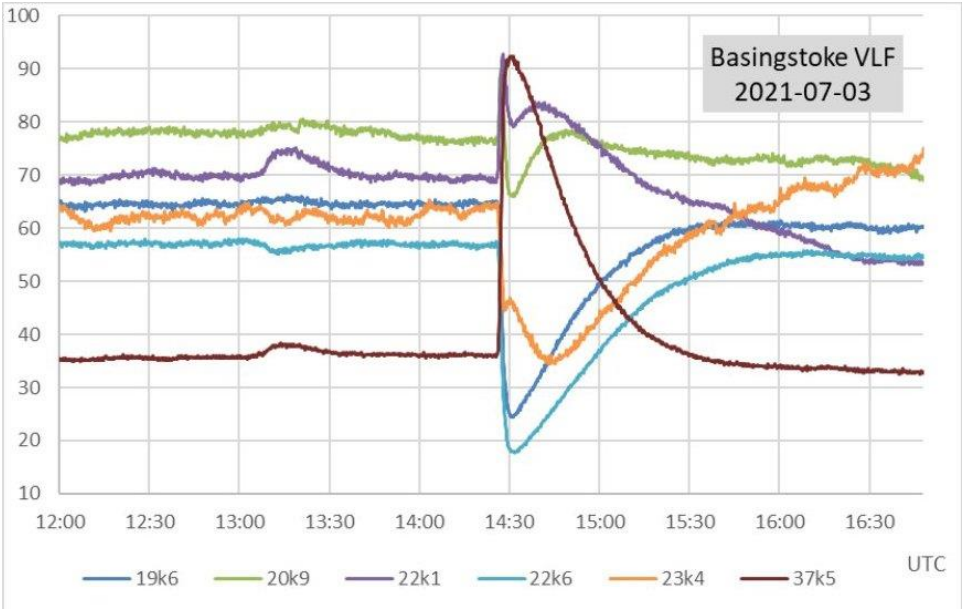

This recording by Paul Hyde shows a variety of SID profiles from the flare. The 37.5kHz SID is a conventional rising 'shark's fin', while the SID at 22.6kHz is inverted. The 23.4kHz signal shows a mild 'spike and wave' pattern as the phase shift between ground and sky waves moves from cancelling to adding and back again. 22.1kHz shows an inverted version of the 'spike and wave'. What is clear from them all is the very rapid rise time of the disturbance. The earlier C1.9 flare is just visible around 13:10-13:30UT.

Radio noise was also recorded at 151MHz, 408MHz and 610MHz by Colin Clements, and at 28MHz by Colin Briden as shown in the charts on the next page:

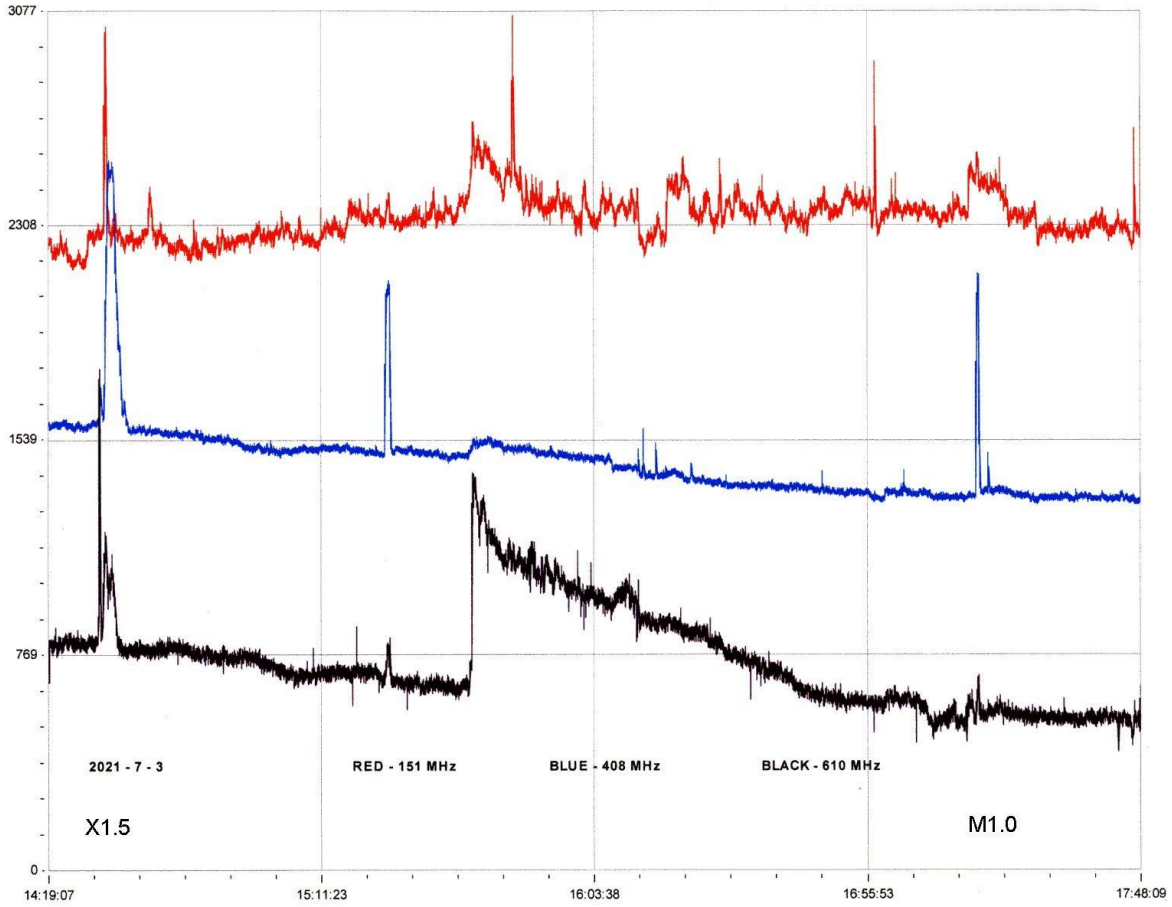

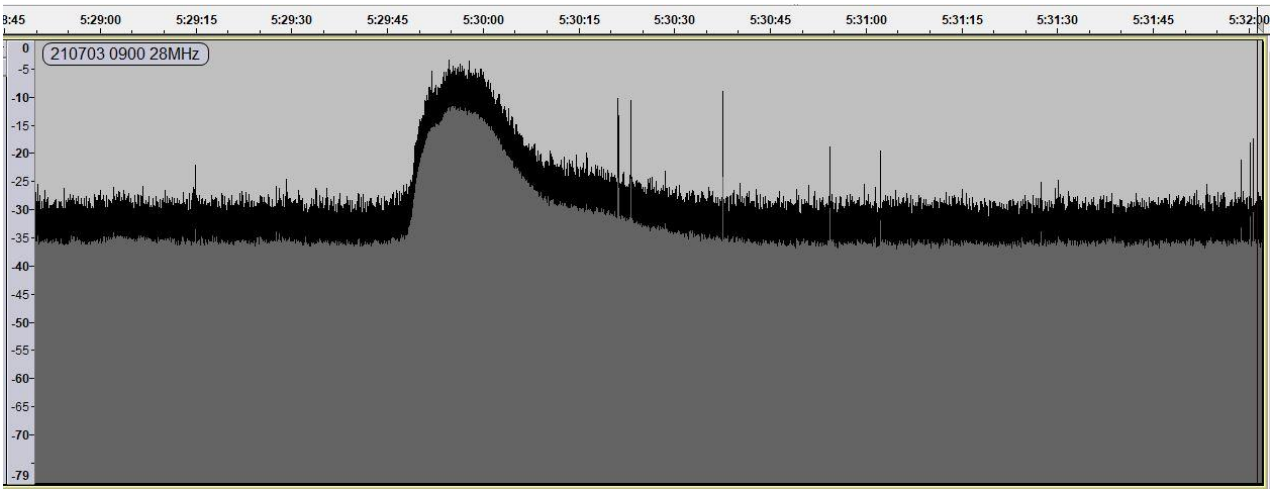

In Colin Clements' recording, 610MHz (black trace) shows a strong spike at the peak of the X1.5 flare, followed at about 15:32 by a sharp rise and long decay in signal strength. The X1.5 shows at all three frequencies, but the later M1.0 flare is only really strong at 408MHz (blue trace).

Colin Bridens' recording shows the 28MHz signal at the time of the X1.5 flare, lasting about 55 seconds before settling at its pre-flare level. The grey band is the signal average, the black band showing signal strength peaks.

The recording from Mark Prescott shows the full day's activity, starting with the M2.7 flare peaking at around 07:20UT. The C1.9 flare shows best at 20.9kHz, despite the noisy signal. The M1.0 flare is also clearly shown, although for some reason 23.4kHz has responded rather weakly to all of the events.

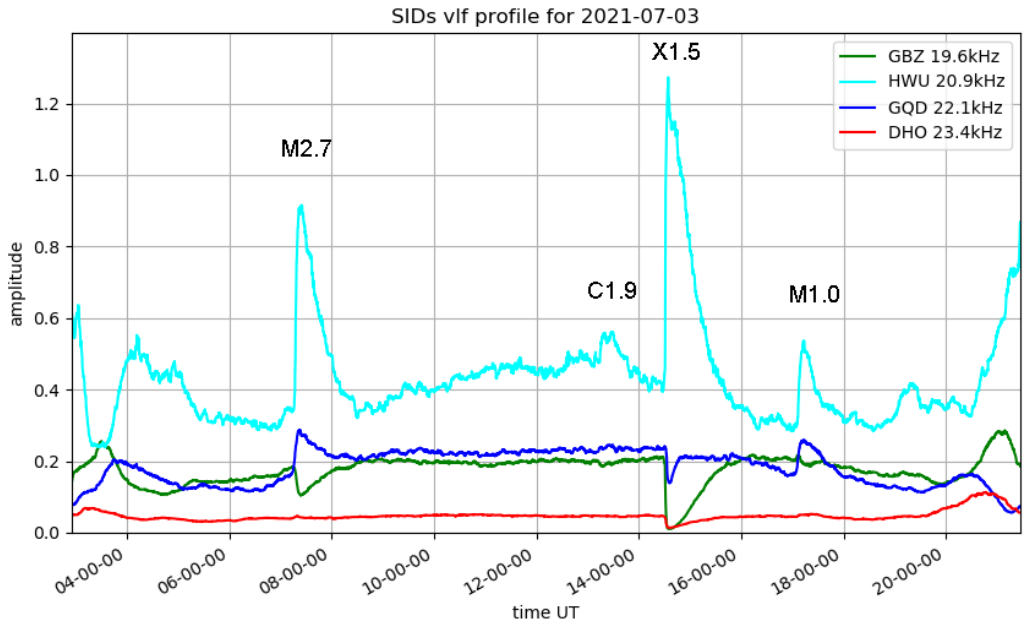

There was another M1.5 flare early on the 4th, after which the sun remained fairly quiet until the 9th when we recorded more strong C-class flares. Colin Clements' recording shows the three stronger events:

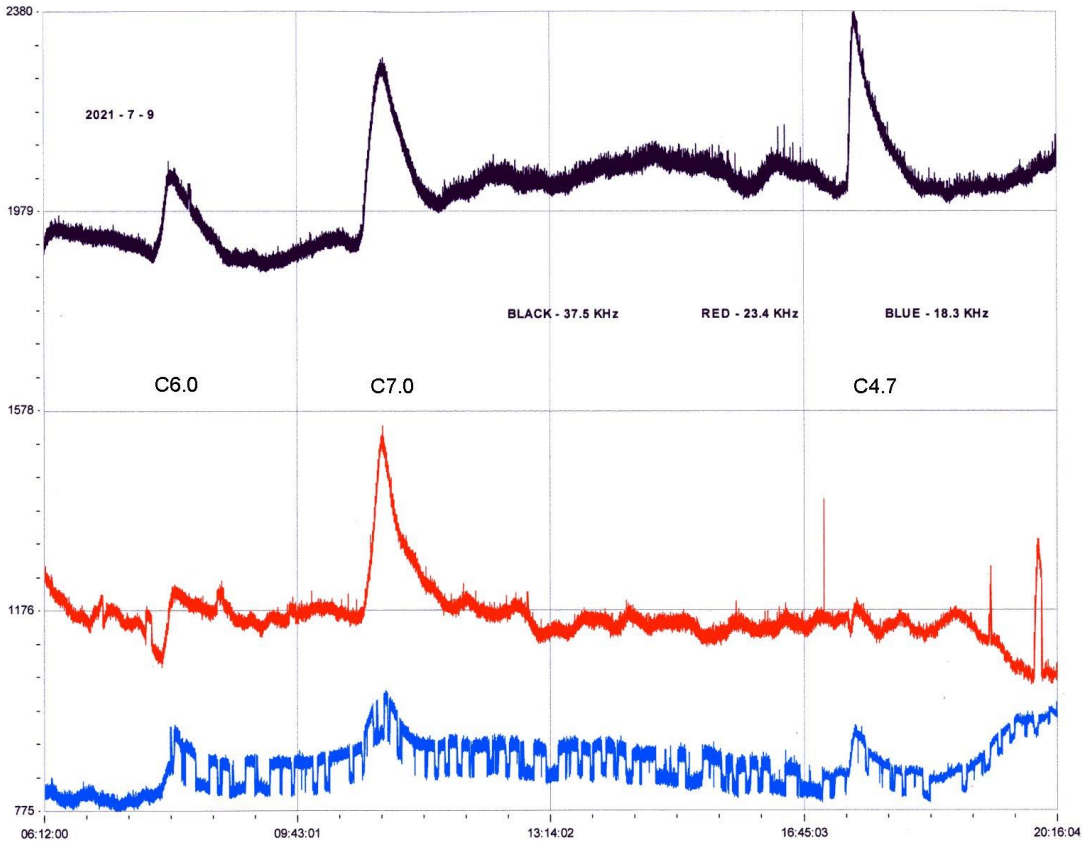

23.4kHz again shows some strange behaviour, with the C6 flare barely visible while the C7 flare produced a clear SID. The later C4.7 flare is also hidden in the noise. There is strong local interference at 18.3kHz, but the SIDs can still be seen. Colin also recorded some VHF activity with these flares. The rest of the month was much quieter with mostly B-class flares, the majority far too weak for us to record.

MAGNETIC OBSERVATIONS

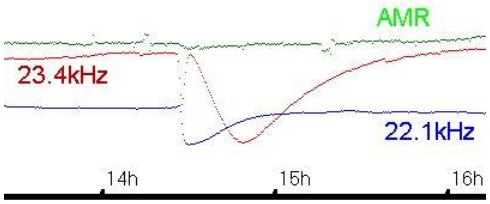

The X1.5 flare on the 3rd produced a magnetic SFE (Solar Flare Effect, or crotchet), shown in the green magnetometer trace in my recording. The SFE is quite small in amplitude (about –10nT) but the dip in the trace matches the upper peak of the 23.4kHz SID. The rectangular disturbances seen either side of the SFE are from local interference. The SFE is also indicated in the month's activity chart from Stuart Green:

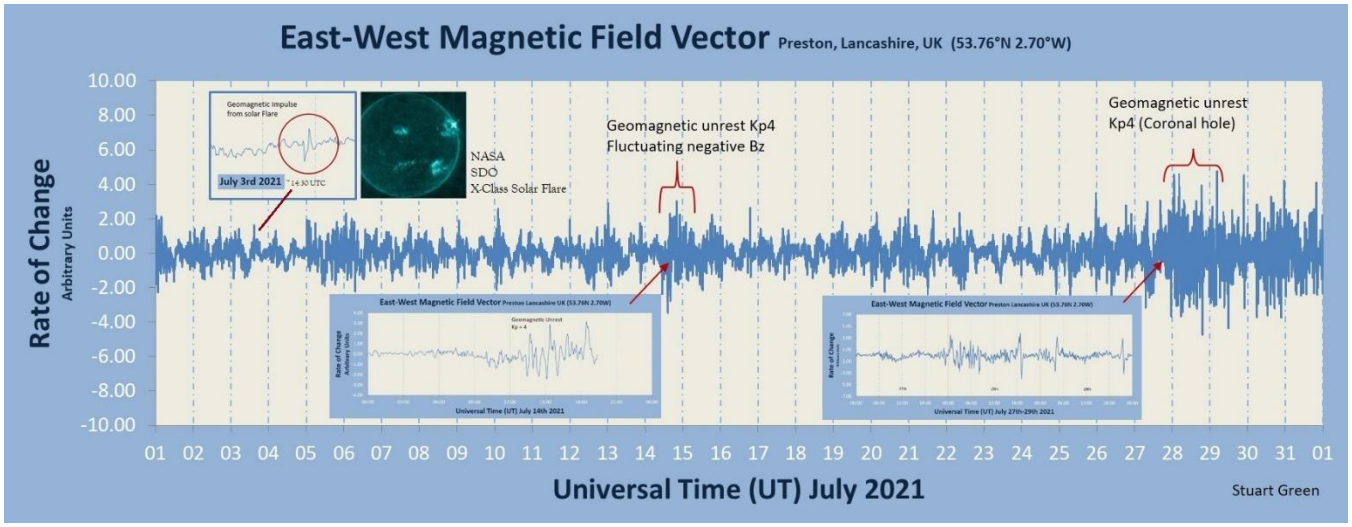

There was a CME from the flare, but occurring right on the solar limb it was not Earth directed. More CMEs were seen in satellite images, but none caused any magnetic disturbances. A generally higher speed solar wind was present mid-month, creating some periods of mild disturbance. The recording by Paul Hearn shows activity on the 14th:

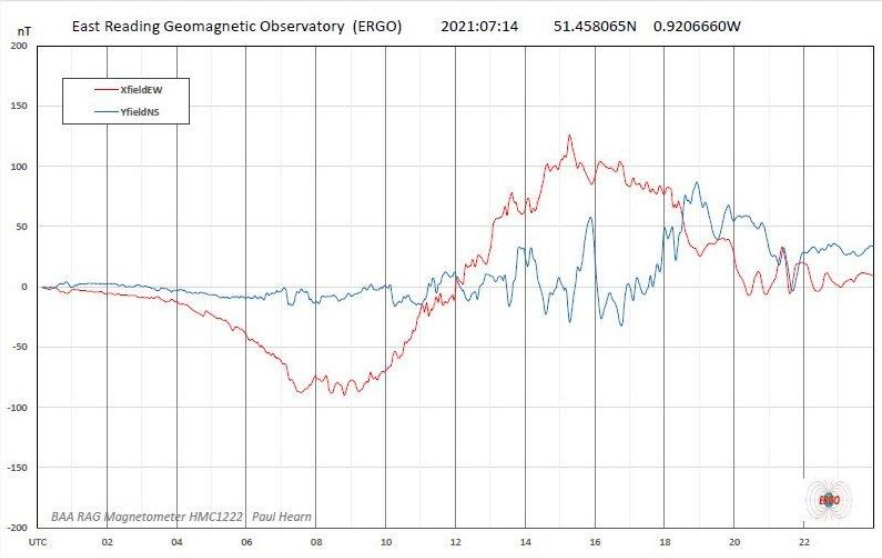

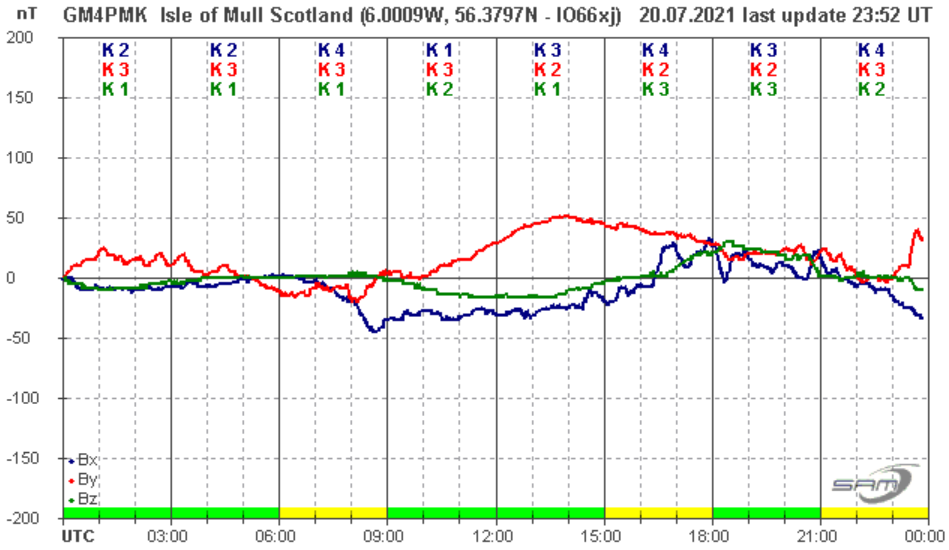

Mild disturbance was also seen on the 20th, shown above in Roger Blackwell's recording. Towards the end of July a pair of coronal holes became effective with a stronger solar wind. This recording by Nick Quinn shows activity on the 28th:

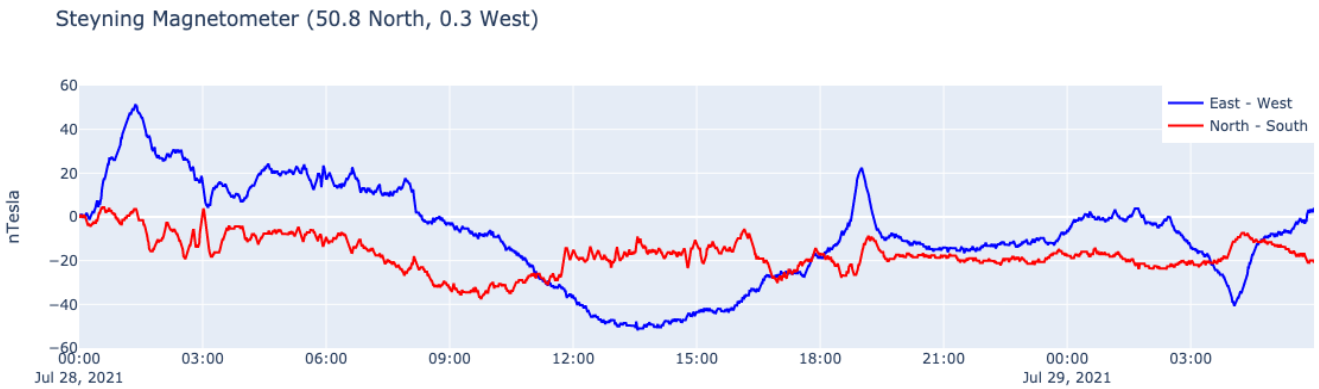

Magnetic observations received from Roger Blackwell, Colin Clements, Stuart Green, Paul Hearn, Nick Quinn and John Cook.

Our series of web-based meetings continues with a GNU radio training seminar on September 18th. Details of how to join the meeting can be found at www.britastro.org along with a programme of future events.

BAA Radio Astronomy Section **2021 August**

The few sunspots present in the first half of August were fairly small and inactive, with just a few B-class flares shown in the satellite X-ray data. The second half was rather more active with some more complex regions present. The strongest flare was the M4.7 peaking just after 06UT. This was rather early in the morning, but it was well recorded. This chart shows the SID recorded by Mark Prescott:

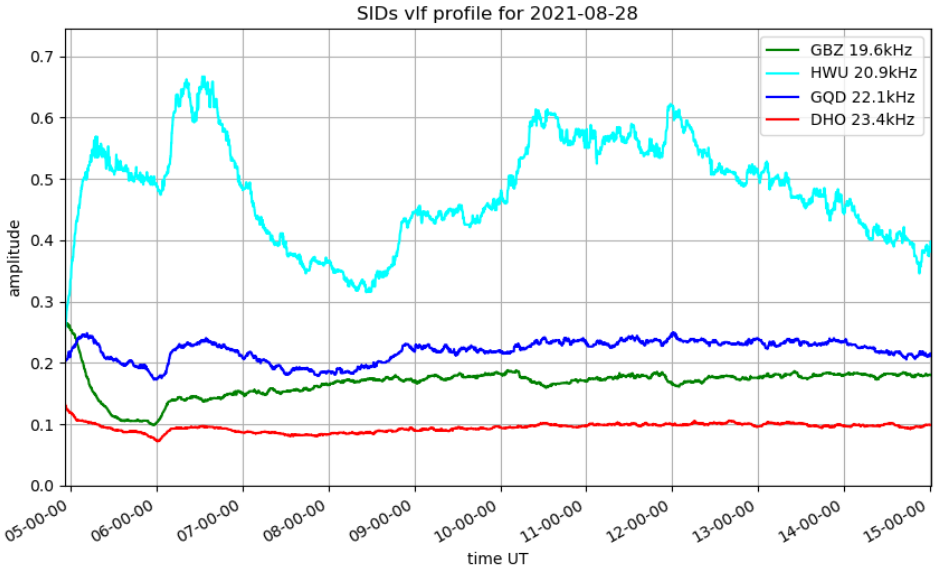

Having multiple signals does make it easier to identify the SID at 19.6, 22.1 and 23.4kHz. The response at 20.9kHz is strange in that it appears to start at the peak time, decaying over about 2.5 hours. Reading it as an inverted SID puts the peak back at 06UT, with a start around 05:15. The GOES satellite data gives an X-ray start time of 05:39, so not at all clear. Most probably the signal was still recovering from sunrise, and that has contaminated the effects of the flare. The C2.7 flare at 12UT was much weaker, but is just visible at 19.6 and 22.1kHz. There is also a response at 20.9kHz, but on a much noisier signal it is less obvious.

The most widely recorded flare was the C8.1 mid-morning on the 29th. The same active area, AR12860, was responsible for both of these flares. It was quite a large and complex group spread over a large area.

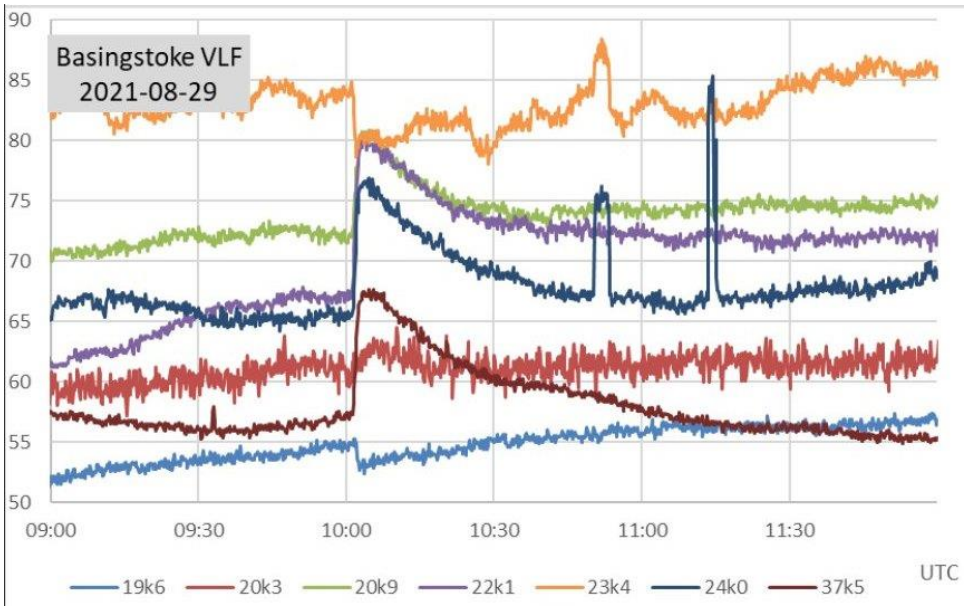

This recording by Paul Hyde shows the C8.1 flare peaking at 10:05UT. Most of signals show a very clear SID, although 23.4kHz is very noisy with a less obvious SID. There are also some strong interference spikes at the higher frequencies from 10:45 to 11:15.

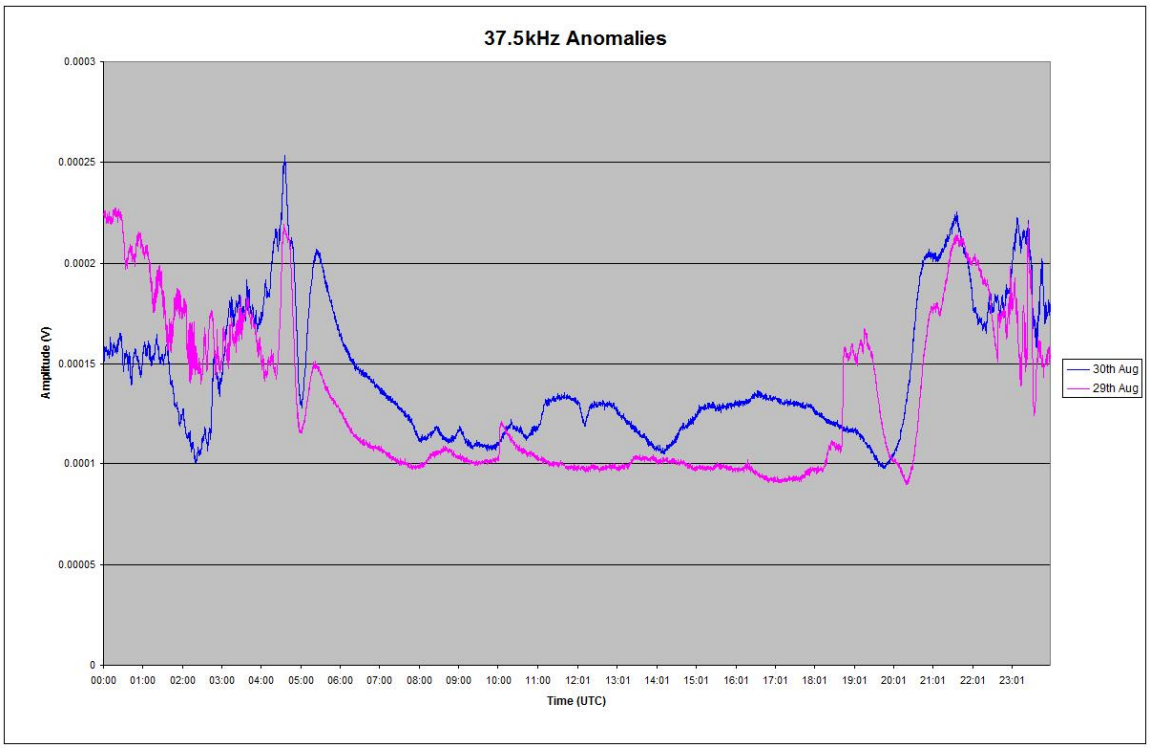

This recording by Mark Edwards shows the C8.1 flare at 37.5kHz on the pink trace. The blue trace shows the same signal on the 30th, with some unusual behaviour during the day. The only notable flare on the 30th was the C1.1 at 09:36UT. There is also a sudden large rise in the signal at 18:43 on the 29th, just before the expected sunset. There seems to have been a very turbulent solar wind over this period, with a large change in polarity at 12:12 on the 30th, corresponding to the dip seen in the 37.5kHz signal.

MAGNETIC OBSERVATIONS

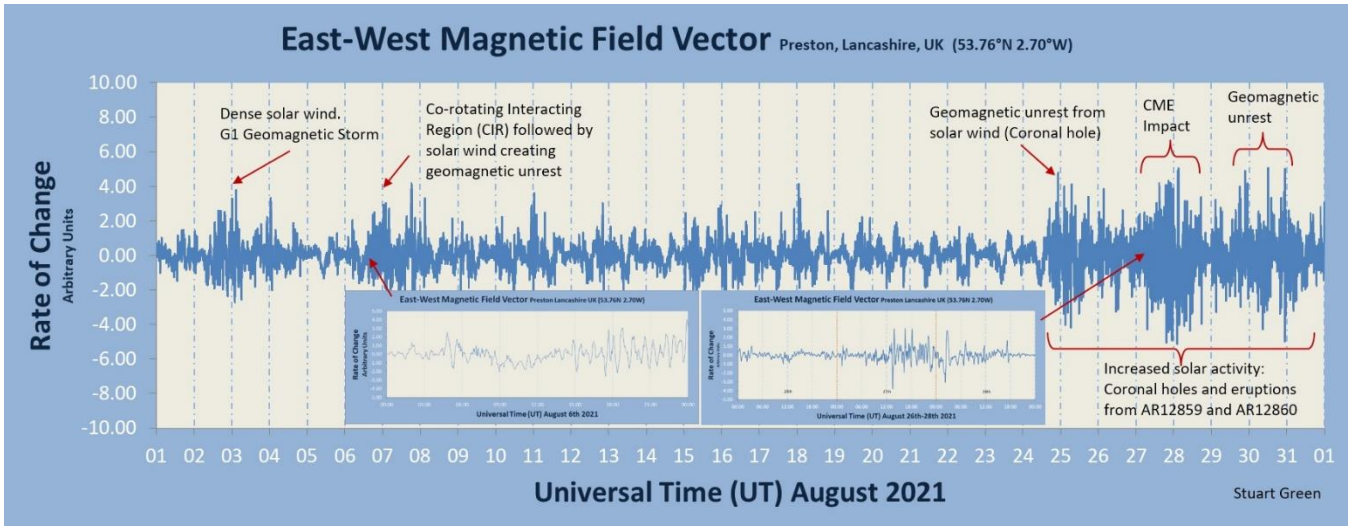

The magnetic summary for August by Stuart Green shows strong activity at the end of the month, matching the increase in solar flares. There is also a period of activity starting on the 2nd, resulting from a CME recorded in satellite images from late July. The recording by Nick Quinn shows this activity:

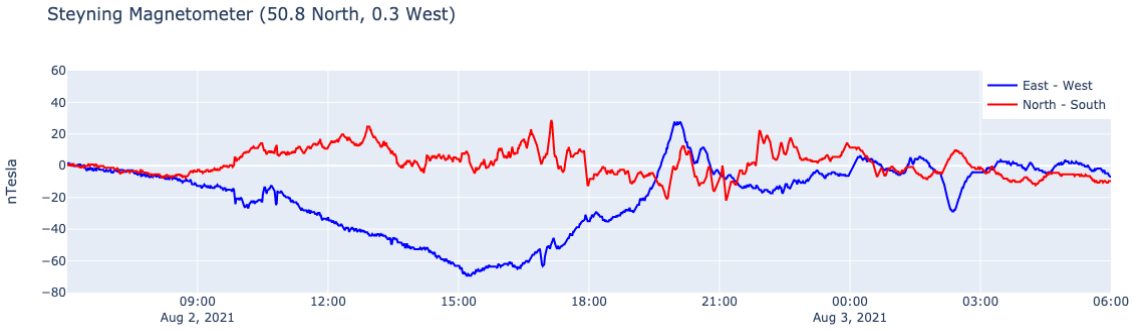

The north-south field in particular is very turbulent through the afternoon and into the early morning of the 3rd.

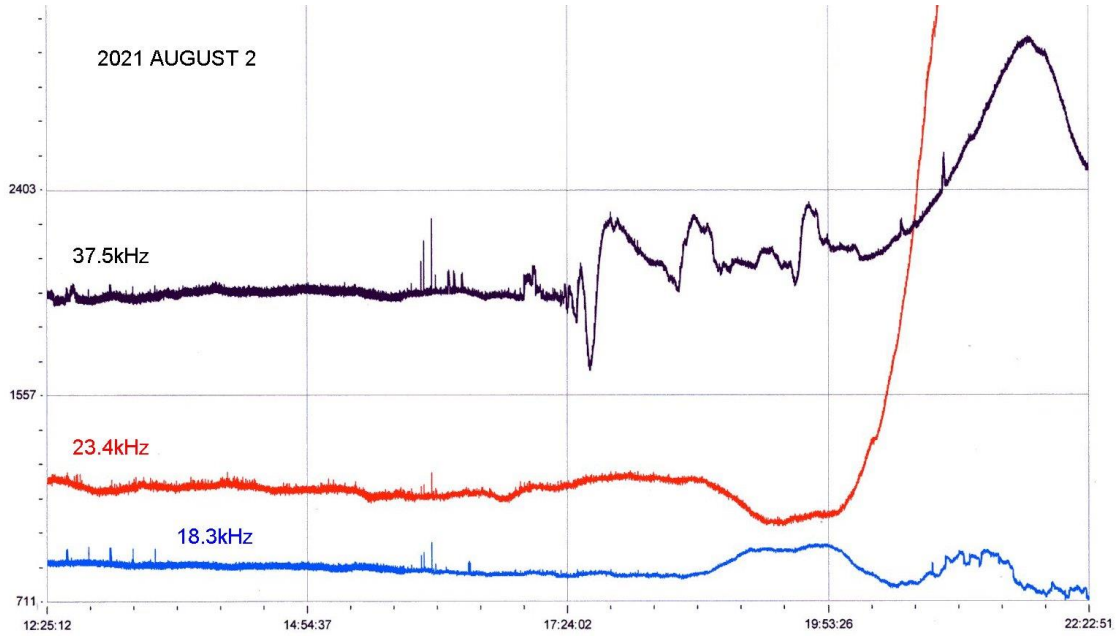

The recording by Colin Clements shows the 37.5kHz response to the magnetic disturbance, starting around 17:30 and continuing until sunset takes over. The other signals show more normal curves, with the sunset dominating. There is some minor local interference around 16:00UT.

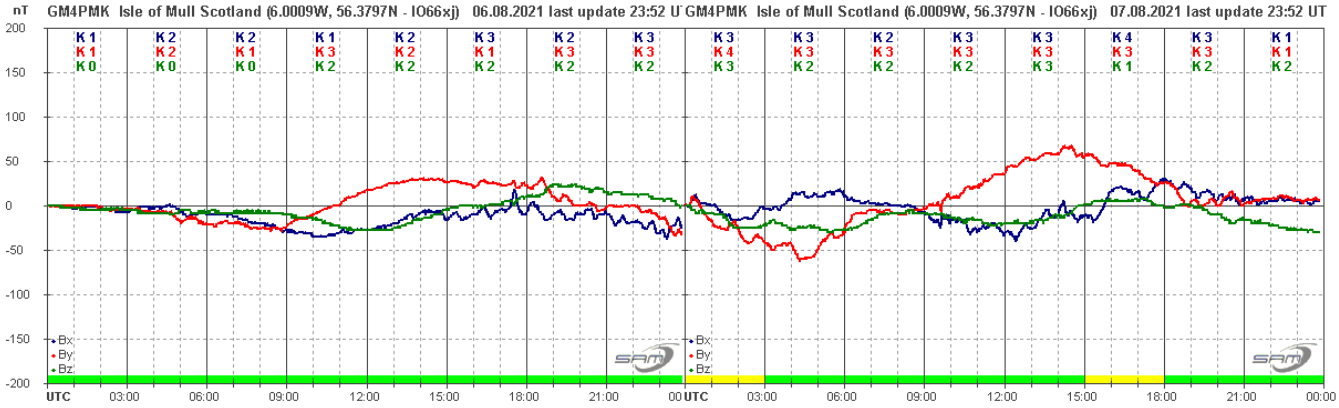

A north polar coronal hole produced a mild disturbance over the 6th and 7th, shown in this recording by Roger Blackwell. There were periods of rapid oscillation, although the magnitude remained quite low. Another north polar coronal hole was responsible for a minor disturbance in the afternoon of the 15th and early morning of the 16th. It is barely visible in the summary chart by Stuart Green, but was recorded by Colin Clements:

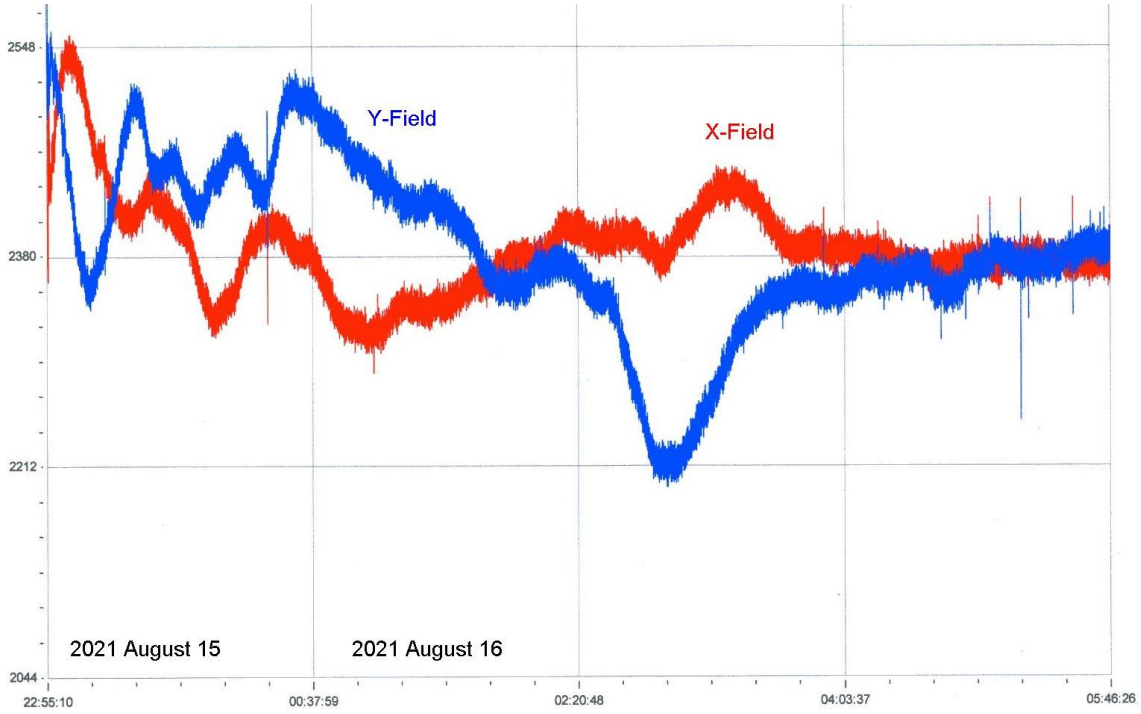

Activity increased again on the 25th, with a combination of coronal holes and CMEs. Disturbance from the high speed wind on the 25th was fairly mild, with a further mild period on the 26th. The CME impact was recorded just after 01UT on the 28th, shown in this recording by Roger Blackwell:

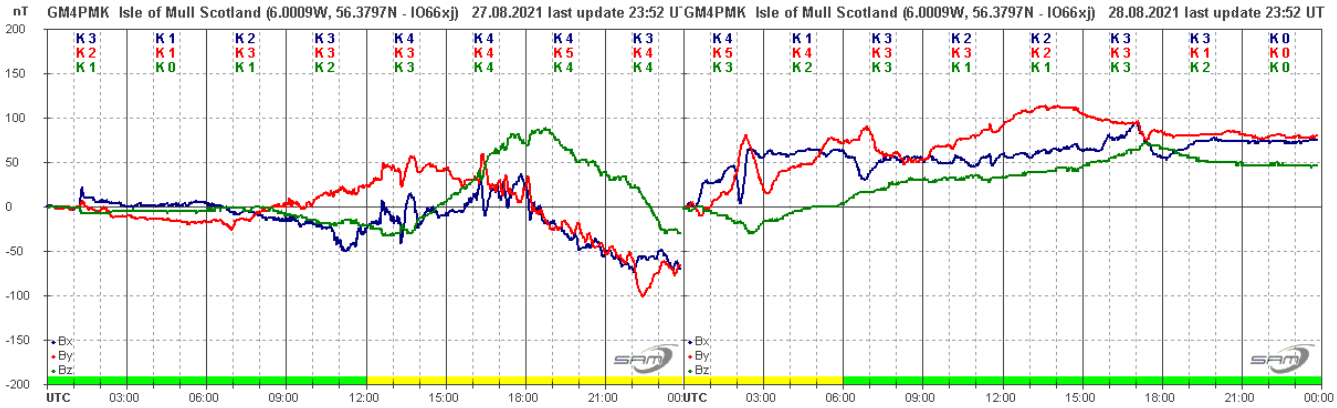

Magnetic activity increased around 11:00UT, continuing through to the evening of the 28th, with +/-100nT shown in Roger's recording. Note that the midnight discontinuity is due to the sensor being reset. Paul Hearn made this recording from the 28th:

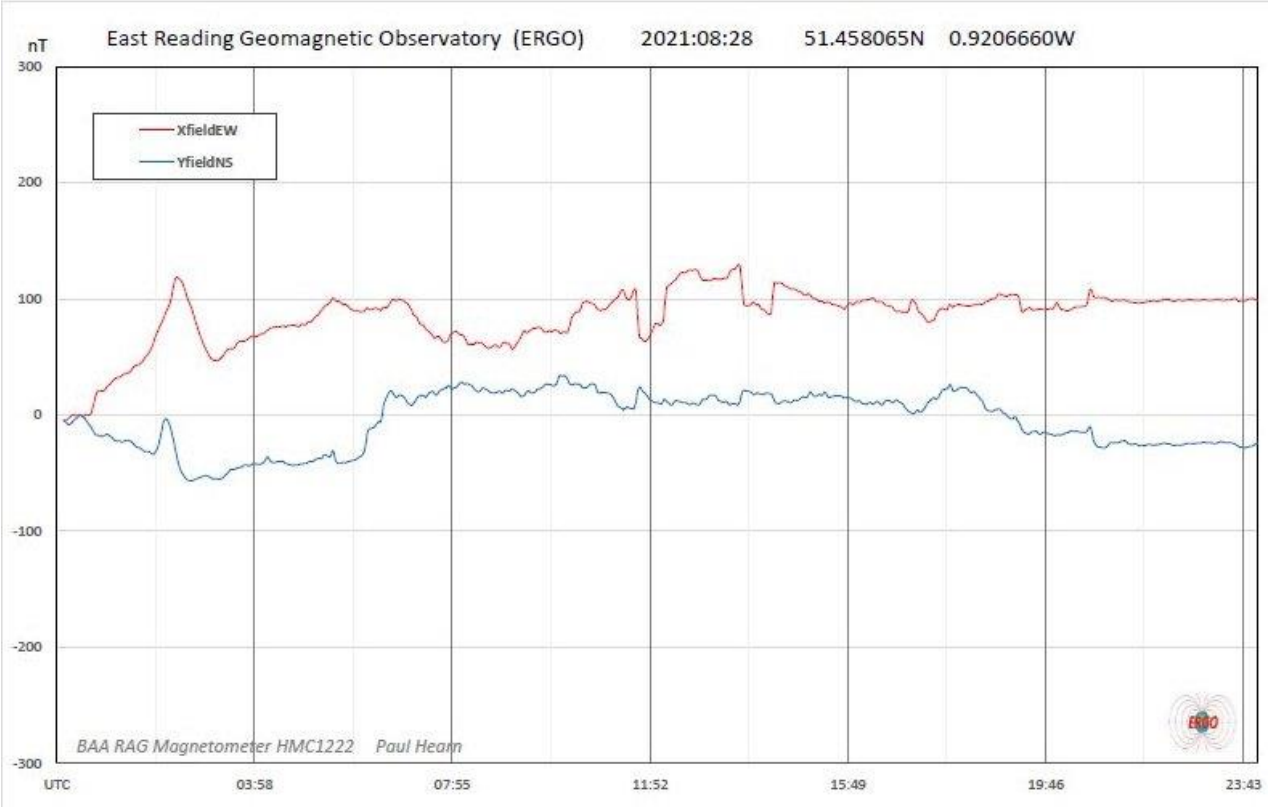

Magnetic observations received from Roger Blackwell, Colin Clements, Stuart Green, Paul Hearn, Andrew Thomas, Nick Quinn and John Cook.

SOLAR EMISSIONS

Colin Briden has been making 28MHz recordings of solar radio emissions. These are not always directly related to larger solar flares, and he recorded a series of three type III emissions on August 30th. During that period, satellite X-ray data shows nothing stronger than B6, and SWPC timings do match well with his recordings. Equipment used included an Icom R70 receiver and a half-wave dipole aerial.

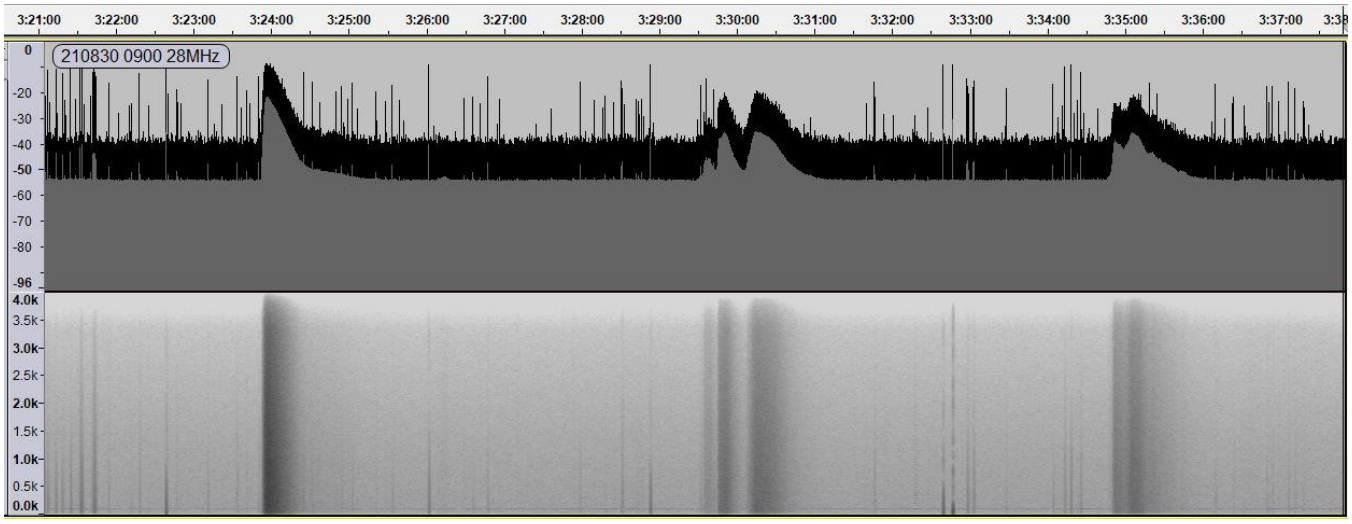

The first peak measures about 30dB above noise level, slightly lower for the others. Local interference can be a problem, but the signals here are quite strong.

PERSIED METEORS

August is of course the month for meteor watching, with the Perseid shower peaking around the 13th. This year there was the extra surprise of a further peak on the 14th. This chart of Perseid counts by Christopher Bailey compares activity in 2021 with 2020:

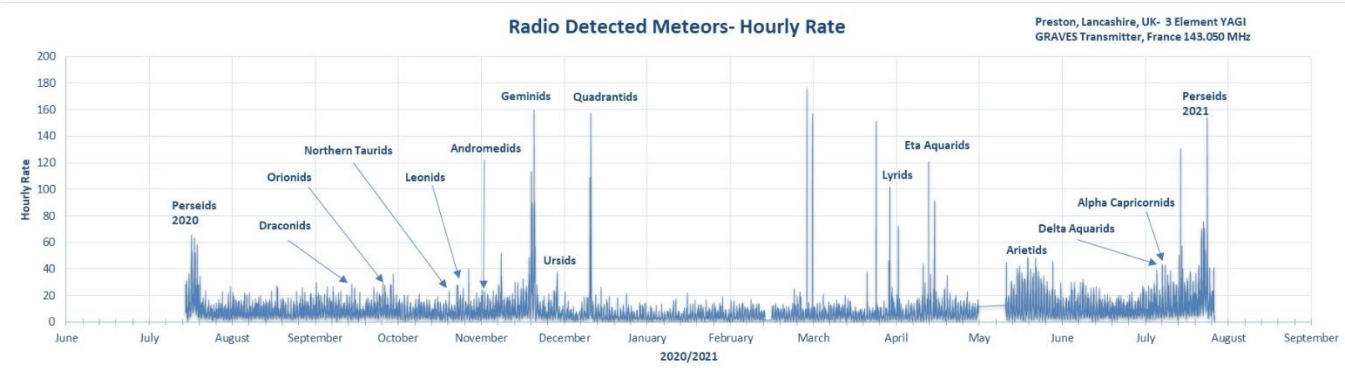

In 2020, activity levels on the 12th and 13th were very similar, with a lower count on the 14th. This year, the activity increased each day, with the morning of the 14th giving the highest counts. Each column on the chart covers a one hour period, showing the number of echos exceeding 10dB. Non-meteor echos have been removed as far as possible. Stuart Green made similar observations, with 30 minute intervals. The lower panel of rolling hourly rates shows the peak on the 14th very well:

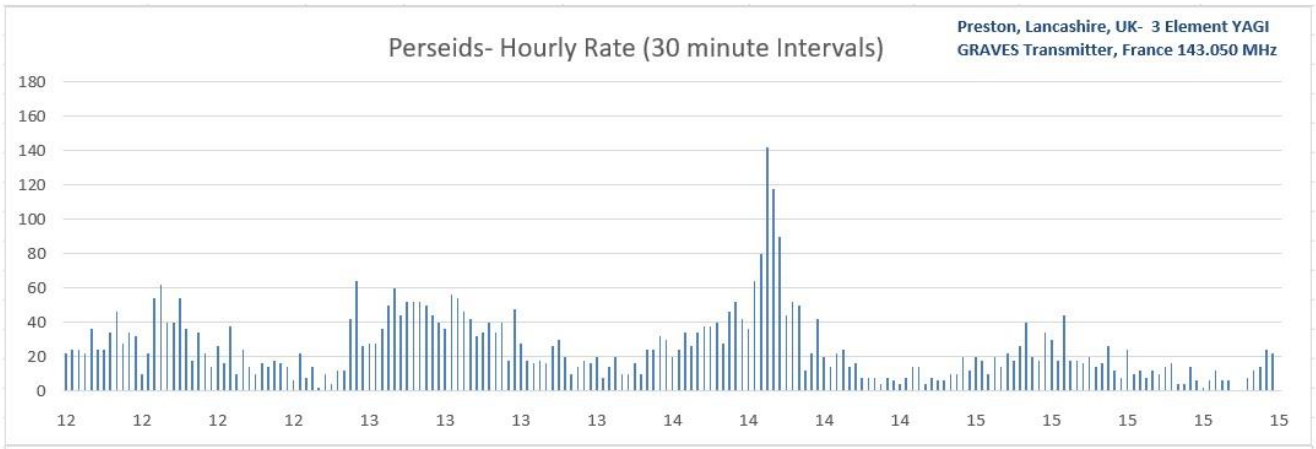

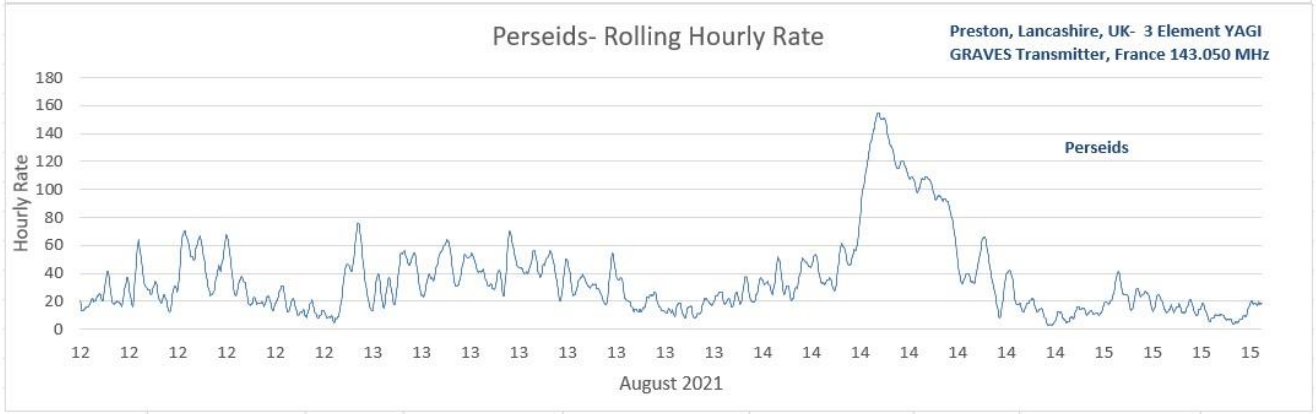

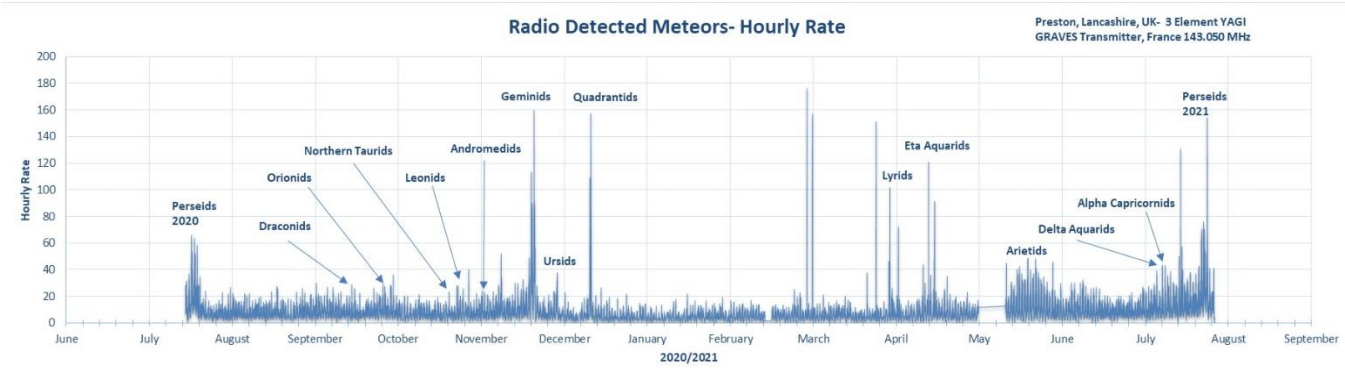

Stuart has also made a chart covering the last 12 months, starting with the 2020 Perseids. Most of the major showers show good peaks, but the 2020 Orionid and Leonid peaks are very weak. It will be interesting to see how they compare this year. Colin Clements also made Perseid counts with the GRAVES signal, covering the expected peak late on the 12th and into the morning of the 13th. Unfortunately the recording period did not cover the unexpected peak on the 14th.

VLF emissions from meteors have bee discussed before, and there is a paper by David Morgan covering this topic. Chris Bailey has been experimenting, and in a session in the morning of August 10th recorded 42 such signals. Two of these matched the timing of meteors caught on camera, and so could possibly be connected. A 25,000 turn coil was used as the aerial.

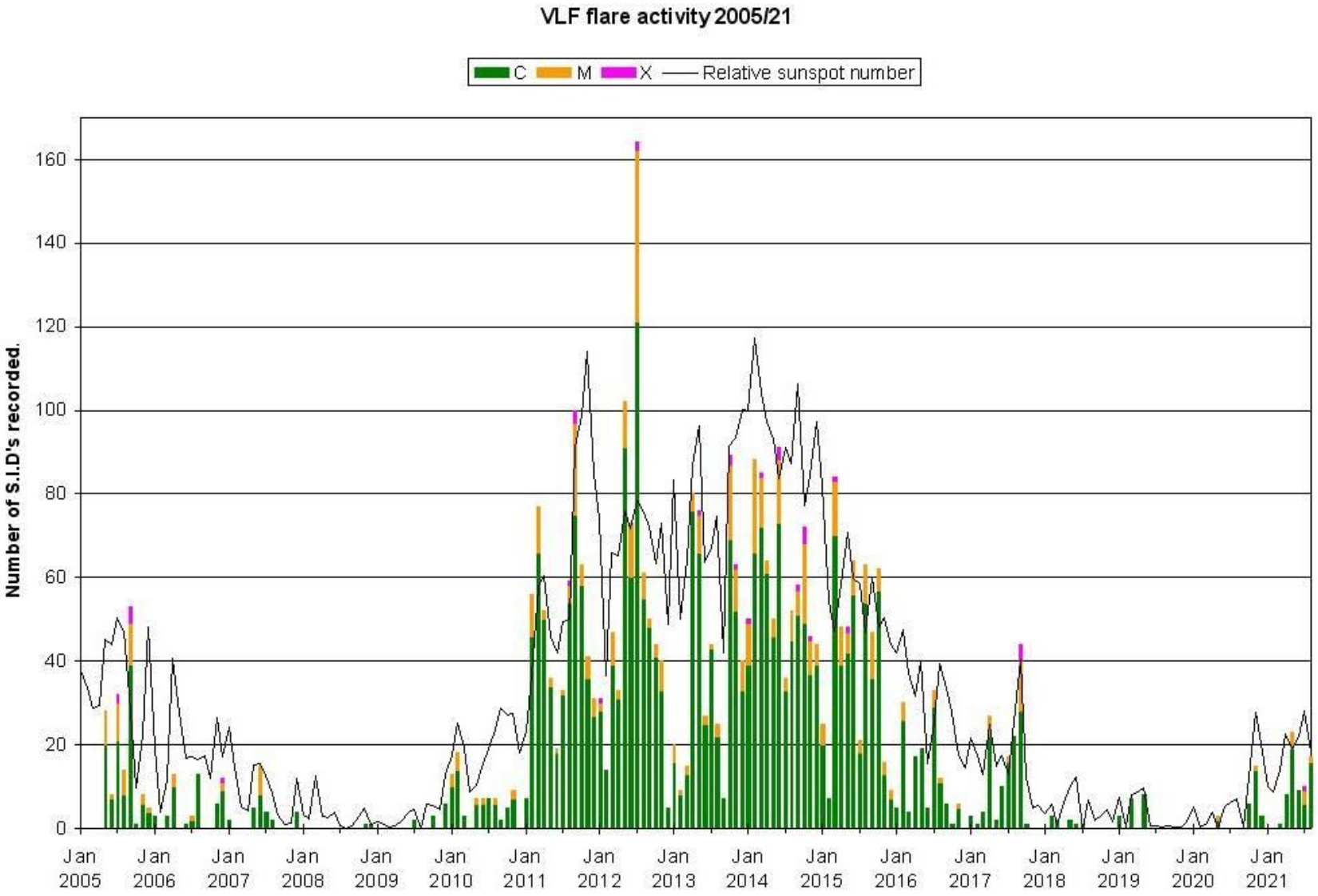
VLF flare activity 2005/21
C
M
X
Relative sunspot number
Number of S.I.D's recorded.
0
20
40
60
80
100
120
140
160
Jan 2005
Jan 2006
Jan 2007
Jan 2008
Jan 2009
Jan 2010
Jan 2011
Jan 2012
Jan 2013
Jan 2014
Jan 2015
Jan 2016
Jan 2017
Jan 2018
Jan 2019
Jan 2020
Jan 2021

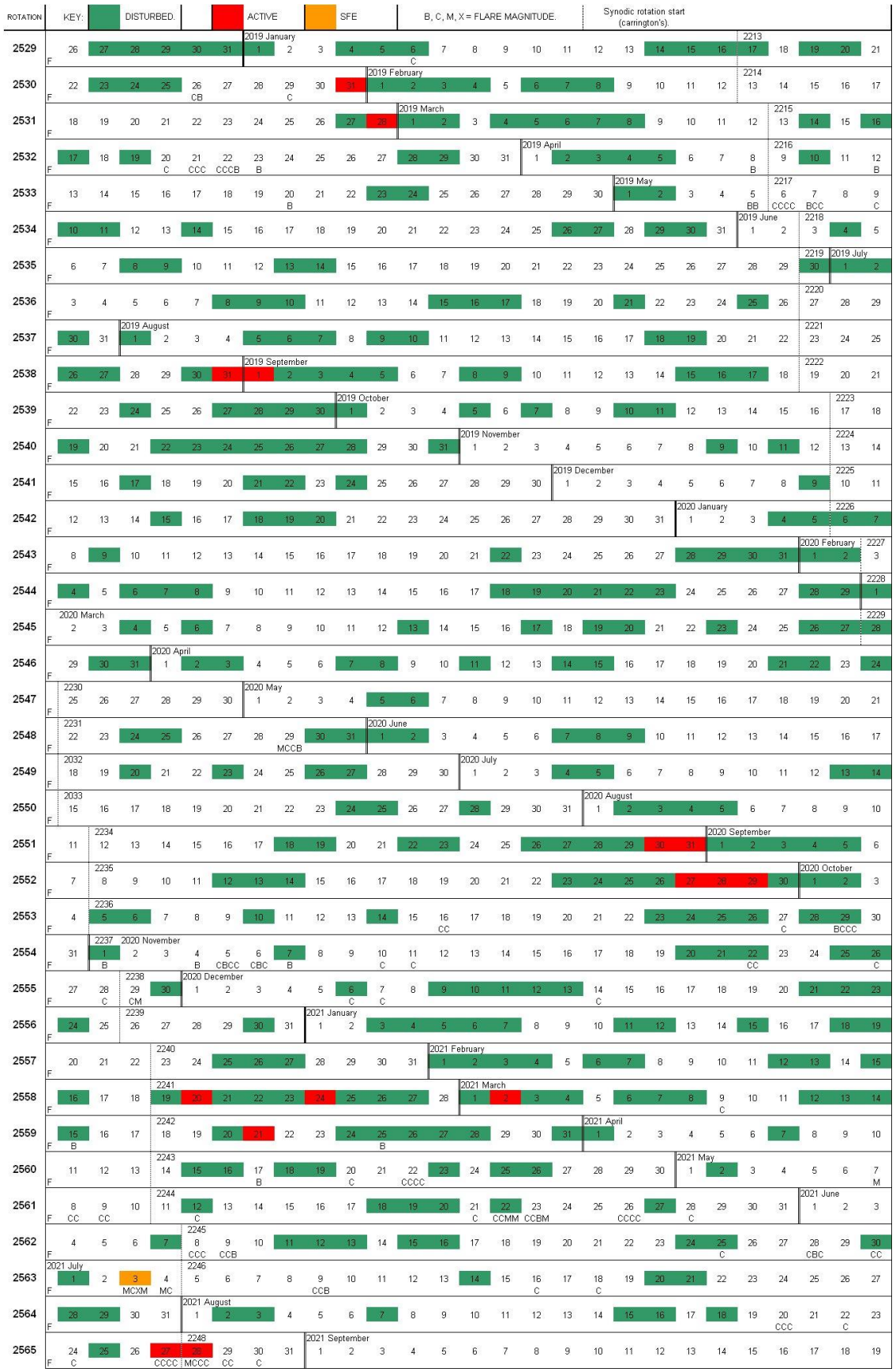
ROTATION
KEY:
DISTURBED.
ACTIVE
SFE
B, C, M, X = FLARE MAGNITUDE.
Synodic rotation start (carrington's).

British Astronomical Association
Supporting amateur astronomers since 1890
Radio Astronomy Section

BAA RA Section Winter programme 2022

Dec 10th 19:30 GMT (19:30 UTC)	Christmas Lecture	Prof. Anna Scaife. Professor of Radio Astronomy at the University of Manchester and Head of the Jodrell Bank Centre for Astrophysics **'Jodrell Bank, the cold war and the space race'**
Jan 7th 19:30 GMT (19:30 UTC)	Alexander Josephy	**'CHIME, Magnetars and Fast Radio Bursts'** Alex has done major foundational work both on CHIME and scientifically.
Jan 15th GNU II Training seminar 14:00 GMT (14:00 UTC)	Marcus Leach	**Unpacking more mysteries of GNU Radio** Canadian Centre for Experimental Radio Astronomy
Feb 4 th 19:30 GMT (19:30 UTC)	Chris Steyaert	**'VHF Meteor Observations, the IMO, and corelation'** Following the main presentation there will be opportunity for members to update us on their observations and techniques.
Mar 4 th 19:30 GMT (19:30 UTC) (This will be a joint session with the 'Arora and Clouds and Polar Mesosphere Summer Noctilucent Cloud' Section of the BAA.) Note: GMT to BST Sunday March 27th.	Dr David Hooper	**'Ice Crystals at the edge of space - Noctilucent Echoes'** David is a STEM ambassador working for the STFC at the Rutherford Appleton Laboratory. The main presentation will be followed by Sandra Brantingham, Noctilucent Section Director.
Apr 1st 19:30 BST (18:30 UTC)	Prof. Carole Mundell	**'…on Fast gamma ray bursts'** Carole Mundell is Professor of Extragalactic Astronomy at the University of Bath. She is an observational astrophysicist who researches cosmic black holes and gamma ray bursts.

If you have any suggestions for the summer 2022 term do let me know. Our meetings are open to all. Once you are registered on the RA Section email list the Zoom link will be sent out to you before the meeting. If you are not on the email list, please request registration from Paul Hearn (paul@hearn.org.uk).

All recordings will be posted on our BAA YouTube channel.
https://www.youtube.com/user/britishastronomical/playlists

Driven by substantial upgrades in recent years to existing facilities and the construction of new radio telescopes, the capabilities for low frequency radio science are greatly expanding. Significant progress is being made in high redshift 21-cm cosmology including the cosmic dawn and epoch of reionization, pulsar and transient science, and the understanding of planetary and exoplanetary magnetospheres, radio sky surveys, space weather, and solar physics. The Science at Low Frequencies (SALF) conference provides a forum for astronomers to share and discuss science results, techniques, and technologies, as well as to plan a coordinated path forward to future projects and facilities.

The format will feature 2-hour blocks distributed every 8 hours to allow most people in the world to participate in person in a somewhat favorable time zone. All talks will be recorded, so you can also peruse the presentations afterwards. There will also be a Slack channel dedicated to the meeting to encourage conversations to extend over the different time zones. An online social event will also be encouraged mid-way through the meeting. If you have any questions or comments, please email Joe Callingham (jcal@strw.leidenuniv.nl) and Jason Hessels (hessels@astron.nl).

Registration and abstract submission: To register and submit an abstract for a talk please fill in the following form: https://forms.gle/x1qsQy4nfsxsdACD6. Please note that abstracts will be assessed by the SOC with all identifying information removed. Therefore, please do not include details in your abstract that will unambiguously identify yourself.

We predict we will likely have a large over-subscription factor (SALFVII had a factor of 8 oversubscription rate). To alleviate that somewhat, everyone that submits an abstract for a talk will also be given the opportunity to present a 2-minute lightning talk. These lightning talks will be hosted on YouTube and were incredibly popular during SALFVII. Invited speakers will be sourced from the pool of successful talk abstracts, as opposed to being approached before abstract submission.

Key Dates:

- Abstract submission deadline: Friday October 8th, 2021
- Preliminary Schedule Announced: First week of November 2021
- Registration deadline: Friday December 3rd, 2021
- Conference period: Monday 6th to Thursday 9th of December, 2021

Registration Fee: There is no registration fee for the conference.

Science Organizing Committee:

- Rick Perley (NRAO)
- Natasha Hurley-Walker (Curtin)
- Jason Hessels (ASTRON/UvA)
- Joe Callingham (Leiden/ASTRON), Chair
- Monica Orienti (INAF)
- Poonam Chandra (NCRA)
- Tao An (SHAO)
- Nichole Barry (UMel)
- Ryan Lynch (GBO)
- Paul Scholz (UofT)

Local Organizing Committee:

- Jason Hessels (ASTRON/UvA)
- Joe Callingham (Leiden/ASTRON)
- Ralph Wijers (UvA)

Wednesday-Friday, December 1-3, 2021

The need for a high-performance solar radio telescope in the United States has been recognized for many years. The FASR (Frequency Agile Solar Radiotelescope) concept represents such a telescope, one that provides high-resolution imaging over a broad range of frequencies, sufficient to probe the solar atmosphere from the mid-chromosphere to the mid-corona, with high time and spectral resolution. EOVSA implemented many FASR design elements and, as such, has served as a valuable pathfinder instrument, spectacularly validating both the fundamental concept of time-resolved broadband imaging spectroscopy and the science it enables. In the meantime, science and technology have advanced and the need for full implementation of the FASR concept has only grown more important.

In anticipation of upcoming funding opportunities, this workshop is being convened to highlight progress in solar physics over the past decade and to take stock of the unique contributions enabled by the current suite of new radio instruments, to refine the science goals and requirements of a next-generation solar radio facility. The workshop will provide a forum to discuss relevant new and emerging technologies that will enable this new science. We invite colleagues with an interest in solar physics and radio technology to help explore the frontiers of science and technology that will guide updates and refinements to the FASR concept.

Registration: The FASR 2021 Workshop will be free, 100% online, and centered on US time zones.
There is no registration deadline, but if you want to contribute, please fill out the registration form by November 1st: https://forms.gle/TKcavxC4a7mVoPJP8

(If you are currently undecided about a contribution, you may register now, and re-register later with a contribution (but remember the November 1st cutoff.))

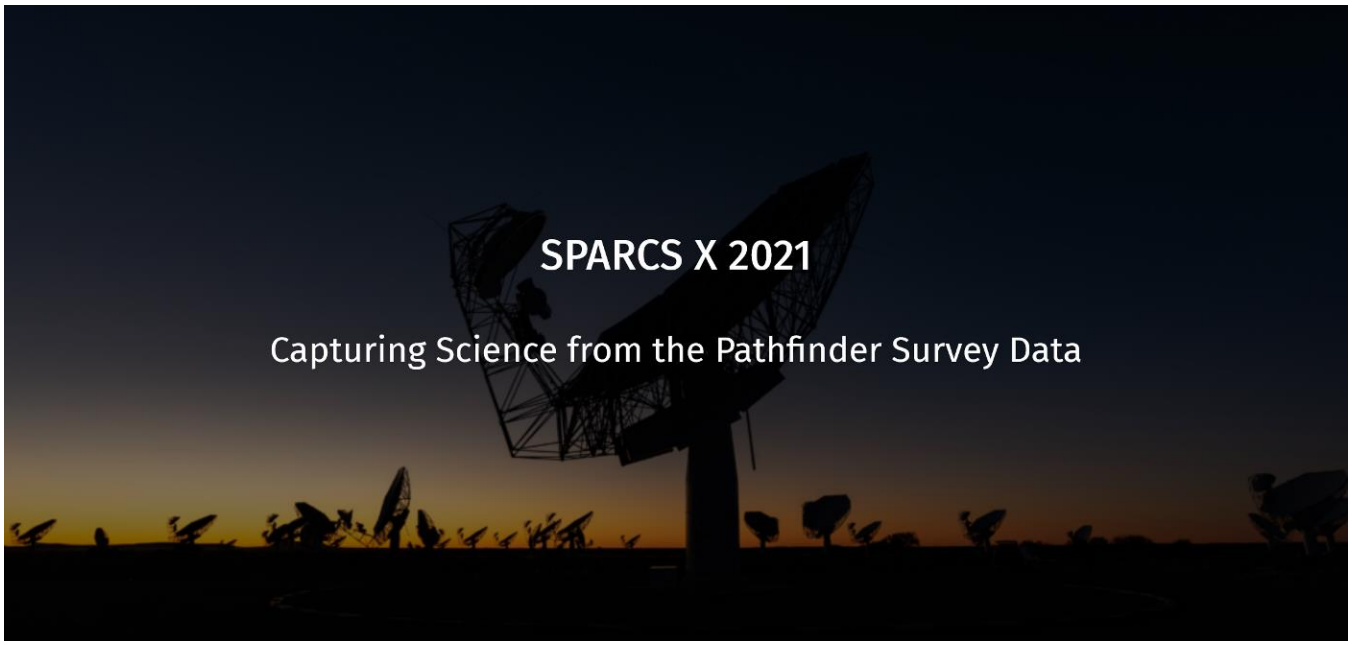

The 2021 meeting of the **SKA Pathfinders Radio Continuum Surveys** (SPARCS), entitled "Capturing Science from the Pathfinder Survey Data", will be held from 15-19 of November as a virtual meeting. The registration and abstract submission is open at https://www.idia.ac.za/sparcs-x-2021/

Priority deadline for talk submission has been extended until October 6th. Talks submitted after this deadline may be considered but talks cannot be guaranteed. Talks can be on scientific results (Galactic, extragalactic, Clusters, cosmology, etc) or more technical in nature. Registration (without a talk submission) will remain open after that date and there is no registration fee.

Details on the program and connection details will be updated on the webpage once available. The meeting format will be all online with zoom with 1 to 2 talk sessions per day, offset in time to accommodate different time zones. Please feel free to forward this message on to any relevant mailing lists or interested parties (apologies if you receive this more than once).

SPARCS Wiki: http://spacs.pbworks.com
SPARCS SLACK INVITE: https://join.slack.com/t/sparcs-team/shared_invite/zt-tj3rhbev-VZTOuROctIgxRzCWoFKcMg

2021 is an exciting time for continuum pathfinder surveys from the low frequency sky with the new release from the LOFAR Two-metre Sky Survey and the upcoming MWA GLEAMX to the mid frequencies with ASKAP's EMU starting a second pilot survey and MeerKAT results coming out (and a whole lot more). Science results are coming out now from many pathfinders. Developments from the many surveys and facilities continue to provide important scientific and technical direction for the next generation and due to the unfortunate global circumstances in 2020 with COVID-19 there was no SPARCS 2020 meeting. This means there will be so much for us to share and discuss this year.

Feature Articles

Development of a Telescope Tracking System

Jack H. Lobingier

Introduction

This article is the first in a series of articles describing the development of a tracking control system for my three meter antenna. This design does not use available rotators, but is more generalized to use almost any dc motor and gear train along with incremental digital encoders. First in this series will be the design of the altitude and azimuth position system, using incremental encoders. Figure 1 shows the Dish as it is currently installed.

Figure 1: 3m with Tracking System

Figure 1 is really the second dish and the third mount that I have built over the last number of years. This is partly because of redesign and partly because of hurricanes. I started by using the TVRO mount that came with the dish, but I quickly found out that, in my opinion, it was not suited for alt./az. positioning or tracking. This current design uses a four inch pipe, embedded in a ton of concrete. The top part of the mount is another pipe that is coaxial with the four inch pipe. This upper pipe is in turn coaxial with a large spur gear. Driving of this large gear is then done by another small spur gear driven by a 30:1 worm gear box, all connected to a 24 VDC right angle gear motor. Figure 2 is a picture of the setup. The altitude drive consists of a 30 inch linear actuator. This is also a 24VDC drive. This is shown in Figure 3.

Figure 2: Azimuth Drive

Figure 3: Altitude Drive

What is not shown in the above is the 2000 ppr digital inclinometer for the altitude axis and the 400 ppr encoder for the azimuth axis. These two encoders provide the 0.18 degree and 0.15 degree per pulse resolution for the altitude and azimuth axes, respectivly. In the case of the inclinometer, only 90 degrees of rotation is used, and on the azimuth the encoder is driven by a 6:1 pinion spur gear, off the main gear. I should point out that higher ppr encoders are now available to achieve a higher resolution, as needed.

Position Encoder and Local Display

This brings us to the subject of this article, the encoder readout, both local and that which is part of the position control system. Figure 4 is a block diagram of the encoder and position system, which is part of the overall tracking system. The encoders are brought into a quadrature decoder circuit that extracts both position pulses and direction pulses. These pulses are then up/down counted, and the resulting count represents the position. This part of of the system is supported by battery back-up for at least four hours with any loss of power, thus ensuring that there is no loss of position information. Position is then displayed by a small local readout and retransmitted over Ethernet into the tracking system computer and software in the house. The design of this system is such that both local and remote position display and control is available. Figure 5 is a close-up of the local position display.

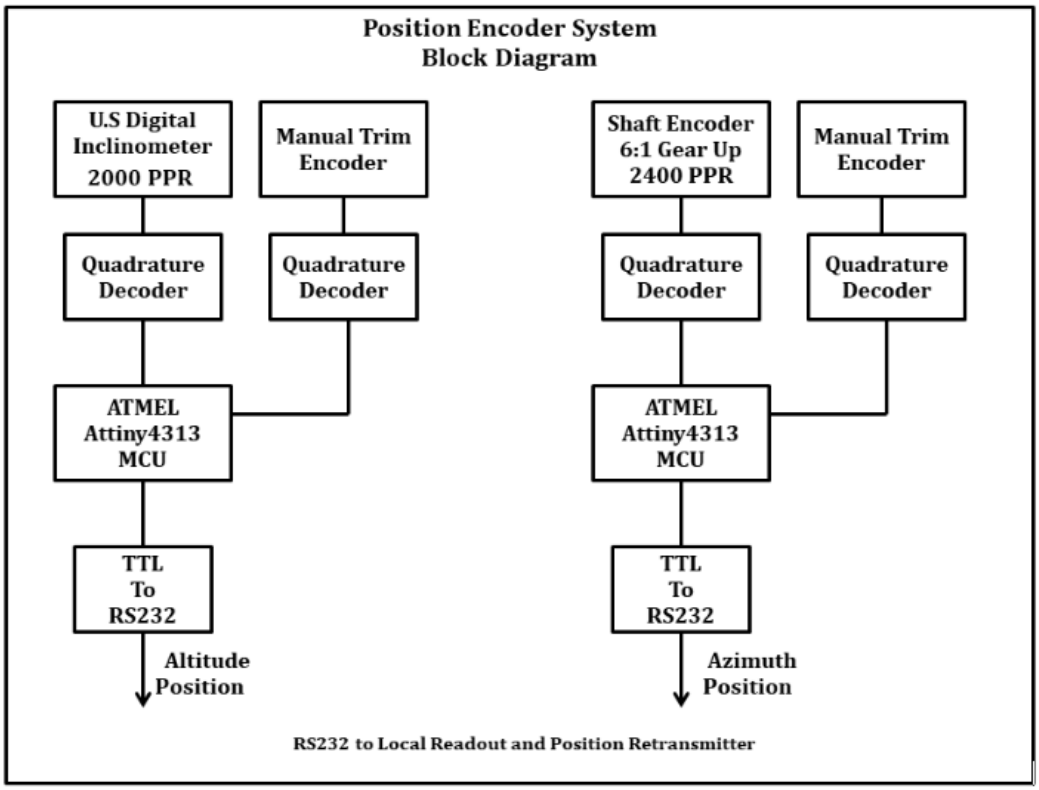

Figure 4: Position Encoder System and BBU

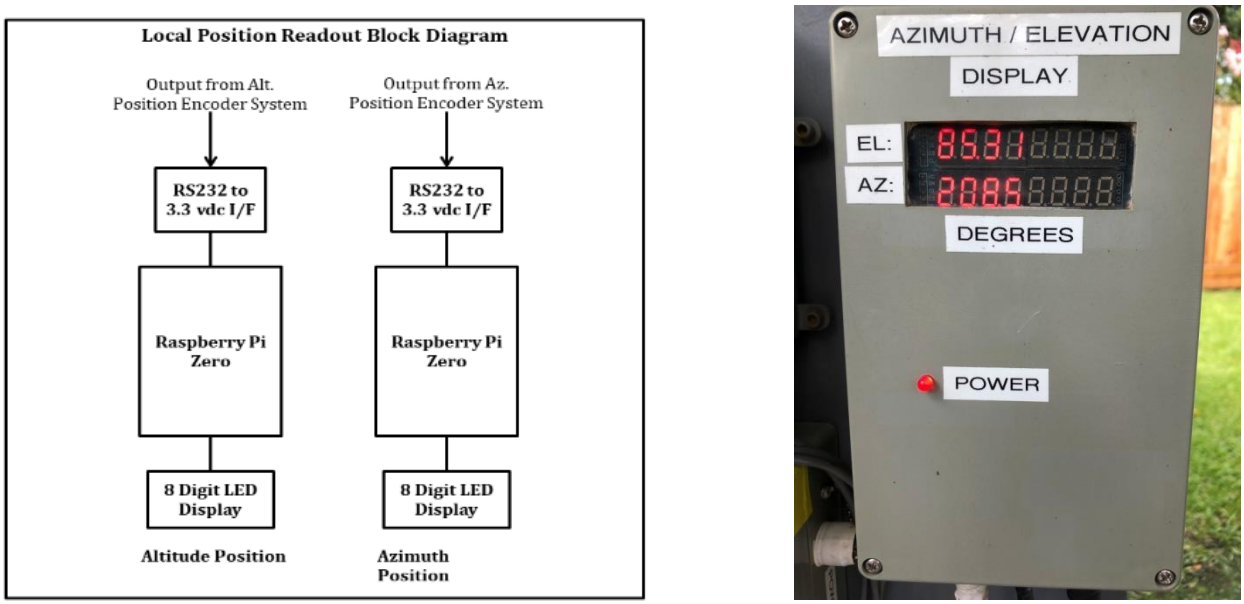

Figure 5: Local Position Display

Position Retransmitter System

So far, all of the position information is local to the antenna. For the overall positioning and tracking system to be integrated, that data needs to be communicated to the computer running the tracking program. The position retransmitter is basically a dual serial to Ethernet server that connects position data to the tracking program. Figure 6 is the current Position Retransmitter.

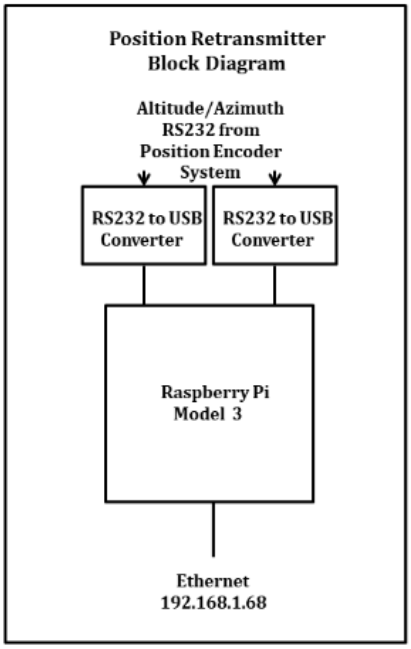

Figure 6: Position Retransmitter

Conclusion

As you might guess, this overall position system grew in stages. If I were building this now I would have most likely put all the functionality into a single box, and cut down on the number of processors that the current system uses. Also, the system needs to be enclosed in a metal box and grounded well, in addition to chokes on all signal lines. I am more than glad to provide the schematics of the sub-assemblies, and the model numbers of the major devices upon request. Having said all that, the system has been very reliable as it is currently configured.

Another feature of the positioning system is the ability to reference, or index, the position to a fixed point that is illuminated by a laser pointer. That pointer is fixed to the dish mount such that it moves with both altitude and azimuth. Once the position is known, say by pointing accurately at a source, the LED is turned on and displays a dot on the wall of my garage. That spot is marked, and can be used to set the positioning system, using the manual trim encoders, if positioning is lost.

Follow on articles will describe the local and remote motor drive and PWM motor control system, along with the Python software used for positioning and tracking. All of the remote parts communicate by TCP over Ethernet, on fiber.

About the author: The author has been interested in radio astronomy since about 1983. He worked as a Systems Consultant for Honeywell, and is now retired. His main interests are in the areas of hardware and software improvement moving towards lower system temperature along with Hydrogen line and Pulsar hunting. You can contact the author at 49jhanl@gmail.com.

Callisto and LWA Antenna Installation at HAARP, Gakona, Alaska

Whitham D. Reeve

A new radio telescope installation was completed at the HAARP facility near Gakona, Alaska in September 2021. In addition to a Long Wavelength Array (LWA) antenna, the installation consists of two Callisto radio spectrometers, a dual up-converter for observations in the HF and lower VHF ranges, LWA Power Coupler and supporting equipment and cabling. The system was installed at the Modular UHF Incoherent Scatter Radar (MUIR) site at 62° 23' 20.66" N, 145° 08' 15.65" W.

First light was achieved at 2302 UTC on 2 October, only two days after the installation was completed, by the reception of weak Type III fast-drift solar radio bursts (figure 1). At the time of the bursts, the Sun was 22° elevation and 204° True azimuth. Additional solar radio bursts were received before the end of the UTC day. The emissions also were received at higher frequencies on a similar system at the Cohoe Radio Observatory about 400 km to the southwest.

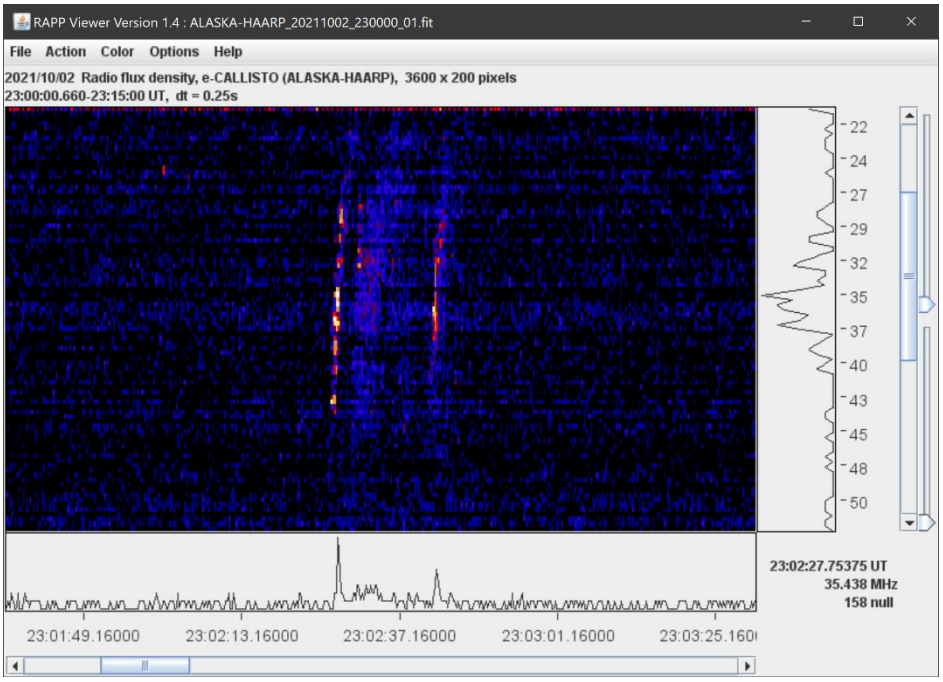

Figure 1 ~ First light! Dim but obvious Type III fast-drift radio bursts observed at 2302 on 2 October between 24 and 45 MHz. Additional radio bursts were received over the next couple hours. Frequency in MHz is shown on the right and time in UTC is along the bottom. The colors indicate relative intensity with black-blue being lower and red-yellow being higher. The text in the lower-right corner indicates the time, frequency and relative intensity of the cursor location when the image was taken (the cursor is not visible in these images).

According to the Space Weather Prediction Center's Events report {SWPC-EVNT}, the radio bursts at 2302 were simultaneously received at Palahua, HI, USA (PAL) and Learmonth, Australia (LEA), where they were classified as a relatively minor intensity Type VI burst. A Type VI consists of a series of Type III bursts over a period of 10 minutes or more with no period longer than 30 minutes without activity. Only a few Type III – components of the Type VI – were detected by the new installation at HAARP, probably due to the low elevation of the Sun and the weak nature of the bursts. See {SOLAR} for information on the types and characteristics of Type III, Type VI and other solar radio emissions.

The antenna (figure 2) and radio spectrometers (figure 3) replace a single Callisto that was previously installed and connected to the TCI-540 antenna about 2 km west-northwest {see (Reeve19}). The earlier installation was decommissioned in May 2021 when the TCI-540 antenna was converted for transmitter operation and subsequently used for some non-solar radio experiments.

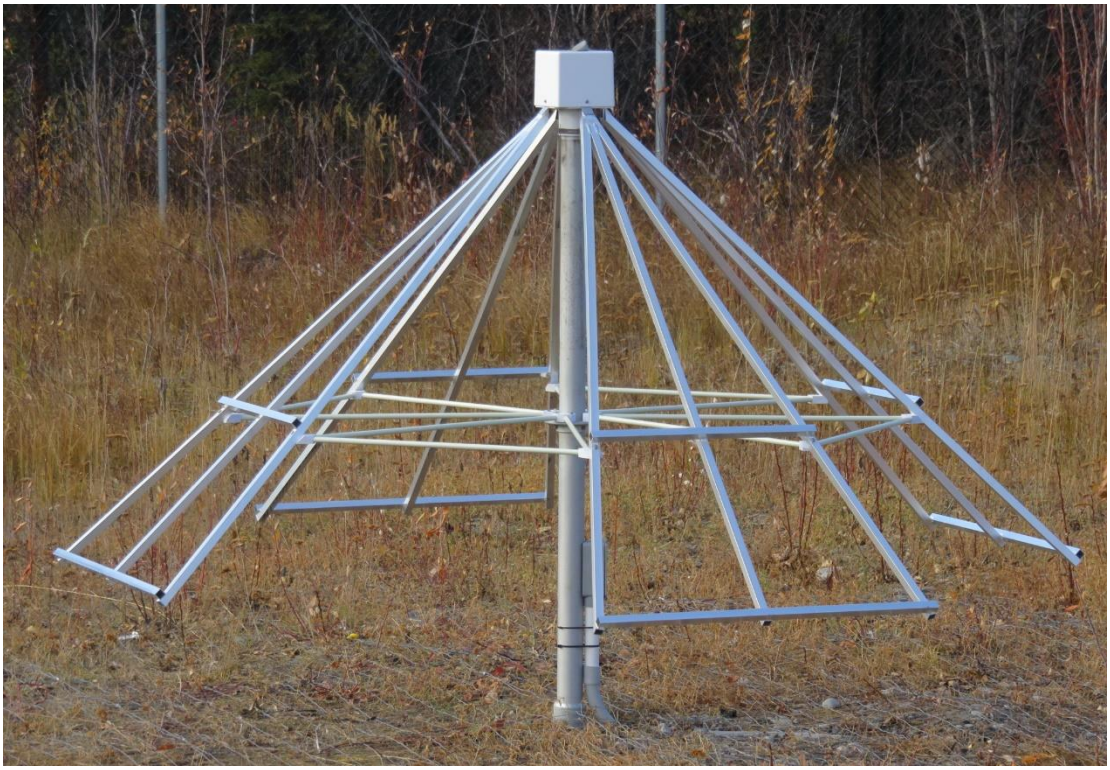

Figure 2 ~ LWA Antenna installed at the Modular UHF Incoherent Scatter Radar (MUIR) site on the HAARP facility. The antenna consists of aluminum, tied-fork, crossed-dipoles supported on a 1.5 m steel mast. Frequency range is approximately 10 to 100 MHz but is usable only to about 85 MHz because of FM broadcast station interference. Image © 2021 W. Reeve

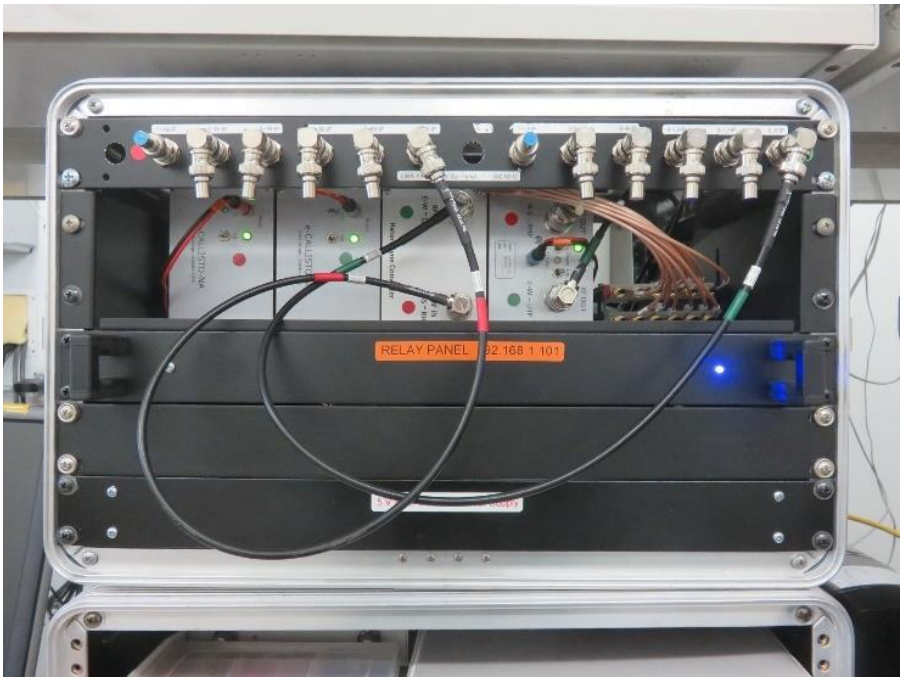

Figure 2 ~ All electronics were installed in an equipment cabinet (of the type used by musicians) and placed in the MUIR enclosure. The two Callistos are at the upper-left. Next to them, and in the middle, is the UPC-590L dual up-converter and to its right is the LWAPC-Q power coupler. The RF patch panel along the top of the cabinet is connected to two 6-port splitters on the far-right next to the LWAPC-Q. Immediately below is the LAN-controlled relay panel for remotely cycling the dc power to the Callistos. At the bottom of the cabinet are the 5, 12 and 15 Vdc power supplies. Not shown are the PC, LAN/WAN components and Uninterruptible Power System.

An LWA Antenna installation was planned prior to converting the TCI-540 antenna but its installation was temporarily stalled until a new site could be found. A survey of potential new sites was completed in May 2021 with selection of the MUIR site and associated heated-cooled equipment enclosure (figure 4). Installation of the LWA Antenna was completed in early September and required only a couple days for site preparation and installation. All electronic equipment was preinstalled in a cabinet and tested in Anchorage before deployment.

Figure 3 ~ MUIR equipment enclosure and associated radar antenna array (left-background). All electronics for the Callisto-LWA Antenna installation were placed in the enclosure at the end of September. A protected coaxial cable entrance facility was installed on the back of the enclosure (not visible in this picture). This picture was taken the day before the weather station and lightning sensor was installed on the enclosure. Image © 2021 W. Reeve

A block diagram of the new installation shows the RF components (figure 4). The two crossed-dipole antenna polarizations are connected through 6-port splitters to an RF patch panel that allows connection of the up-converters and Callistos as well as other receivers. Power is provided to the LWA Antenna Front-End Electronics (FEE) by an LWA Power Coupler with Quadrature Coupler (LWAPC-Q). The quadrature coupler provides right-hand and left-hand circular polarized outputs from the LWA Antenna's linear polarized dipoles.

The Callisto instruments have an instantaneous bandwidth of approximately 300 kHz and an integration time of 1 ms. The Callisto software collects data as Flexible Image Transport System (FITS) files, which are stored locally. The files also are uploaded automatically to Fachhochschule Nordwestschweiz (FHNW) University of Applied Sciences & Arts website for permanent archiving. Data from the HAARP Callisto installation as well as other stations within the e-CALLISTO network are located at {e-CALLISTO}. Callisto data uploads and local archiving are controlled by System Scheduler software using an FTP script developed by Christian Monstein.

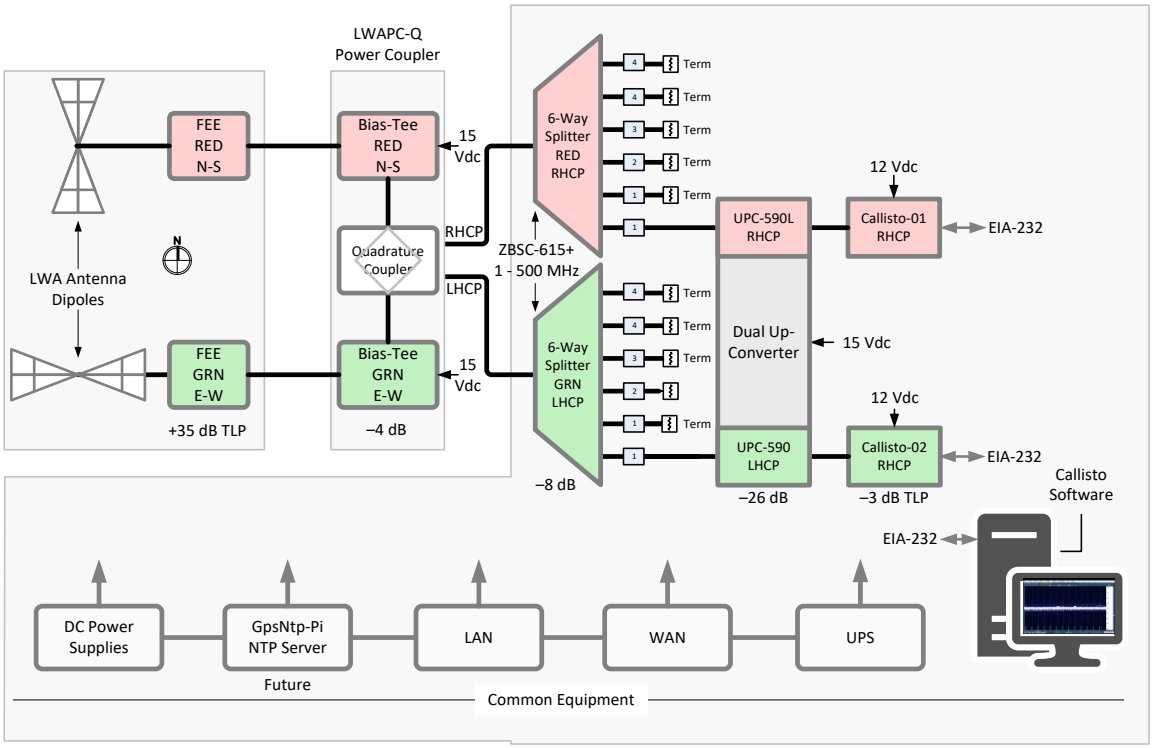

Figure 4 ~ System block diagram shows the components associated with the LWA Antenna and Callisto instruments and the common equipment shared across the observatory. Polarizations are color-coded: Red, RHCP; Green, LHCP. To offset the high gain of the LWA Antenna FEE, the up-converter has an internal 20 dB attenuator in each channel to provides an overall conversion loss of 26 dB. The splitter and quadrature coupler losses add up to 12 dB, resulting in a Transmission Level Point (TLP) at the Callisto RF input of –3 dB. Image © 2021 W. Reeve

References & Weblinks:

{e-CALLISTO} http://soleil.i4ds.ch/solarradio/callistoQuicklooks/

{Reeve19} Reeve, W., New Radio Observatory Established at HAARP in Gakona, Alaska, 2019, available at: https://www.reeve.com/Documents/Articles%20Papers/Reeve_HAARP-System.pdf

{SOLAR} http://www.reeve.com/Solar/Solar.htm

{SWPC-EVNT} ftp://ftp.swpc.noaa.gov/pub/indices/events/

2021-08-07 DSES Open House Trip Report

Bill Miller

Open House Attendance. Sorry if I missed any others.

Current Members

Myron Babcock, Co. Springs
James Burnet, Co. Springs
Floyd Glick, Co. Springs
Dan Layne, Col. Springs
Bill Miller, Co. Springs
Rich Russel, Co. Springs
Marc Slover, Denver
Ray Uberecken, Co. Springs

Interested Visiting Parties:

Vince Bradshaw, Lakewood
Jayson Quilantan, La Junta Arthur
W. Roos Jr., La Junta

Time Lapse Star Trails with Dish, "Skyfall" Photo by Marc Slover

Most of the current members arrived on Friday Afternoon. The temperature at 3PM was 103 Deg. on Friday and didn't cool off until after midnight.
Rich Russel got to the site Friday morning and finished mowing the RV park. This made it much easier to pull the RVs in and set up camp that night. Rich brought all of his equipment including Telescope, 850MHz Interferometer, Itty Bitty Radio Telescope, Optical Telescope and Mini 1420 MH Scope in a Box. The thick smoke, wind and light attendance made it difficult or nonproductive to set most of this up, so the majority of the observations and science were conducted from the Comm. Trailer.
We had 4 RVs plugged into the 20 AMP 120 Volt RV circuits but those are not enough to run the air conditioners so keep that in mind when camping on site. The power did allow fans, microwaves, and refrigerators to work and was a great convenience to all the RVers. Ed Corn installed the breakers for these in the outhouse and they should be turned off when not in use.

Each morning Bill set up a coffee pot outside the trailer to keep us going. Bill also bought and put out 28 solar yard lights so we could see our way around obstacles in the dark.
Rich and Dan set up the equipment and computers to hunt Pulsars on the installed 1420MHz feed. On previous trips they had problems with accurate pointing and receiver settings and had not been able to acquire and pulsars

on 1420. Glenn Davis, Dan Layne and Phil Gage and others had made several calibrations runs in the last several months to solve the pointing error of ~3.5 deg Azimuth and in the last several trips, they fixed it in the software along with other enhancements. During this weekend the pointing/tracking system worked almost flawlessly.

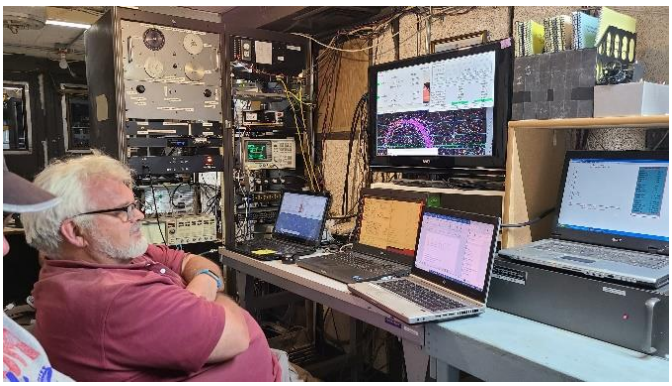

Dan Layne had been experimenting with the B210 Receiver and had found suitable pulsar settings for the 1420 feed system. On Saturday afternoon he started receiving pulsars starting at the top of the signal strength list and bagged 4 by about 10PM. One of these had not been captured on previous 408MHz runs so added to our list of 14 Pulsars so far. This was the first time that pulsars have been detected on 1420 MHz This was done using the new supercomputer provided by Don Latham. Rich and Dan had a competition going about who could receive the most in a single day. Rich had previously bagged 5.

Myron Set up a VHF/UHF Satellite communication system with a Yaesu F736R and two Eggbeater antennas on the Comm Trailer and proceeded to work contacts through the AMSATs. Myron also brought out his new DJI Mavic Mini 2 drone and flew it around the site for about an hour. We can't wait to see the video footage from this.

Ray setup a Flex Radio on the Jupiter dipole antennas and attempted to capture the Jupiter/Io emissions with the RadioSkyPipe and Radio Jove prediction SW. Later Arthur W. Roos Jr. of La Junta brought in his Radio Jove receiver. Bill calibrated it with a reference generator and the Radio Jove calibrator from Rich. Arthur left it with us to use and experiment with until we can fix the old one or get a replacement.

Marc Slover and Vince Bradshaw came down from Denver and set up a number of cameras for time lapse videos. Marc has designed and built his own unique articulated slow moving time lapse camera mount that yields excellent camera position and movement effects.

Marc has posted several of his time lapse videos of the dish on his You Tube channel: Road Trip Ventures at: https://www.youtube.com/channel/UC7xe59SBEdWErd25TZ1Ffkw/videos .

We had some time to set back under the canopies and reflect on the dish, the site and the science of Radio Astronomy and Ham radio. On Saturday night the smoke and wind were too great to cook outdoors so Myron took the cookout to the underground/bunker. He provided hot dogs, beans, potato salad, macaroni salad, watermelon, cake, and lemon aid. After a hot and tiring day, this was very well received and satisfying.

During the weekend Bill and Myron did some more cleanup work on the bunker and installed a 2 inch exhaust pipe out to the surface to exhaust the vacuum for cleaning. This is a great add to allow vacuuming out the bunker without breathing the dust it exhausts inside. The pipe is capped on the outside with a bean can to keep the rain out when not in use. Be sure to remove and replace this can when using the vacuum to clean the bunker.

In previous trips Bob Haggart and Bill discussed various methods of removing the tumble weeks from the bunker ramp including borrowing a chipper/shredder from Bob Sayers. This didn't work so they thought about using a pitchfork to load the weeds onto the tarp then wrapping it up with the rope and dragging it up the ramp to dump away from the bunker. This was far easier than pitching the weeds over the ramp walls as had previously been done. Dan Layne came down about halfway through this exercise and helped shovel weeds. It took only 6 tarps full and two hours to clear the ramp of weeds. (see this video of the tumble weed monster). https://www.dropbox.com/s/k7ar75g0940fcar/20210717_102614.mp4?dl=0

On the previous Monday Bob Haggart met Bill and Myron at Home Depot and we purchased a pallet of Cinder blocks and mortar. Bob hauled them down to Haswell with his trailer and Bill added a tier to the cinderblock wall to stop the mud flow over it. Myron loosened and piled up the mud that had flowed into the ramp.

On the open house trip Jim Burnet helped Myron and Bill shovel the dried mud into his truck and it took four partial loads and a number of wheel borrow loads that Myron single handedly pushed up the ramp to clear most of the mud from the ramp. Thanks to Jim and Myron for this hard work!

The ramp is now clear but will require several more tiers of cinder blocks and biannual maintenance to remove the tumble weeds and keep the mud out of the bunker sump pumps and hallway.

Additional housekeeping during the open house included: Jim bought some fly traps on his side trip to Las Animas. Myron cleaned out a lot of the old, expired food and junk and did many cleaning activities in the bunker. Bill emptied the bunker portable toilet, took out the trash and ran the magnet roller up and down the road and parking area collecting about 2 lbs. for nails and metals.

Overall, everyone learned a lot. We got a lot done, had some good observations, and great comradery even if attendance was light and the heat and smoke was heavy. We hope to have many more observing trips and sponsor a much larger public open house after the pandemic next year.

End of trip report.

Radio Astronomy: Meteor Detection

by Job Geheniau (jobgeheniau@gmail.com)

A meteor itself cannot be recorded by radio, but you can record the so-called ionisation trail left by a meteor. In France, there is the Graves transmitter.

This military transmitter has a power of more than 400 KW and sends out a specific carrier wave. The reflected signal can be received with an antenna and a RTL-SDR. Also in The Hague, where I live, despite of a lot of rfi here.

By the way in Belgium are also 2 beacons (at Ieper and (BRAMS/Dourbes) at the 6 meter band (49.97 MHz), which I also can receive with my second 6 meter band Yagi.

GRAVES

Great Network Adapted for Space Surveillance

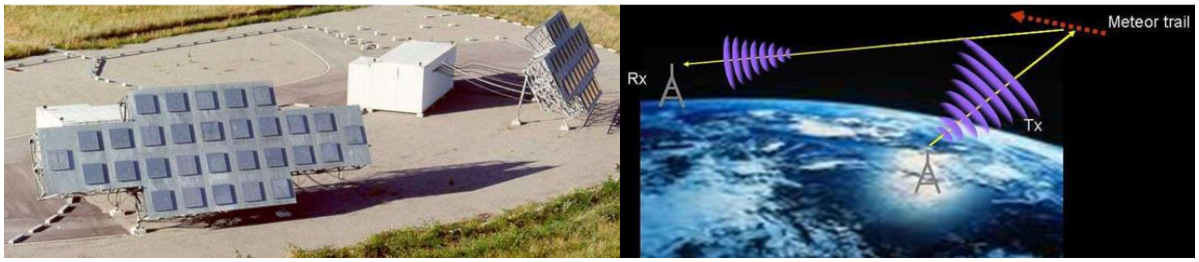

The antenna used is a 2 meter band antenna to receive Graves (143.05 MHz), in this case a 4 element Yagi under an angle of 15 degrees to the South.

The receiver is a RTL-SDR USB dongle. I do not use a lna (Low Noise Amplifier).

The software is CubicSDR for the Mac or SDR-Radio for the PC. These programs generate an audio signal of the offered sdr signal. This audio signal is sent to the application Speclab, a spectrum analysis program for the PC which runs fine on a Macintosh under Wine (a kind of simulation application).

The receiver software (CubicSDR) is set to USB (Upper Side Band).

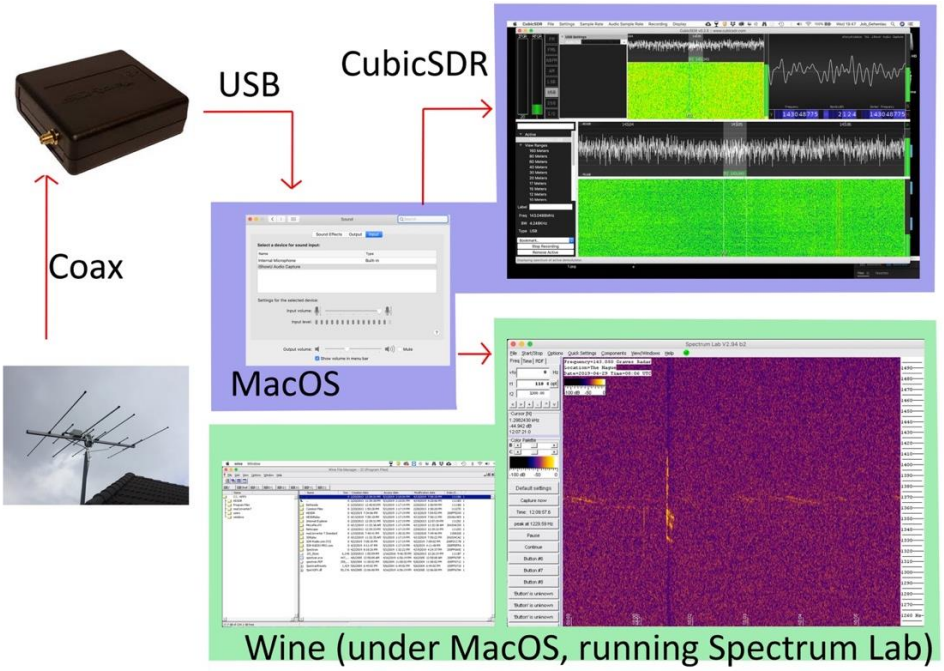

What you will eventually see in Speclab is a so-called 'waterfall', a slowly scrolling screen in which the detected frequencies have been made visible by means of Fast Fourier Transform (FFT). Because the meteor leaves an ionisation trail, there is a Doppler effect (changing tone) in the spectrum, both audible and visible!

The Graves transmitter generates a thin line around 1500 HZ in Speclab. The frequency range I set in Speclab is from 1200 Hz to 1600 Hz.

Meteors are short lines perpendicular to the Graves line, or more visible as a large spot, so called overdense ionisation clouds, which often linger for seconds. Slanting lines are often aircraft, sometimes satellites or very occasionally the ISS if you are lucky. The transmitter is so powerful that an Earth Moon Earth detection can often be seen. A horizontal line visible as separate pulses (Graves transmits in pulses).
With Speclab I also used a technique to count meteors. Speclab can have a plotter running along. In this plotter you script the various frequencies with a minimum and a maximum set sound intensity (dB). When a meteor is detected, it will show a vertical line on the plotter depending on the strength of the signal.

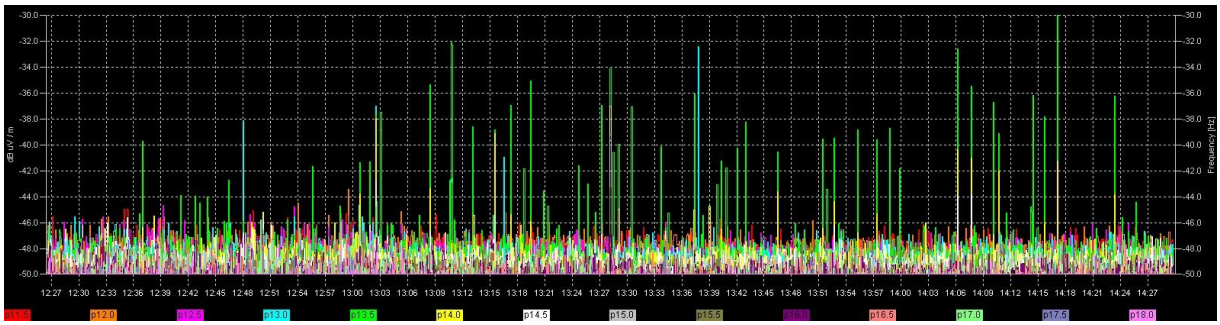

Finally, some results. During the Perseids of 2021, I ran the equipment for 4 weeks. Speclab captures a screenshot every 6 minutes and CubicSDR a WAV audio file every 20 minutes. (300 GByte in total)

On the links below, the complete recording of 4 weeks can be seen as a 10 minutes video. There is also a link to an audio file in which you can clearly hear the meteor.

For some more info/results:
https://jgeheniau.wixsite.com/radioastronomy/radio-astronomy

4 weeks of meteors during Perseids (17 july – 15 August)
https://youtu.be/VQyxxQmvaiI

audio:
https://jgeheniau.wixsite.com/radioastronomy/copy-of-nice-overdense

2 big dense clouds (the small vertical lines are very small meteors):
Horizontal the time, vertical the frequency.

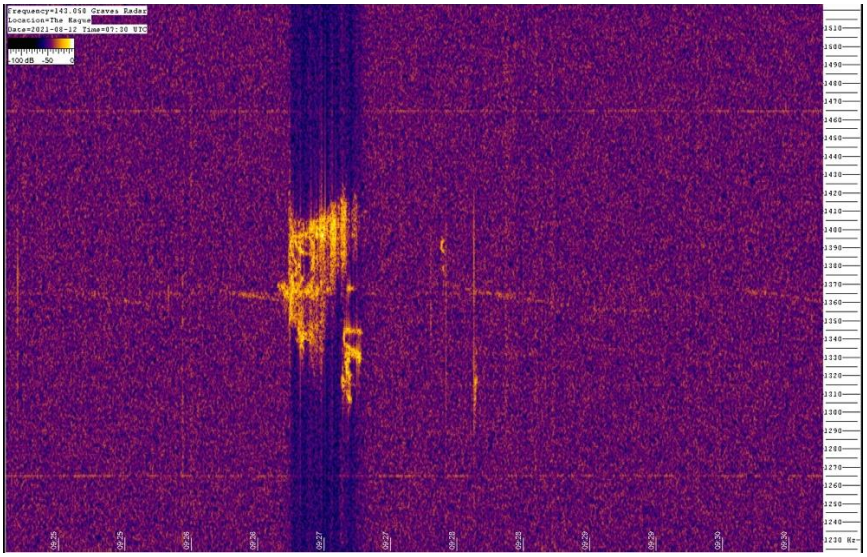

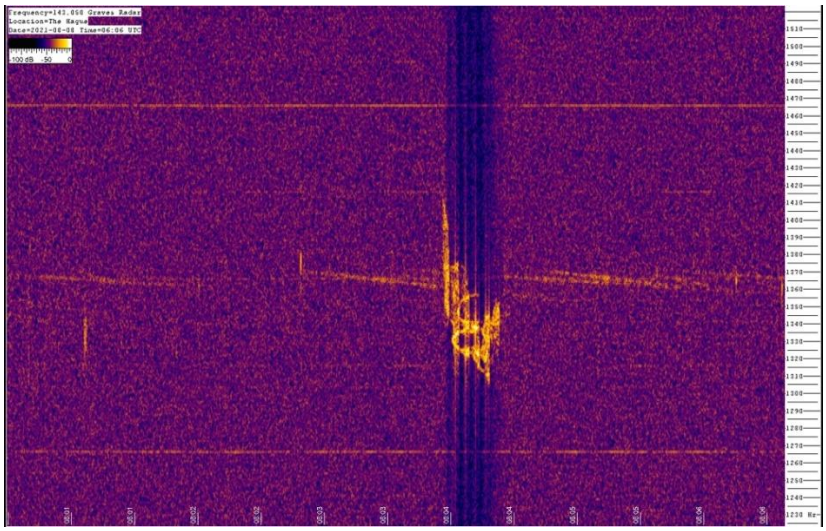

Moonbounce (the horizontal dotted line, not completely horizontal, because the moon moves! So doppler here also):

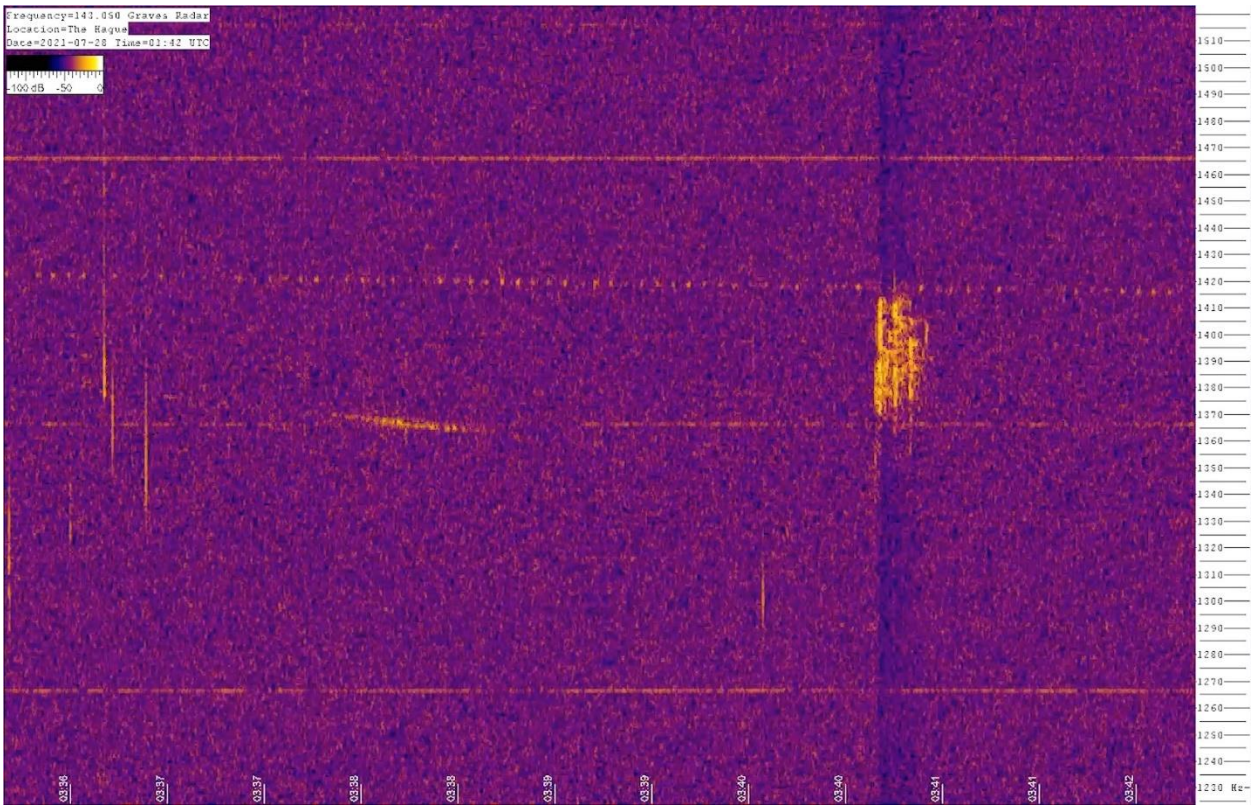

SpaceX satellites (which I don’t like as an amateur astronomer):

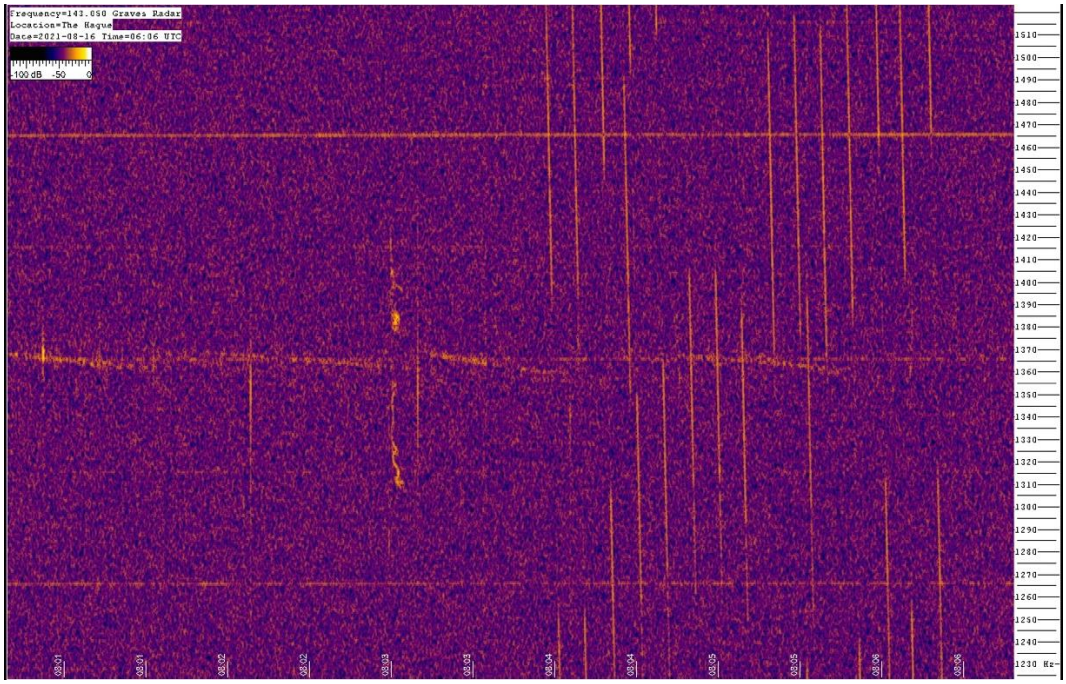

Summary of Geomagnetic Effects Observed During a Solar Cycle

Whitham D. Reeve

1. Introduction

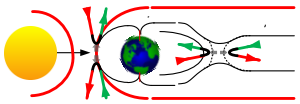

A recent article showed the types and characteristics of solar radio emissions that might be detected throughout a solar cycle {Reeve21}. In addition to the radio phenomena received at Earth, geomagnetic effects and disturbances may be observed. These result from the interaction of Earth's magnetic field with the interplanetary magnetic field (IMF) and solar wind, both of which are controlled by the Sun. An indicator of solar activity is the number of sunspots. Sunspots follow a cyclic pattern lasting about 11 years from minimum at the beginning through maximum to minimum at the end when the Sun's magnetic field polarity reverses and the next cycle starts. Solar cycle 25 started December 2019. For a regularly updated plot that shows the progress of the solar cycle, see {NOAA25}.

Geomagnetic disturbances are initiated by solar phenomena. The major causes are flares, coronal mass ejections (CME), coronal hole high-speed streams (CHHSS), corotating interaction regions (CIR), and solar sector boundary crossings (SSBC). Because of relatively long travel times, magnetic observations on Earth may be delayed from hours to days or weeks with respect to a particular event at the Sun; however, strong solar flares can have an almost immediate effect on the geomagnetic field because flare x-ray radiation, which induces the disturbance, propagates at light-speed.

Solar activities, such as sunspots and coronal holes, that persist for more than one solar rotation cause recurring geomagnetic effects at about 27-day intervals. Some geomagnetic activity has no obvious source but is interesting nonetheless. Even time periods when Earth's magnetic field is very quiet are interesting, especially at higher latitudes because they are so rare (figure 1). Very quiet days, when the K-index was zero for a full 24 hours, have been recorded only twice at Anchorage in 11 years of observations of solar cycle 24 by the SAM-III magnetometer.

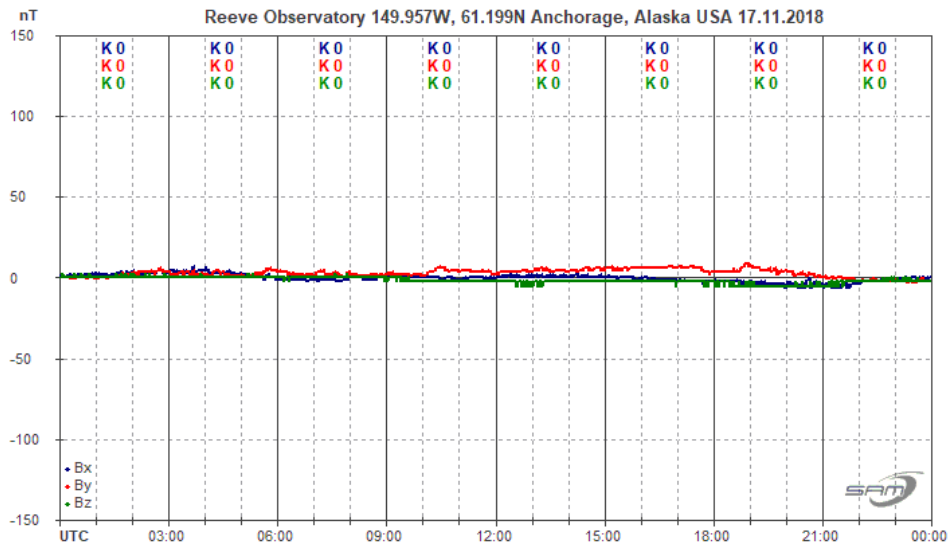

Figure 1 ~ Very rare magnetically quiet day near the end of solar cycle 24 was observed at Anchorage, Alaska on 17 November 2018 with the SAM-III magnetometer. All magnetic components indicate a K-index of zero in each of the eight 3-hour synoptic periods. The system sensors are oriented according to the geographical coordinate system and measure Bx (blue, north-south), By (red, east-west) and Bz (green, vertical).

This article briefly describes each of the phenomena listed above and their geomagnetic effects. All are illustrated through solar images and magnetograms from solar cycle 24, which began December 2008 and ended December

2019. The magnetograms were produced by the SAM-III magnetometer at Anchorage, Alaska, 61.7° north latitude {SAM-III}. All solar images were obtained from NASA. Readers interested in the general topic of geomagnetism may find the tutorial at {Reeve15} useful.

Many government agencies use data from ground magnetometers in *space weather* prediction and research. The Space Weather Prediction Center (SWPC) in the USA provides a lot of free information called *products* and *data* that are useful for correlating with local geomagnetic observations. SWPC regularly produces dozens of reports, observations, models and data summaries related to space weather. Good places to start are the Space Weather Dashboard {DSHBD} and the Products and Data tab on that webpage. Other countries provide similar space weather services, including Australia {SWS} and European Space Agency Space Weather Service Network (ESASWSN). These agencies generally are collaborative with SPWC but tailor their reports and products to their geographic regions.

---

2. Phenomena

Flare: A solar flare is a huge explosive event on the Sun's surface resulting from magnetic instabilities associated with sunspots (figure 2). A flare can last from minutes to hours. The sudden release of magnetic energy causes an intense burst of electromagnetic radiation over an extremely wide frequency range. Particles – electrons, protons, and heavier particles – are accelerated by a flare and, if *geoeffective*, can lead to a number of effects. Geoeffective means the particles are moving in such a way that Earth intercepts them as they travel outward from the Sun. Flares and related phenomena are most common near the peak of a solar cycle when sunspot numbers are high but are unpredictable and may occur any time, even at solar minimum.

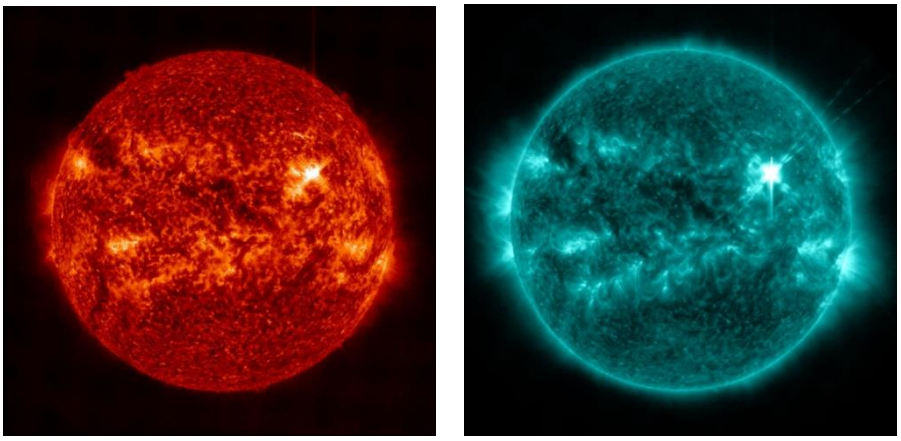

Figure 2 ~ X1.0 solar flare imaged at 30.4 nm (left) and 13.1 nm (right) wavelengths on March 29, 2014. The flare is the bright area on the right above the equator. The 30.4 nm wavelength shows the region between the chromosphere and corona, and 13.1 nm wavelength shows material with a temperature of 10 million kelvin. This flare produced a magnetic crochet described below. Image source: NASA/SDO

The x-ray radiation from a flare propagates at light-speed and reaches Earth after a little more than 8 minutes. When detected, the times of solar events are reported with respect to *Coordinated Universal Time* (UTC). If a part of the flare has a very sudden optical brightness increase (within about 1 minute), it is called an *impulsive flare*. If it also is very strong, the associated x-ray radiation quickly increases the ionization and, thus, the electrical conductivity in the D- and E-regions of Earth's ionosphere. The increased conductivity leads to increased electric currents in the electrojets, which, in turn, produce a sharp change in the magnetic field measured on the ground. As the flare tapers off and the burst of radiation subsides, the ionosphere, electric currents and magnetic field return to their preflare conditions.

When such an event occurs, a real-time trace of the magnetic field measured on the ground has the shape of a crochet hook used for knitting. Thus, the trace on a magnetogram is called a *magnetic crochet*, but its more formal name is *Solar Flare Effect*, or SFE. Magnetic crochets are rare and usually are observed only on Earth's dayside. Locations where the Sun is directly overhead at the time of the flare have the highest likelihood of observing a magnetic crochet when it occurs, but other locations are possible. For example, a weak magnetic crochet produced by the X1.0 flare shown above was observed at Anchorage, Alaska about 4 hours before solar transit (figure 3).

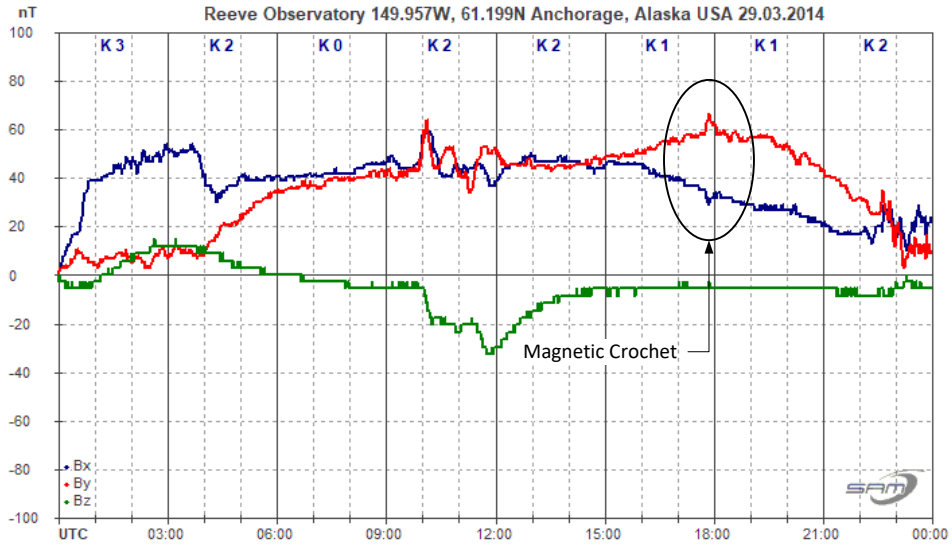

Figure 3 ~ Normalized magnetogram showing measurements at Anchorage, Alaska for the 24 h period on 29 March 2014 near the peak of solar cycle 24. An X1.0 solar flare caused a rare magnetic crochet, which is circled and indicated by the black arrow in Bx and By at 1748 UTC (9:48 am local). This crochet was observed only 2 hours after local sunrise and 4 hours before solar transit. In addition to this crochet, the flare produced numerous radio emissions and an HF radio blackout. The trace colors are as in the previous magnetogram and shown in the lower-left corner. This and subsequent magnetograms have the K-index for each 3-hour synoptic period shown along the top; the vertical scale is magnetic flux density in nT normalized at the beginning of the UTC day.

Coronal mass ejection: The energy released by a strong solar flare can accelerate a huge mass of charged particles, mostly hydrogen and helium ions and electrons, away from the corona above sunspots. The event is appropriately called a *coronal mass ejection*, or CME (figure 4). Not all flares produce a CME and not all CMEs are produced by flares, but most are. A CME can travel at speeds up to 2000 km s^{-1} and, if geoeffective, reach Earth in as little as a day. However, most CMEs have speeds in the 500 to 700 km s^{-1} range and arrive within a week. A fast CME will overtake the slower ambient solar wind and produce a shock front that travels outward.

The CME carries a portion of the Sun's magnetic field into interplanetary space; that is, the field is *frozen-in* to the ejected plasma and moves with it. The vector magnitude of the interplanetary magnetic field, or IMF, at a distance of 1 astronomical unit (AU) from the Sun is on the order of 5 to 8 nT but can increase with solar activity such as a CME. The magnitude of Earth's magnetic field at about 10 Earth radii on the dayside toward the Sun is comparable to the IMF. If the CME is geoeffective, it can disturb the geomagnetosphere as described below.

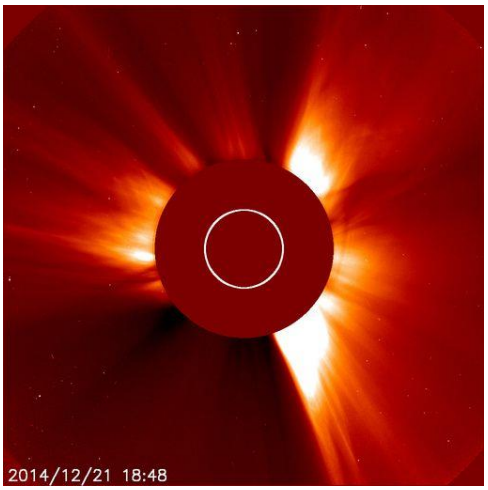

Figure 4 ~ Coronal mass ejection on 21 December 2014 seen as the bright areas. The Sun itself, shown by the white circle, is blocked by an occulting disk in the spacecraft imaging device. This CME intercepted Earth on 23 December only 2 days after leaving the Sun. A CME is a huge 3-dimensional moving mass of charged particles generally with higher density and speed compared to the ambient solar wind. When a geoeffective CME impacts Earth's magnetosphere, the magnetic field is disturbed and oscillates. This generates electric currents in Earth's ionosphere and near-Earth space environment. The electric currents in turn generate additional magnetic field variations and often a geomagnetic storm. Image source: NASA/SOHO/LASCO

Refer to the numbers in figure 5, which shows a conceptual sequence called the *Dungey Cycle* to describe the IMF and magnetosphere interactions when the IMF has a southward component: 1. When the interplanetary magnetic field embedded in the solar wind has a southward component, opposite to Earth's magnetic field, the two fields merge on the dayside of the magnetosphere in a process called *magnetic reconnection*; 2. The formerly closed geomagnetic field lines facing the Sun open as they merge with the IMF. The IMF and magnetosphere are now linked and solar wind plasma can enter the magnetosphere at high latitudes; 3. The open field lines are carried over the Earth's poles by the solar wind. The field lines are stretched out on Earth's nightside in the region called the magnetotail; 4. As they stretch out, the open-field lines move toward the center plane of the tail where they reconnect again, closing the magnetic flux that was opened on the dayside. The time from 1 to 4 is on the order of 1 hour; 5. Part of the flux moves down-tail away from Earth, but, of interest here, part of the magnetic flux returns by internal flows to their origin; 6. This process carries plasma resident in the magnetotail toward Earth; 7. The highly energized electrons in the plasma are trapped by the magnetic field and are further energized when they arrive within a few Earth radii by voltage variations along the magnetic field lines. The cycle may repeat in a quasi-cyclic process called a substorm with a period of roughly 1 to 3 hours. If the IMF is northward, it is deflected around Earth and there is no reconnection.

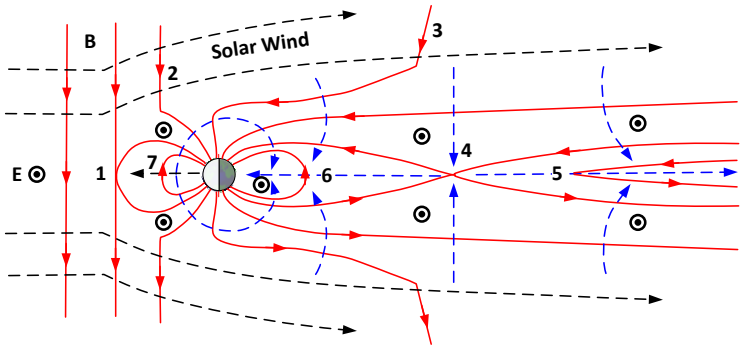

Figure 5 ~ Conceptual drawing of magnetic reconnection. The numbers indicate the sequence described in the text. The Sun is to the left out of view, and the solar wind is shown by the black dashed lines flowing left-to-right. The magnetic field (B) is shown in red; the IMF is southward. Earth is the circle with the sunlit side facing the Sun and has a northward magnetic field. Current flow (E) is into the page shown by the circled dots. Magnetic flux movement is shown by blue arrows. Diagram adapted from: [Seki]

When the charge particles stored in the magnetotail are energized and travel back toward Earth along the stretched out magnetic field lines, they interact with the upper atmosphere at approximately 100 to 300 km altitude to produce aurora. The energy transfer can also produce strong geomagnetic disturbances and a storm (figure 6). It should be noted that simply having a southward component in the IMF does not always lead to a

disturbance. Generally, the southward component has to have a large enough magnitude, say > –5 or –6 nT, and be sustained for a period of time so that enough energy transfer can take place.

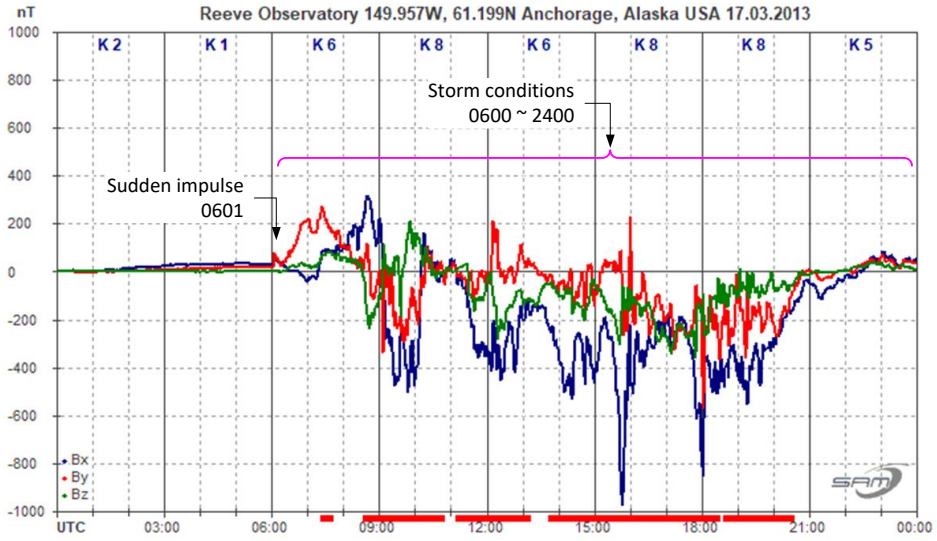

Figure 6 ~ Normalized magnetogram showing a geomagnetic storm observed at Anchorage, Alaska on 17 March 2013 near the peak of solar cycle 24. Although not obvious at this scale, a sudden impulse occurred at 0601 UTC and was followed almost immediately by storm conditions indicated by K-index of 6 during the 0600 to 0900 synoptic period. The storm reached a K-index of 8 for two synoptic periods and lasted the rest of the UTC day. It was caused by a geoeffective CME that occurred 2 days before and traveled with an average speed of almost 900 km s^{-1} to Earth. Note that the magnetic flux density during the storm initially increased but then decreased from normalized levels; the traces show some quasi-periodic structures. These may be due to build-ups and releases of energy in the magnetotail as reconnections took place.

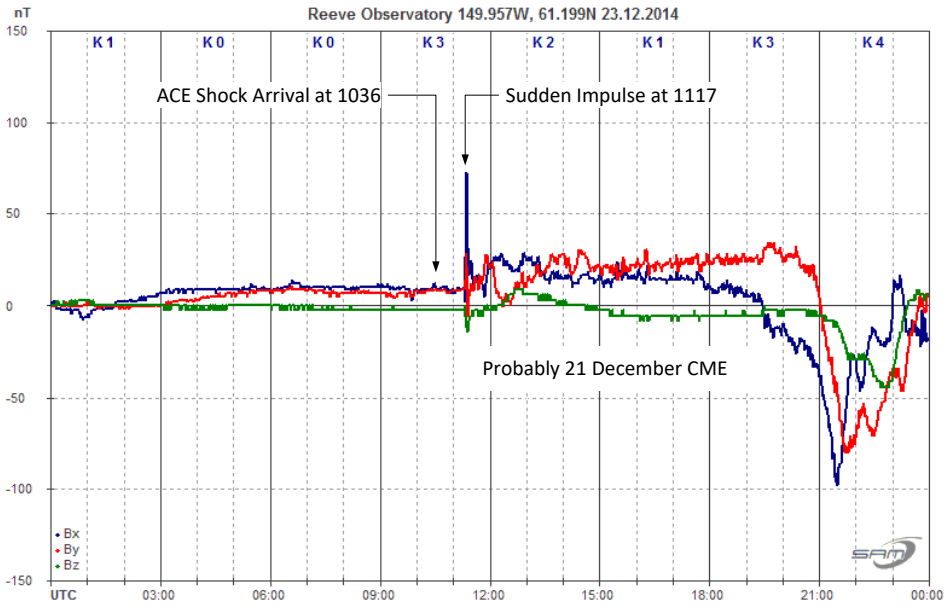

Figure 7 ~ Normalized and annotated magnetogram showing a sudden impulse at 1117 UTC observed at Anchorage, Alaska on 23 December 2014 near the peak of solar cycle 24. Note the vertical scale change compared to the previous magnetogram. The amplitude of this sudden impulse is quite large at about 60 nT. The CME that caused this disturbance is imaged in figure

4. A flare produced the geoeffective CME 2 days before and it arrived at the ACE spacecraft (a sentinel spacecraft $1.5 \cdot 10^6$ km from Earth on the Earth-Sun line) at 1036 UTC and 41 minutes later at Earth. Note the magnetic field disturbances that follow the sudden impulse, especially the bay about 9 hours later, compared to activity before the sudden impulse. The disturbances did not reach actual storm levels until the next day at approximately 1430 UTC.

Disturbances are not limited to situations with a southward IMF. Upon impact, the CME compresses the magnetosphere and suddenly alters the currents flowing in the ionosphere (electrojets), producing a *sudden impulse* (figure 7) or transient measured by ground magnetometers (see {Reeve13} for a more comprehensive discussion of sudden impulses). The sudden impulse may or may not be followed by a storm but often does. *Sudden commencement* is the name often given to a sudden impulse that is followed by a storm.

Coronal hole high-speed stream: Coronal holes are large areas in the solar corona with less dense and colder plasma and where the solar magnetic field lines are able to stretch far into the interplanetary medium (IPM) (figure 8). The wind that originates from a coronal hole is elevated compared to surrounding areas, so it is called a *coronal hole high-speed stream*, or CHHSS. Coronal holes that persist for more than one solar rotation of approximately 27 days are called *recurrent* coronal holes. Coronal holes are the most common source of geomagnetic storms.

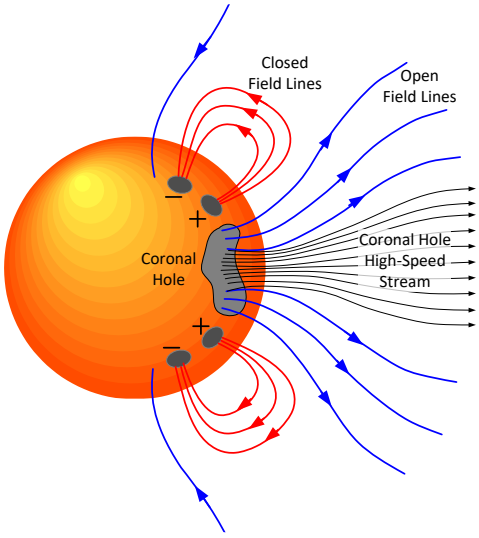

Figure 8 ~ The Sun's magnetic field does not have simple dipole characteristics but is very complex. Closed magnetic field lines shown by the red lines in this conceptual drawing connect the different sunspot polarities and other solar features. Coronal holes have magnetic field lines, indicated by blue lines, that stretch far into the interplanetary medium allowing the solar wind to escape at high speeds. The plasma in the coronal hole regions is less dense and cooler than surrounding areas and the high-speed stream is correspondingly cooler and less dense as well. The Sun's magnetic field lines are frozen-in to the stream and if the stream is geoeffective and has a southward component, that portion of the Sun's field may merge with Earth's magnetic field, leading to a geomagnetic disturbance. The field lines labeled *open* actually are closed but do so at some distance past Earth, so as seen from the perspective of Earth's magnetosphere, they are open.

As the sunspot cycle winds down and goes through the minimum phase, the solar wind is dominated by coronal hole high-speed streams with speeds in the range of 500 to 800 km s^{-1}. The solar wind also has a denser lower speed component of around 300 km s^{-1}. The overall average speed is in the vicinity of 470 km s^{-1}. Larger coronal holes can be a source for high solar wind speeds that buffet Earth's magnetic field for many days. Sometimes a CHHSS becomes geoeffective at about the same time as a CME impacts Earth, leading to a strong geomagnetic storm.

During solar cycle minimum, coronal holes usually are found in the Sun's polar regions (crowns). Because the magnetic fields associated with coronal holes are extremely twisted and complex and heavily influence the wind streams, the solar wind from polar coronal holes often reach the ecliptic plane and affect Earth. As the solar cycle progresses and solar activity increases, the coronal holes occur at all solar latitudes. When a coronal hole is near or on the solar equator, its high-speed wind flow has a high likelihood of becoming geoeffective (figure 9).

A coronal hole does not always cause storms, but it can cause increased geomagnetic activity (figure 10). The wind may simply blow around Earth's magnetosphere and continue on its way; however, if the IMF embedded in the

CHHSS has a southward component, the open field lines in the stream can merge with Earth's closed field lines, transferring energy to the magnetotail and manifesting as a geomagnetic disturbance and storm conditions (figure 11) in the same manner as described above for CMEs.

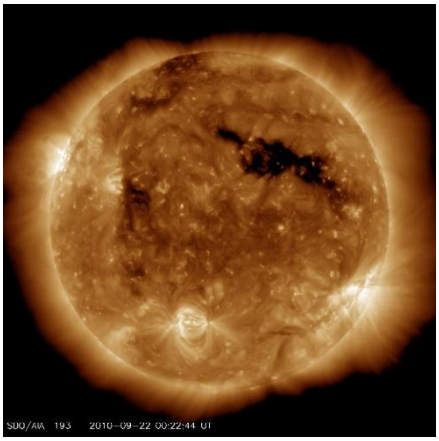

Figure 9 ~ Coronal hole imaged at 0022 UTC on 22 September 2017 during the descending phase of solar cycle 24. Coronal holes are seen as dark areas in images taken at extreme ultraviolet (EUV) and soft x-ray wavelengths. The image shown here was taken at a wavelength of 19.3 nm, which is used to record ultraviolet light coming from gas at a temperature of about 1 million kelvin. The dark areas, such as the elongated black stripe at the upper-right of the solar disk, are cooler and less dense than the surrounding area and have open magnetic field lines that stretch far into the solar system. The open field lines allow the solar wind to easily escape much faster than surrounding areas, the surrounding areas being constrained by closed magnetic field lines. Image source: NASA SDO/AIA

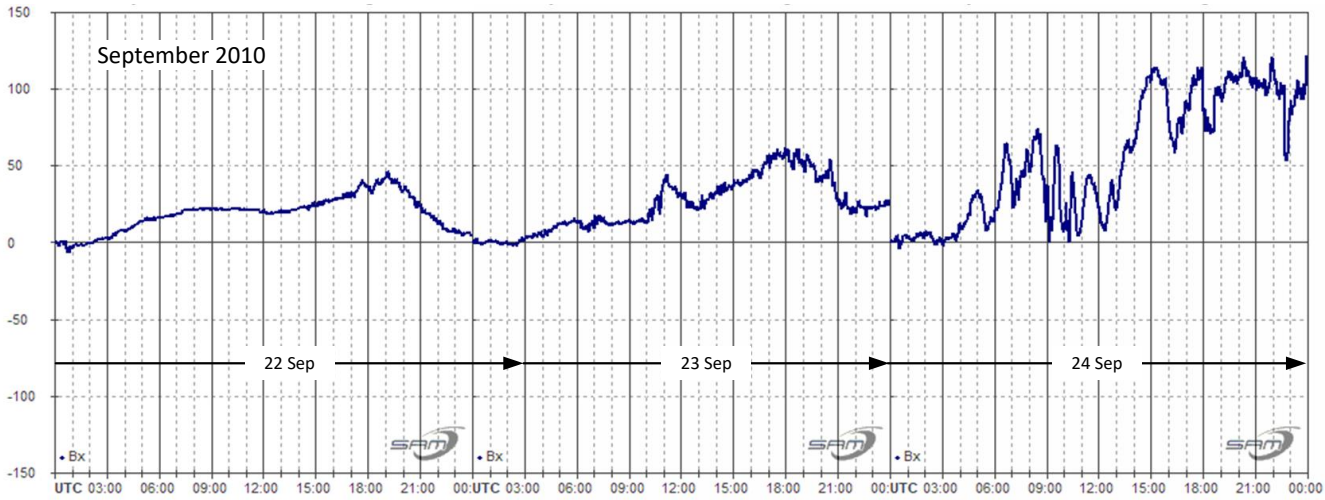

Figure 10 ~ Spliced 24-hour magnetograms at Anchorage, Alaska for the three consecutive days 22, 23 and 24 September 2010 during the ascending phase of solar cycle 24. The trace for 22 September shows a magnetically quiet day before the coronal hole high-speed stream became geoeffective (see previous figure for an image of the coronal hole). The following day, 23 September, also is mostly quiet with some activity starting between 0600 and 1100 as the geoeffective solar wind speed increases and buffets Earth's magnetic field. The CHHSS appears to sweep into full effectiveness (magnetically speaking) starting around 0400 on 24 September. Solar wind velocities increased steadily and reached 600 km s^{-1} on 24 September. The vertical gap at the beginning of 24 September is a plotting artifact due to normalization of the data. These magnetograms were produced by the original SAM magnetometer equipped with a single axis sensor oriented north-south (Bx).

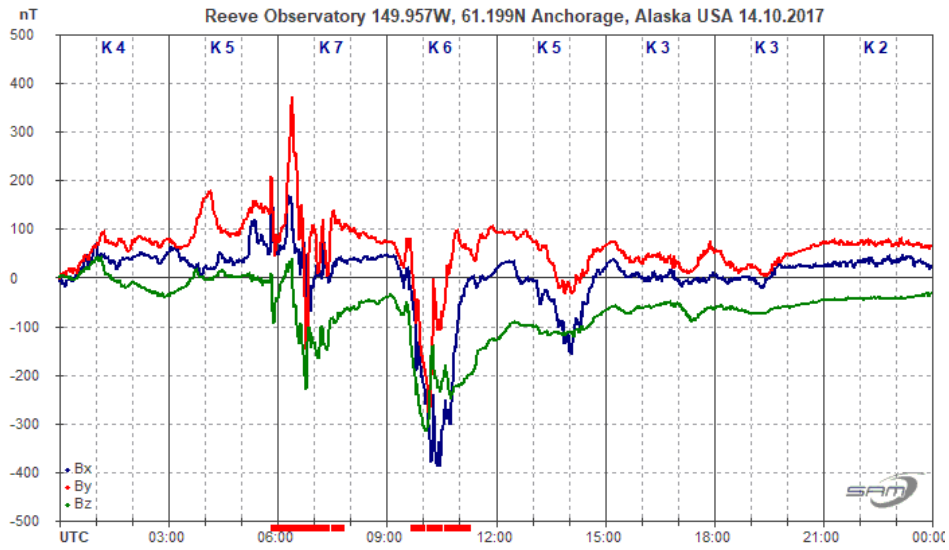

Figure 11 ~ Normalized 24 hour magnetogram at Anchorage, Alaska for 14 October 2017 during the descending phase of solar cycle 24. Storm conditions (K ≥ 5) are indicated during the four synoptic periods from 0300 to 1500, in part caused by the elevated solar wind speeds throughout the 24 h period due to a geoeffective coronal hole in the Sun's polar region. Reconnection was enabled by a southward Bz component in the interplanetary magnetic field, which reached –7 nT.

Corotating interaction region (CIR): The high- and low-speed components of the solar wind form alternating streams in the solar wind flow. They move outward into interplanetary space in a spiral because of the Sun's rotation. As the streams travel away from the Sun, the high-speed flows overtake the low-speed flows, creating a compression region with enhanced plasma density and magnetic flux density. This region is called a *corotating interaction region*, or CIR (figure 12). As viewed by a fixed observer in interplanetary space, the CIR appears to lead the coronal hole high speed stream.

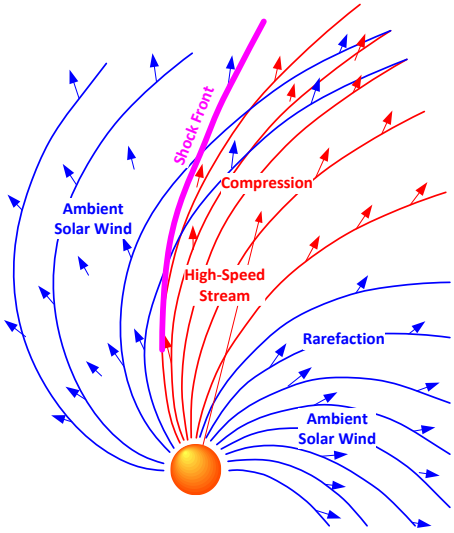

Figure 12 ~ Conceptual illustration of a corotating interaction region looking down on the Sun along its rotation axis. A CIR forms where the low-speed component of the solar wind (blue) is overtaken by the high-speed wind (red) from a coronal hole, forming a shock front (violet) ahead of the compression region. The relatively abrupt changes in the solar wind speed and interplanetary magnetic field at the shock can affect the geomagnetosphere when Earth intercepts it. Because of the spiral structure of the solar wind, Earth intercepts it at about a 45° angle with respect to Earth's orbital direction.

The CIR can result in plasma density enhancement and IMF flux density increase that precedes the onset of the CHHSS lower density and higher wind speed. When Earth intercepts the CHHSS, sentinel spacecraft detect it as an increase in the solar wind speed and temperature and a decrease in plasma density. After passage of the CIR and upon transition into the CHHSS flow, the overall IMF strength near Earth will normally begin to slowly decrease.

Generally, coronal holes located at or near the solar equator are most likely to be geoeffective and result in a CIR passage or higher solar wind speeds, or both, observed at Earth. CIRs and the following CHHSS do not necessarily

induce geomagnetic storms but they may have some effect (figures 13, 14 and 15). However, strong CIRs and faster CHHSS can cause periods of increased geomagnetic activity and storming, particularly if the embedded magnetic field has a southward component.

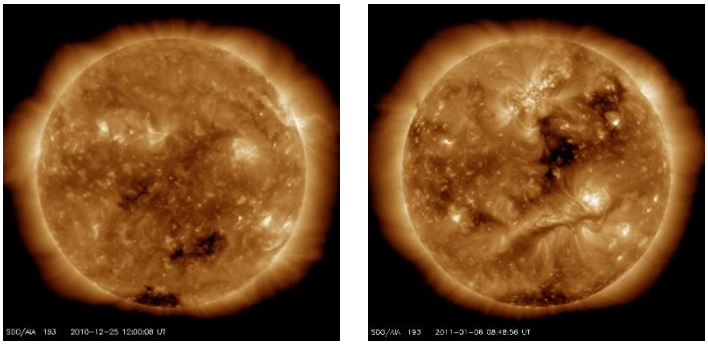

Figure 13 ~ Images at 19.3 nm wavelength of the Sun showing coronal holes in view on the dates of the two magnetograms shown below. Neither coronal hole is particularly large. Left: 25 December 2010; two small coronal holes, one at south pole and one just above the south pole and to the right; Right: 6 January 2011; three coronal holes, south pole, just above the equator near the meridian and one not quite visible in this image at the north pole. Image source: NASA SDO/AIA

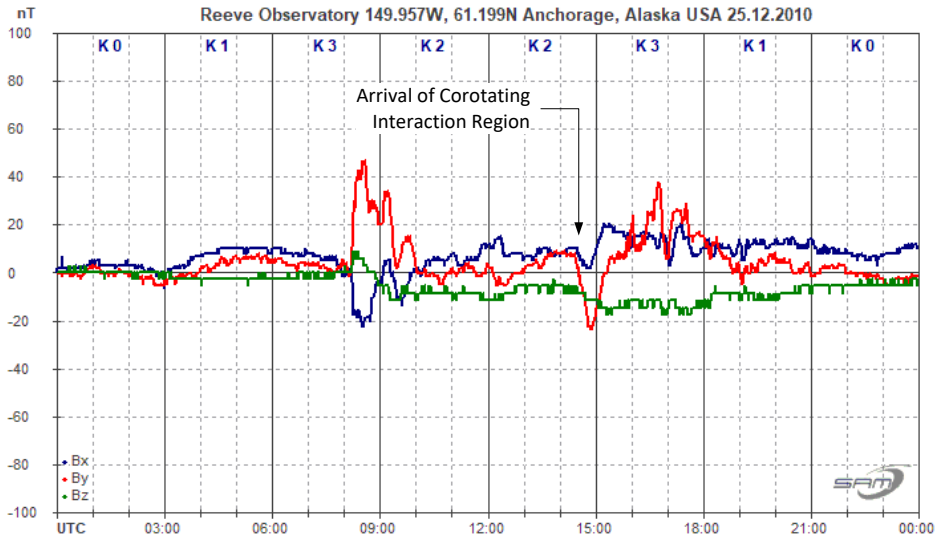

Figure 14 ~ Corotating interaction region on 25 December 2010. Although a coronal hole high-speed stream very likely followed the CIR, it was not reported. Note the dip in both Bx (north-south) and By (east-west) magnetic components immediately after the CIR was intercepted at 1430 UTC. The minor disturbance earlier at 0800 probably was related to the CIR.

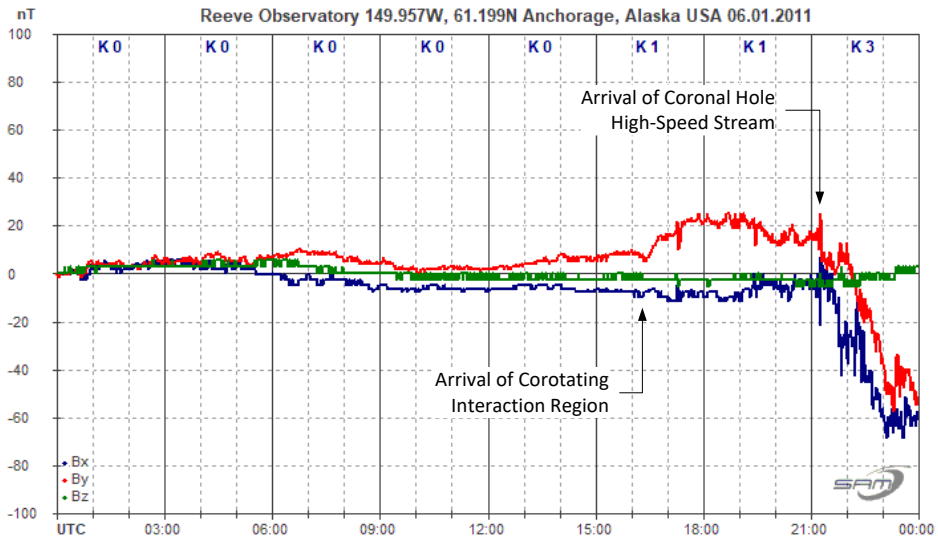

Figure 15 ~ Corotating interaction region followed by a coronal hole high-speed stream on 6 January 2011, about 2 weeks after the previous magnetogram. Note that the CIR had relatively little geomagnetic effect, but the CHHSS that followed about 5 hours later caused a bay, or reduction in measured flux density. Some sharp transients were recorded between the CIR and CHHSS; their source is unknown but they possibly were caused locally (road grader).

Solar Sector Boundary Crossing (SSBC): As previously noted the solar wind carries part of the Sun's magnetic field as it flows away from the Sun, and the solar wind has a spiral shape as it extends out from the Sun due to the Sun's rotation. The Sun's north and south hemispheres have opposite polarity that flip every 11 years, corresponding to the sunspot cycle (22 years for a full magnetic cycle). Along the solar magnetic equator the opposite polarity field lines are parallel, creating a current sheet between them called the *heliospheric current sheet*, or HCS (figure 16, left].

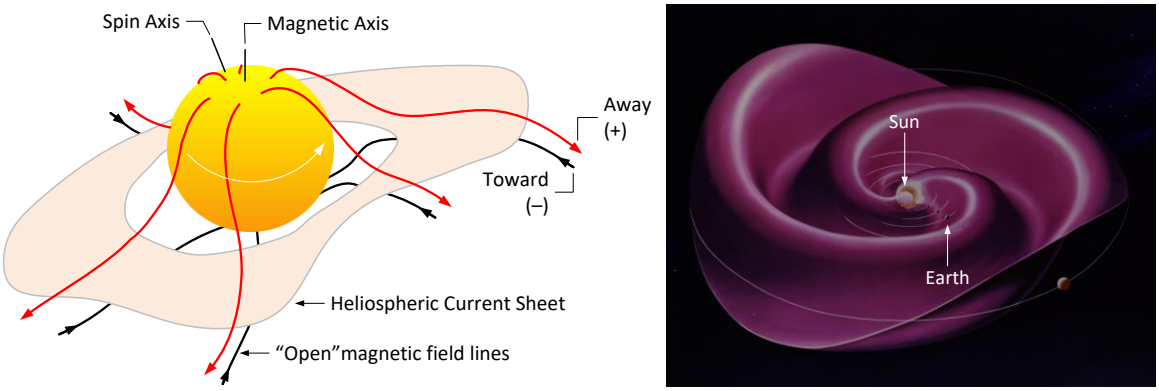

Figure 16 ~ Left: Heliospheric Current Sheet forms between opposite polarity open magnetic field lines from above and below the Sun's magnetic equator (adapted from [Smith78]). Right: The wobbling of the Sun due to misalignment of its rotation and magnetic axes creates folds, or sectors, in the HCS that interact with Earth's magnetic field (adapted from Stanford Solar Center, {STNFRD}). Each passage through a sector is called a solar sector boundary crossing.

The current sheet is warped and develops folds, or sectors, because the Sun's rotational and magnetic axes are not always aligned and it wobbles (figure 16, right). Along the ecliptic plane, the IMF generally has two or four fold-sectors per solar rotation (27 days each). When Earth crosses one of these folds there is a change in the solar wind's magnetic orientation, or polarity, called a *solar sector boundary crossing*. A well-defined sector boundary crossing has a uniform field direction (as measured by sentinel spacecraft) for about 4 days before and after the crossing. The polarity change can simply jostle Earth's magnetic field (figure 17) or, if it includes a southward magnetic field component, merging and disturbance of Earth's magnetic field may result.

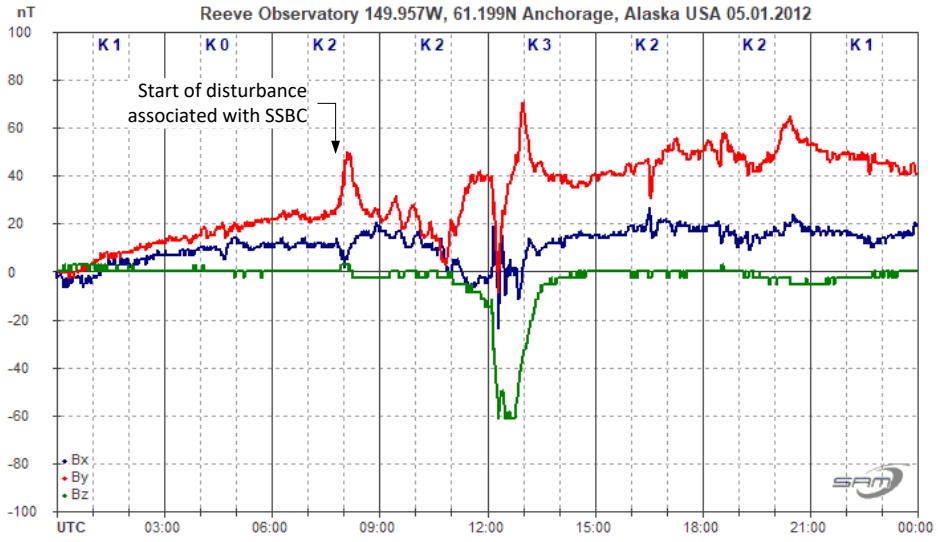

Figure 17 ~ Unsettled conditions possibly caused by SSBC when effects were indicated just before 0800 UTC on 5 January 2012, approximately 4 years into solar cycle 24. This disturbance produced only a K-index of 3 during the 1200 to 1500 synoptic period. According to spacecraft data, the SSBC showed stable magnetic field polarities 7 days before and 4 days after the SSBC, which actually occurred the next day.

Other interesting phenomena: The magnitude of magnetic variations caused by a coronal hole high-speed stream or other solar phenomena may be relatively minor but those variations may include interesting structures, such as *ULF* (ultralow frequency) *waves*, also called *magnetic pulsations* and *micropulsations*. These are periodic variations in Earth's magnetic field with periods from fractions of a second to several minutes. Note that the maximum sample rate of the SAM-III magnetometer is 1 Hz, so fractional second variations cannot be resolved by it.

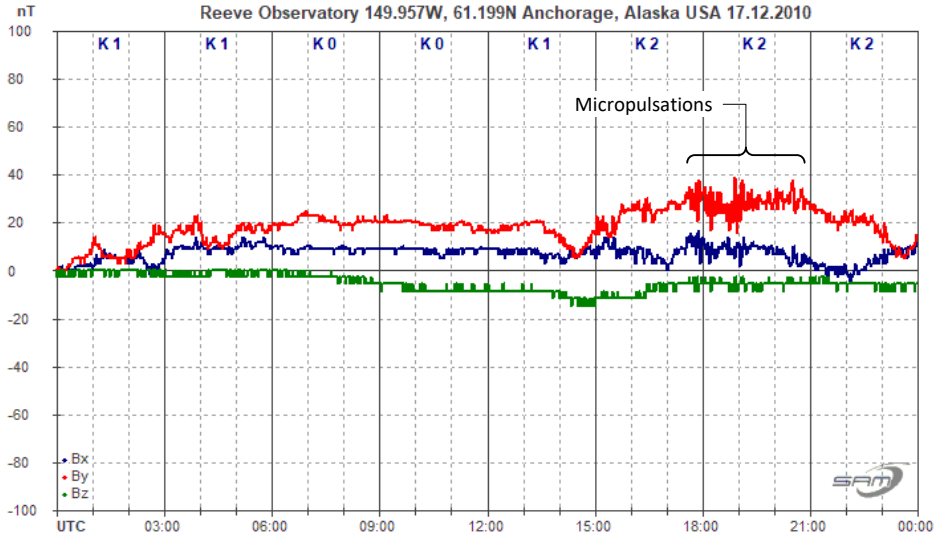

Figure 18 ~ ULF waves possibly instigated by multiple CHHSS on 17 December 2010. The traces throughout the day show some relatively smooth and typical variations. However, at about 1730 UTC, the field experienced short-period pulsations with peak-to-peak amplitudes of about 20 nT. There also is evidence of the waves a few hours before and after this main period. These measurements were made by the SAM-III while set to 0.1 Hz sample rate (10 second sampling period).

There are many causes of ULF waves, all related to wave interactions and resonances in the geomagnetosphere cavity and waveguide where they originate. The solar wind dynamic pressure and external perturbations work in concert with Earth's magnetic field to influence their generation. The pulsations can be irregular (Pi) or continuous (Pc) and their characteristics as measured on the ground depend on many factors including geographic location, particularly latitude, and whether the magnetometer station is on the dayside or nightside of Earth. Historically,

pulsations were observed on telegraph wires by rapid changes in the current polarity; early formal observations in the 1850s used a microscope at the end of a very long compass needle.

---

3. Comments

Earth's magnetosphere never responds the same way twice to a given type of phenomena. Generalizations can be made but there are just too any variables involved including solar wind speed and the strength and characteristics of the embedded magnetic field. These may be estimated through modeling but predictions are very difficult. Observations of a given phenomenon with ground magnetometers depend on geographic locations, latitudes and local magnetic environments and whether they are on the dayside or nightside when the event occurs; no two magnetometers will show exactly the same response.

Some observations are not easily explained. Magnetic field measurements may show unexpected variations or none at all from a solar event. A solar event may have occurred days or weeks before making time correlation especially difficult. Multiple flares, CMEs and coronal holes that become geoeffective about the same time have complicated interactions because they unpredictably mix together. Having regular reports from organizations such as SWPC greatly aids identification of an event, particularly at higher latitudes where the magnetic field is naturally more active and subtle changes may be buried in the natural variations.

---

4. Weblinks & References

{DSHBD} https://www.swpc.noaa.gov/communities/space-weather-enthusiasts

{NOAA25} https://www.swpc.noaa.gov/products/solar-cycle-progression

{Reeve13} Reeve, W., Geomagnetic Sudden Impulses, 2013, available at: http://www.reeve.com/Documents/Articles%20Papers/Observations/Reeve_GeomagSuddenImpulses.pdf

{Reeve15} Reeve, W., Geomagnetism Tutorial, 2015, available at: http://www.reeve.com/Documents/SAM/GeomagnetismTutorial.pdf

{Reeve21} Reeve, W., Summary of Solar Radio Emission Types and Characteristics, 2021, available at: http://www.reeve.com/Documents/Articles%20Papers/Reeve_SolarRadioCycle25.pdf

{SAM-III} http://www.reeve.com/MagnetometerM3.htm

[Seki] Seki, K., et al, A Review of General Physical and Chemical Processes Related to Plasma Sources and Losses for Solar System Magnetospheres, Space Science Reviews, August 2015, DOI 10.1007/s11214-015-0170-y

[Smith78] Smith, E and Tsurutani, B., Observations of the Interplanetary Sector Structure up to Heliographic Latitudes of 16°: Pioneer 11, Journal of Geophysical Research, Vol. 83, No. A2, February 1, 1978

{STNFRD} http://wso.stanford.edu/SB/SB.html

{SWPC} https://www.swpc.noaa.gov/

{SWS} https://www.sws.bom.gov.au/

{ESASWSN} https://swe.ssa.esa.int/current-space-weather

Author: Whitham Reeve obtained B.S. and M.S. degrees in Electrical Engineering at University of Alaska Fairbanks, USA. He worked as a professional engineer and engineering firm owner/operator in the airline and telecommunications industries for more than 40 years and now manufactures electronic equipment used in radio astronomy. He also is a part-time space weather advisor for the High-frequency Active Auroral Research Program (HAARP) and a member of the HAARP Advisory Committee. He has lived in Anchorage, Alaska his entire life. Email contact: whitreeve@gmail.com

Speeding Up Search Folding for Amateur Pulsar Hunters

Peter W East

Abstract

Search folding is the process whereby the epoch folding algorithm is repeated over a range of parameter values to extract detailed pulsar information from recorded data. Processing large observation data files necessary to detect and analyze weak pulsar signals can be a long and computational intensive process. Professional software including PRESTO seems to have solved this problem and manages to produce a comprehensive printout in a minute or two. In this article, a simple concept is described, suitable for amateurs to apply which can speed up analysis of targeted pulsars by first compressing the data files whilst ensuring negligible information loss. The technique is suitable for speeding up data searches of period, P-dot profiles and improving the accuracy of the pulsar dispersion searches. It has particular benefit in reducing the computation time of the 2-D period/period rate graphic that is featured in PRESTO pulsar recognition plot.

Introduction

A Fast Folding Algorithm or FFA was first proposed in 1969 as a method of searching recorded data for new pulsars having a wide range of possible periods and unknown phases [1]. The method is based on the divide-and-conquer successive block halving rule, as used in the Fast Fourier Transform (FFT), to minimize redundant calculations. Even so the computation load was still high and the more straightforward FFT spectrum harmonic summing technique has tended to be preferred by professionals. Recently the FFA idea has been developed and shown that folding really does offer better sensitivity in finding new pulsars than the common FFT spectral methods[2].

The name, Fast Folding Algorithm implies that it is a faster process than the standard epoch folding algorithm, but this is not so as they address different problems. Whereas the folding algorithm usually folds de-dispersed pulsar data at a known period value, the FFA scans a wide range of period and dispersion ranges to determine the presence and periods of unknown pulsars. The 'fast' prefix means that the process is designed to be faster than simply repeating the basic folding algorithm for discrete pulsar test values over an extensive search range. Even so, when processing very wide pulsar period ranges, (tens of ms to tens of seconds), the computational load can still be very high. Reference 2 looks at a number of methods to speed this up with the aim of searching large dish data to find new pulsars at lower signal-to-noise ratios by exploiting the sensitivity advantage of period folding to spectrum harmonic summing. Reference 2 also discusses the necessity of pulsar pulse matched-filtering to achieve the optimum signal-to-noise ratio as is incorporated in the processes suggested here.

For amateur purposes, in seeking known pulsars in data using system clocks with doubtful accuracy there is an interest in testing a much narrower range of periods to determine the best folded response and to investigate the pulse peak roll-off either side of the matched period. Presently this is tested by repeating the folding process on all the data over a small a range of periods about the expected value and producing a manual plot.

This article investigates how this latter search process can be automated and speeded up by first compressing the detected data file whilst ensuring minimum information loss.

Pulsar Period Search Strategies

1. Standard Search

Pulsar period search is used to indicate an accurate value for the observed pulsar period by determining the point of pulse amplitude maximum. The data is folded at a number of discrete periods around the predicted value, the period being changed typically in fractional parts per million. Figure 1 depicts the effect of changing the correct period duration *P* by -*p* parts per million (ppm).

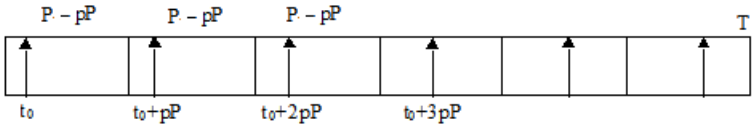

Figure 1. Period Search Parameters - search period reduced by *p* ppm from test value *P*

Normally, as in Figure 1, the total record, covering an observation time *T* is divided into blocks equal in length to the test pulsar period *P.* The first pulse arrives at time t_0 after the record start. In the matched period case, the pulsar pulse will occur in the same relative position t_0 in all periods and when the period sections are summed (or folded), the pulses add linearly and any noise present adds as the detected voltage square root, improving the SNR by the square-root of the number of sections.

When the period is reduced by *p* parts per million the pulsar pulse is delayed in increments of *pP* in successive periods as indicated in Figure 1. These delays may be small but, if not matching the true pulsar period, will tend to spread the observed pulse on folding and reduce the summed amplitude.

The typical adjustment increment to ensure finding a reasonable pulsar maximum is of the order *W/T*, where *W* is the pulsar pulse width and *T* the observation duration (see Reference 3; part reproduced in Appendix 1). So if the pulsar period uncertainty is large, many folded search attempts will be required. For example, for a 2 hour observation with a possible system clock accuracy and offset up to 10 ppm, to search for pulsar B0329 (*W* = 6.5 ms), searching a 20 ppm range in 0.5 ppm steps could require $40*T/(6.5*10^6)$ full folding operations, numbering approximately 45 worst case.

2. *Period Rotate Search*

In this alternative method, when searching for the correct period, a fixed initial period value *P'* is chosen close to the expected value. Then, if a pulsar is present with a period slightly greater than *P'* by a factor (1+*p*), the pulse positions will be linearly delayed in successive periods as shown in Figure 2.

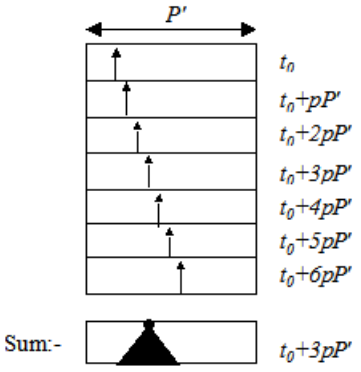

Figure 2. Position offsets with Pulsar Period Greater than Test Period *P'* before Rotation Alignment

Direct summing an offset period results in a reduced amplitude, broader pulse width result as shown in Figure 2. Since the test period *P'* is normally divided into a number of bins and the period-to-period pulse delay is linear, instead of adjusting the initial period *P'*, we could rotate each period's bins, towards the left (in this case) linearly increasingly with period number until the pulsar positions align vertically and so on summing, maximising the

output pulse amplitude. The correct pulsar period correction, (P'-p_m P') can then be calculated from the adjustment required.

Both these methods require quite a lot of computation, since a 2 hour record, downsampled to 1 k samples/s data record may contain typically 7.2 million samples of around N = 10800 pulsar periods, where each period may be folded into, for example, some 700 bins.

Speeding up the Search Process by Data Compression

As described, there is probably not much processing time-wise to choose between the above two methods, but there is some benefit in both schemes by applying some data compression ensuring minimum information loss.

This is possible if groups of say 'q' single periods could be pre-summed together to produce a new smaller data file before searching; so reducing the computation load by the factor N/q (where, N is the total number of periods in the data file.

For negligible signal-to-noise ratio (SNR) loss and little pulse width stretching then qp_rP', the q^{th} period pulse maximum delay (see Appendix 1.), must be much less than W, the pulsar pulse width.

For example, suppose we wish to search over a range of p_r = ±50 ppm, and P'/W = 110, then if the acceptable maximum pulse shift in a block (qp_rP') is less than $W/2$ and SNR reduction < 6% (see next paragraph), then,

$$q < \frac{10^6}{2p_r}\frac{W}{P'} \qquad (1)$$

so in this example, q <91 and we can safely pre-fold, $R = N/q$ ≈120 data blocks before search folding or fold rotation.

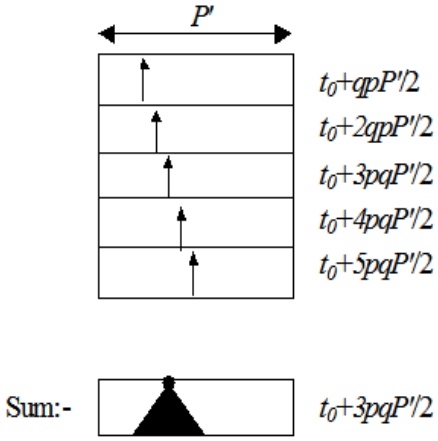

Figure 3. Folding and Combining q-Period Data Blocks with p ppm Period Offset

Figure 3 shows the result of folding and combining q-period data blocks with p ppm period offset.

The halving factor in the delayed pulsar-sum positions, aligns the combined/folded block pulse centre, being halfway between the initial pulse position t_0 and the final block period delay $t_0 + qpP'$.

This technique potentially cuts the example overall search processing time by a factor of q = 91 with just a small reduction in integrated pulsar pulse amplitude.

For the example, using Equation A.1. of Appendix 1, for R = 110, P' = 714.5 ms, W = 6.5 ms and p_r = ±50 ppm, the folded peak amplitude factor drops by 6% at the search limits, with just a similar slight increase in observed pulse width.

The implications of this minimal data loss compression is far-reaching. Whilst it doesn't match the wide range of the Fast Folding Algorithm, it is useful for speeding up the analysis of known pulsars for more computational intense detailing tasks such as multi-band de-dispersion and 2-dimension period/p-dot search.

The next question to resolve is, how many bins to fold the compressed data in? Basically there is no restriction if pulse width matched-filtering is incorporated; but for convenience, one to four bins/ms is recommended to simplify band de-dispersion and folded data pulse width determination. Of course, if the search range required is much less than the ±50 ppm example discussed, then much greater data compression is possible.

Note that, once the compressed data file is defined, then for further folding to achieve optimum recovered pulsar signal, the bin number replaces the test period value in the folding equation.

Data Compression/Fold Procedure (Method 1)

The compressed data processing sequence diagram is shown in Figure 4.

The processing sequence is,

1. Synchronously, based on the period P, partition the data file into R sections ($R = N/q$, where, N is the number of periods in the data file and q is calculated from Equation 1).
2. Fold the R sections, each into B bins (for ease of pulse width checking, B can be chosen into equivalent ms time bins)
3. Serially combine the R section fold results to form a new data time series file of RB samples.
4. Standard fold the new data file with search period offsets $pp.N/R$, over the range ±PP specified, but now with an effective period 'B'.

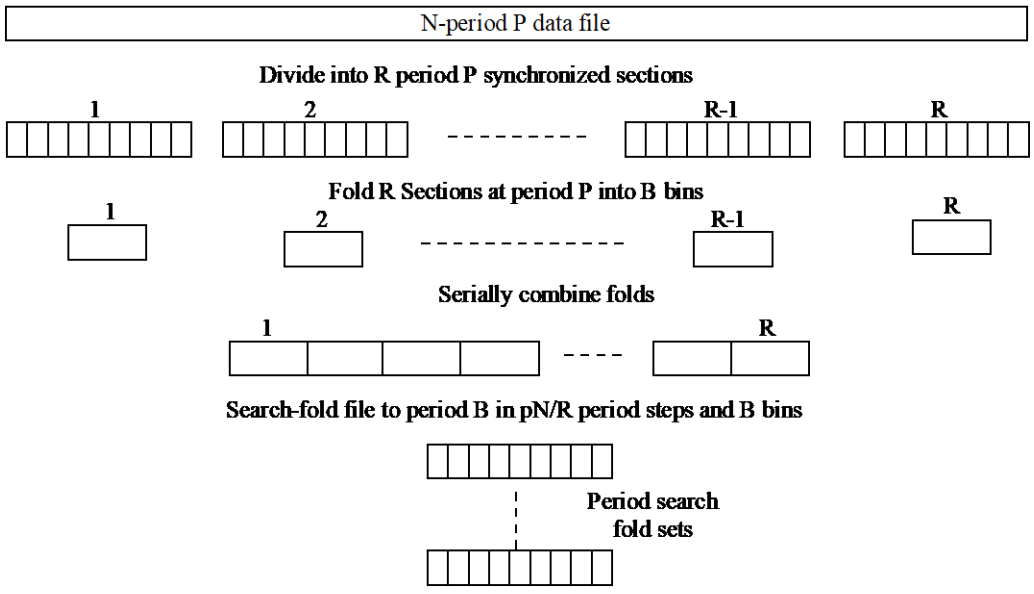

Figure 4. Compression/Search Sequence

This is achieved by applying the fold algorithm (MathCad code is listed in Appendix 2) with the parameters as specified below.

Step 1,2.

$$Fb^{\langle r \rangle} := Fold\left[B, 1, P, Dat, r \cdot \frac{Mx}{R}, \frac{(r+1) \cdot Mx}{R}, pw \right] \qquad (2)$$

where,
B is the number of fold bins
P is the search test pulsar period in ms
Dat is the data file name
Mx is the number of data file samples (assumed 1 kpps)
r is the section number *R* range variable
pw is the search pulsar pulse width in ms (*W*)

Equation 2 produces a 2-D matrix which is converted to a series file - in MathCad this is achieved simply with the instruction,
Step 3.

$$Fs_{k+r \cdot K} := Fb_{k,r} \qquad (3)$$

where, *k* is the bin number range variable .

Finally, the period search folding set can be completed.
Step 4.

$$Fn^{\langle pp+PP \rangle} := Fold\left[B, 1, B \cdot \left(1 + \frac{pp}{10^6} \cdot \frac{Mx}{R \cdot P} \right), Fs, 0, R \cdot B, pw \right] \qquad (4)$$

Note: For the new compressed series data file *Fs*, the period is reset to reflect the bin number (ie, *P* -> *B*)

Also, *PP* is the period search ± extent and *pp* is the period search range parameter. The factor, Mx/RP (or *N*/*R*), modifying *pp* in Equation 4 compensates for the data compression of the method.

The Data Compression/Fold procedure for the alternative data rotation version, Method 2, is listed in Appendix 3.

Proof of Principle

To demonstrate the operational advantages of the processing proposed, a data file was simulated with 7200000, 1ms samples containing two similar level fake pulsars of 6.5ms half-height pulse width. One offset by -45 ppm and the other by +8 ppm from a test period value of 701.1 ms. The base noise was generated by a MathCad function that produced a Gaussian/Normal file matching the length of the pulsar example.

1. Initial Check

Figure 5 compares the final folded results of the full (blue) and the compressed (red) folded data (*R* = 90 pre-averaged sections) on one of the test pulsars (+8 ppm), showing negligible final folded differences. Those apparent can be explained by the double matched filtering occurring with the compressed data process smoothing out some of the faster data variations. The number of bins into which the data is folded was chosen as 1402, or 0.5 ms/bin to simplify pulse width checking.

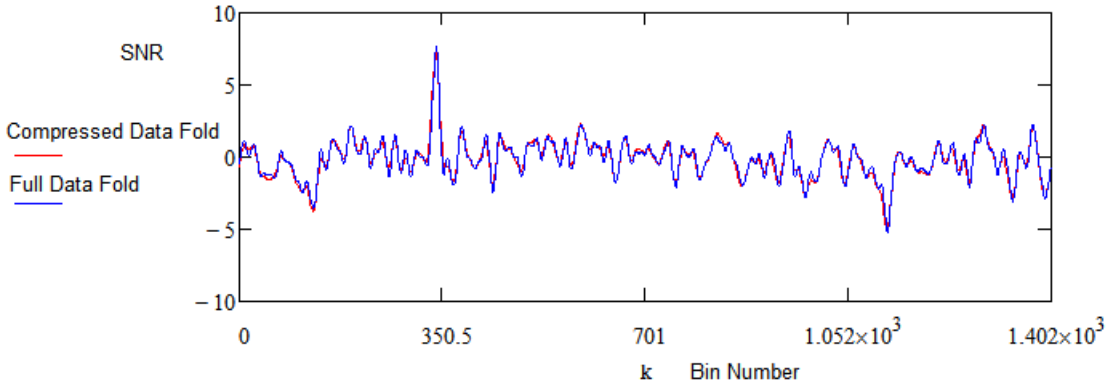

Figure 5. Comparison of Compressed Data Folding (red) with Full Data Folding (blue)

2. Period Search Examination

Figure 6 displays the plot of Equation 4 for all bin values over the period range 701.1 ms ±50 ppm in 0.5ppm steps. It shows two clear peaks at -45 ppm and +8 ppm identifying the fake pulsar offsets, as defined in the initial example. Other peaks are evident and these are easily identified and corresponding folded time peaks can be investigated. It is noted that with the test peaks around 7.5:1 folded SNR levels the base noise shows relative peaks up to 3:1 SNR as expected. Also, the presence of the base noise influence is evident in the asymmetries in the shapes of the fake pulsars.

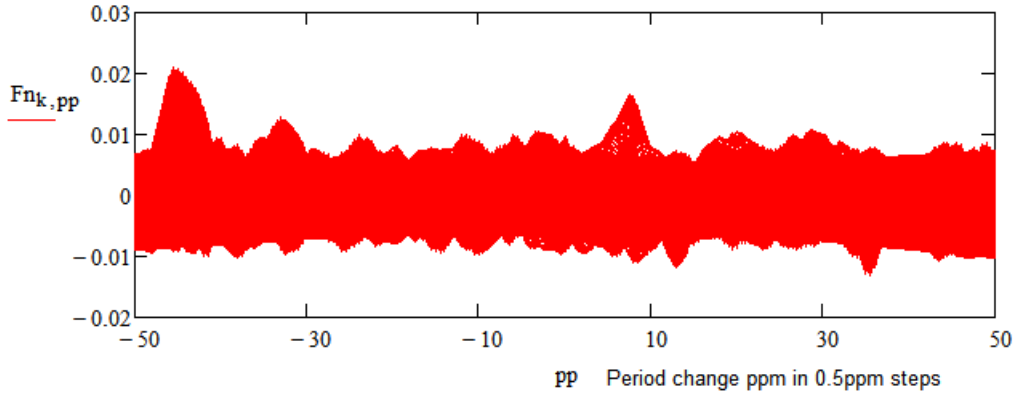

Figure 6. Period Search Result - all bins and *pp* range over ±50 ppm and all *k*, the bin number range variable (200 x 714 = 142800 data points plotted)

3. Extracted Final Folds.

From the resulting data produced by implementing Equation 4, some detail can be extracted and the final folded results of the two example pulsars is reviewed in Figure 7. Both pulses integrate to about 7.5:1 SNR.

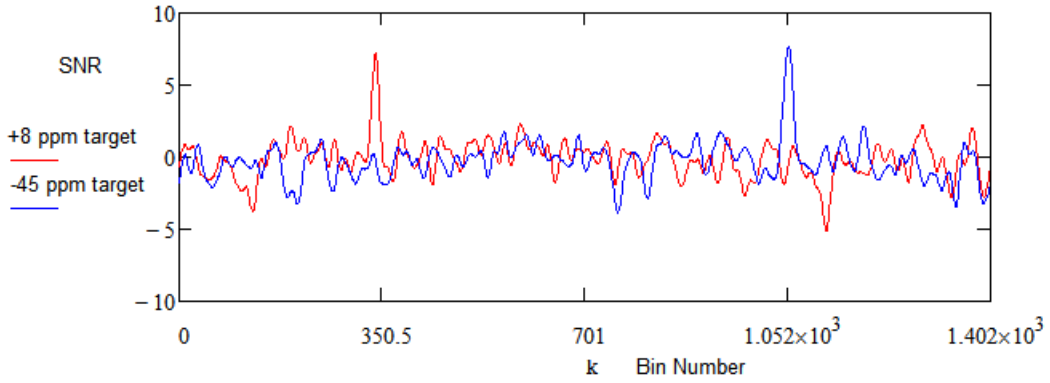

Figure 7. Final Folded Plots of the Two Example Target Pseudo-Pulsars

The next most significant peak at *pp* = -32.5 in Figure 6 produced a folded peak at bin 913 with an SNR of 3.0:1 with a pulse width of 12 ms - a typical noise peak.

4. Period Search Data Analysis

Figure 8 summarizes some detail that can be extracted from Equation 4 - period search analysis carried out on the example data. The brown curve records the maximum amplitude over all phases at each test period change, whereas the red and red-dashed curves report the amplitude at the optimum target phase and calculated response of the 8ppm offset target respectively (blue and blue dashed correspond to the -45 ppm target). The predicted/calculated results follow the analysis given in Appendix 1.

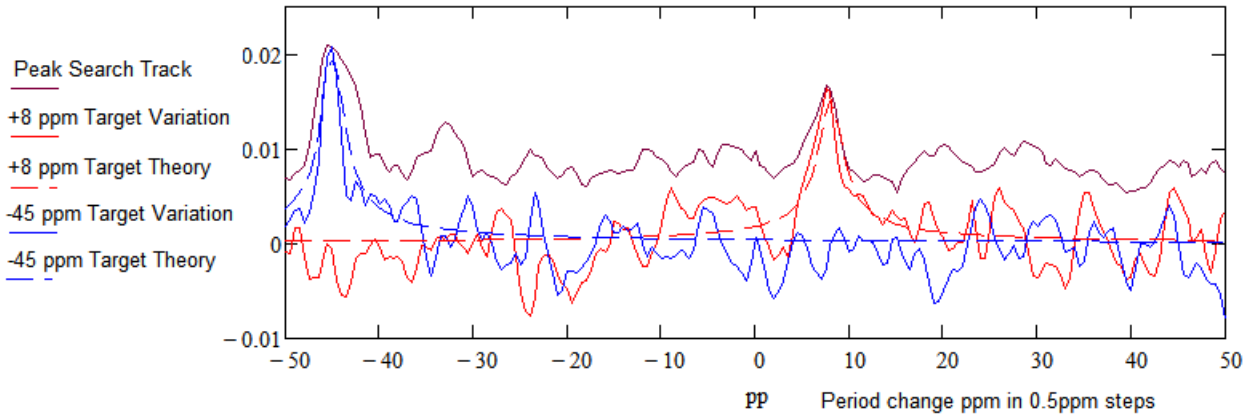

Figure 8. Period Search Data Detail.
brown - peak search; blue, -45ppm target; red, +8ppm target

The small deviation of the measured and calculated target plots arises due to two main causes. The first is the influence of the base noise which is indicated by the asymmetry noted above and also due to the fact that peak values are plotted which does not take into account the pulse width broadening, due to the finite target pulse width (the broadening effect is evident in Figure A.2 in Appendix 1).

5. Timing Comparison

For a straight 200 point (±50 ppm in 0.5ppm steps) full period search, the number of averaging operations is equal to 200x10800periods = 2160000.

For the compressed data model, the number of operations is one full fold (1x10800) for producing the 90 sections, then 200 compressed data folds (200*90periods = 18000) to produce the search data.
The ratio of these process averages is 2160000/(10800+18000) ≈ 75.
A MathCad timing comparison gave a result of 320s/9s ≈ 36.

Either result shows a significant computation time advantage and as the Figure 4 indicates, with negligible data/information loss.

Implications and Potential for Real Data

The proof of principle using the fake pulsars has shown that,

1. For defined period parameter ranges, data compression is a valid technique
2. The computational load of fold-processing large data files can be reduced significantly.
3. Time resolution improvement by using large bin numbers is feasible.

These properties can be achieved with negligible data loss. The compression ratio is dependant upon the period range observed and so improves with more accurate knowledge of the observed pulsar topocentric period. Examples using real data follows.

Application to 2-D Period/P-Dot Searching

Figure 9(a) Period/P-dot search plot was produced for Reference 4 from real data in an effort to duplicate the PRESTO *prepfold* plot and it was observed that the MathCad program, listed in the reference appendix took over an hour to produce this output. For comparison, Figure 9(b) operating on the same real data under this new regime, completed the plots in under a minute.

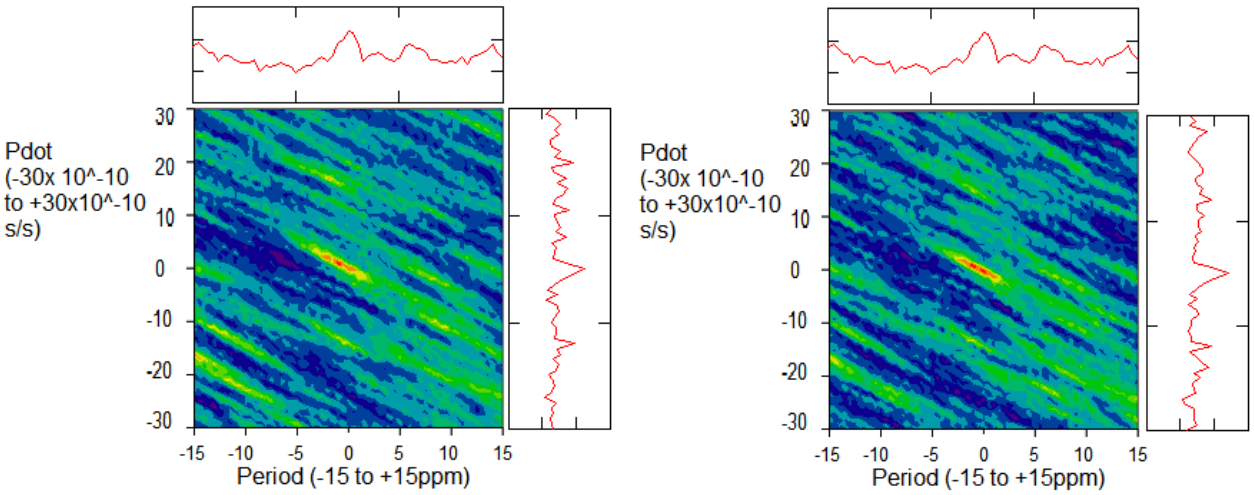

(a) No Data Compression (b) Data Compressed into 50 Sections

Figure 9. 2-D Period/P-Dot Comparison - 60 Period x 60 P-Dot increments

For Figure 9(b) result, the data was compressed into 50 sections and it is clear that these final results match very closely.

Application to De-dispersion

Detected pulsar data prior to de-dispersion usually comprises a set of downsampled files at 1 or 2 k samples/second data rate, representing a time series of the incoming data split into a number of RF bands. This is the typical form in standard filterbank (.fil) files, produced by PRESTO and amateur GNURadio programs [5,6]. The file lengths cover the record observation time.

In PRESTO, the first process is to scan the band files to find and blank RFI sections followed by adjusting the band timings to analyze the target pulsar dispersion. The optimally de-dispersed band files are then suitable for combining to produce a single file for folding, and the subsequent period and P-dot searching processes.

However, once the RFI mitigation has been carried out, the compression method described can speed up the de-dispersion and analysis processes by significantly reducing the multiple band file sizes before dispersion measure (DM) search and final de-dispersion. In addition, the methods detailed can also improve the band file time resolution, so improving the accuracy of band file delays for optimum de-dispersion.

Figure 10 shows the same Reference 4 data folded in 714 bins (upper plot with ~ 1ms time resolution) and with 2856 bins (lower plot with ~0.25ms time resolution), demonstrating an advantage of matched-filtering.

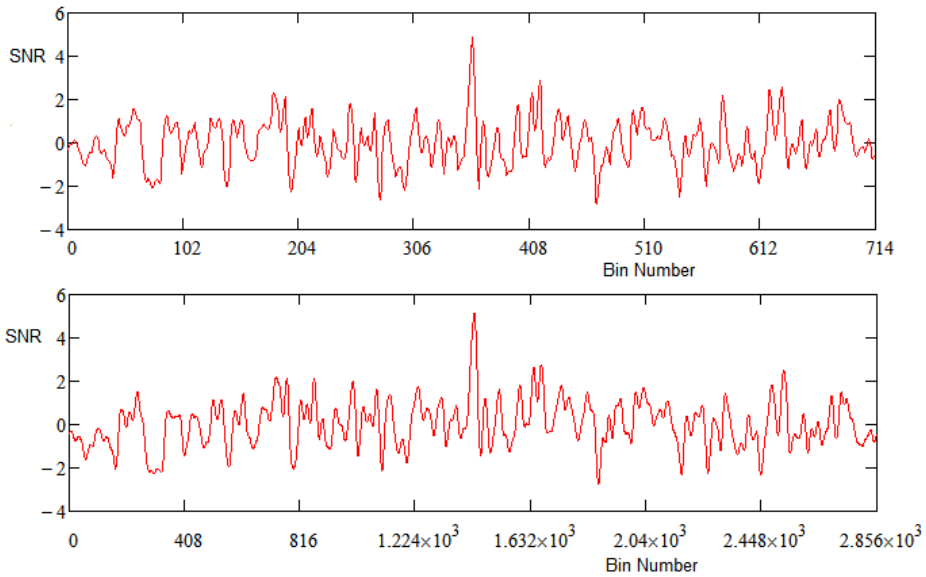

Figure 10. Bin Number Comparison of Time Resolution Improvement with Pulse-Matched Folding

Figure 11 demonstrates the improved Dispersion Measure result from taking advantage of the techniques described. The upper plot mirrors the final DM search result of Reference 4 whilst the lower plot was produced using the new processes described.

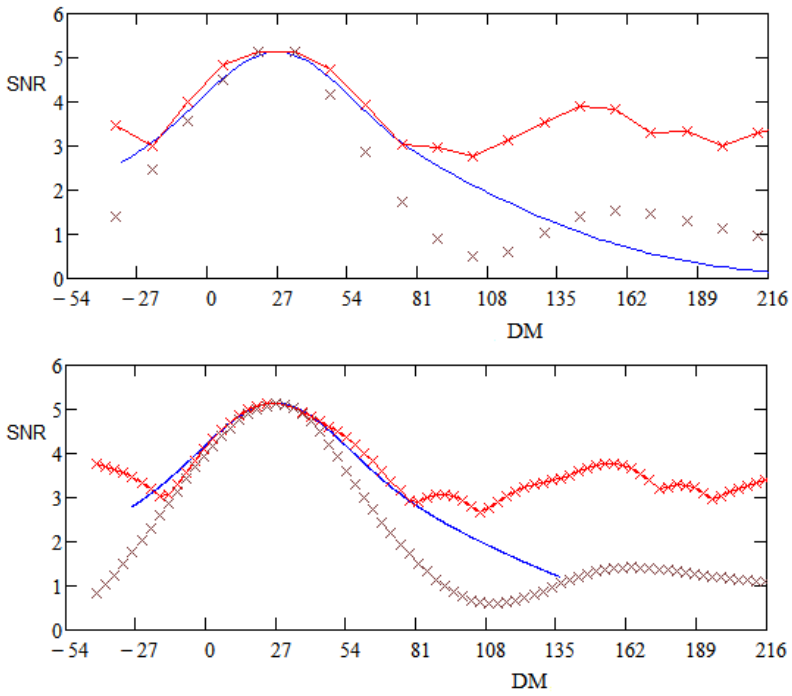

Figure 11 Dispersion Measure Search Comparison with low (1ms) and high (0.25ms) Resolution (red - maximum value; blue - theory; brown pulsar peak value)

The detected data comprised three adjacent 2 MHz bandwidth files with 1 ms sample, detected data resolution. It is noted in the reference that the data needed adjustment in timing by 0.5 ms to compensate for the coarseness of data sampling. The lower plot with 0.25ms equivalent sampling required no post adjustment, as the improved band folding resolution allowed the slight mis-alignment to be corrected prior to the DM search process.

Conclusions

This short investigation to speed up pulsar parameter searching analysis was triggered by having to endure the long waiting time required by MathCad to produce the period/p-dot search 2-D plot needed to emulate one part of the PRESTO *prepfold* analysis output[4,5]. Whilst it is obvious that coding in a high-level language such as any of the members of the C language suite, plus making use of multiple cores now available in computer CPUs, can solve this problem; simplifying the process as here, is another option. It has been shown that, by limiting the period search range, large multi-band detected files of known pulsars can be partially folded and compressed producing improved timing resolution allowing parameter search routines to speed up analysis by factors of ten to one hundred or more.

The alternative, of course is to use PRESTO, but the challenge for amateurs is to understand its processes and adapt them to better suit our purposes.

References

[1] DH Staelin. Fast Folding Algorithm for Detection of Periodic Pulse Trains, Proceedings of the IEEE, P 724, April 1969.

[2] V Morello, et al. Optimal periodicity searching: Revisiting the Fast Folding Algorithm for large-scale pulsar surveys. arXiv:2004.03701v2 [astro-ph.IM], 3 Aug 2020.

[3] PW East. An Analytical Method of Recognizing Pulsars at Moderate SNR., Journal of the Society of Amateur Radio Astronomers. November-December 2018.

[4] PW East. Getting the Best out of PRESTO - Part 3: Waterfalls and Conclusions., Journal of the Society of Amateur Radio Astronomers. July-August 2021.
[5] PRESTO Home. https://www.cv.nrao.edu/~sransom/presto/
[6] MD Leech. pulsar_filterbank, https://github.com/ccera-astro

Appendix 1. Pulsar Period Search Analysis

Pulsar period search is used to indicate an accurate value for the observed pulsar period by determining the point of pulse amplitude maximum. The data is folded at a number of discrete periods, the period being changed typically in fractional parts per million. Figure A.1 depicts the effect of changing the period by *-p* parts per million.

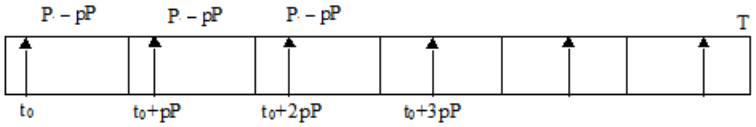

Figure A.1. Period Search Parameters

Normally, the total record, covering an observation time *T* is divided into sections equal to the pulsar period *P.* The first pulse arrives at time t_0 after the record start. In the matched period case, the pulsar pulse will occur in the same relative position t_0 and when the sections are summed (or folded), the pulses add linearly and any noise present adds as the detected voltage square root, improving the SNR by the square-root of the number of sections. When the period is reduced by *p* parts per million the pulsar pulse is delayed in increments of *pP* in successive periods as shown in Figure A.1. These delays although small will tend to spread the observed pulse and reduce the summed amplitude. Similarly for increasing *p* producing a bell-shaped amplitude profile. The peaking effect is shown in PRESTO, but since we know the pulse width, with this analysis, the amplitude curve shape can be predicted with some accuracy. In addition, it is realized that for pulse train existing over the whole record, given a value of *p*, the apparent stretched pulse width and new pulse centre position can also be predicted. This additional predicted information for a continuous pulse train can be compared to actual results to add confidence in real pulsar presence.

In summary, referring to Figure A.1, for pulses,

1. When the folding period matches the pulsar period the pulsar pulses align in each fold window and add to maximize pulsar visibility.
2. Decreasing the fold period slightly causes the pulse to increasingly shift later within the fold period window smearing out the pulse.
3. The maximum shift occurs within the last fold period and totals, *NpP* where *pP* is the fold period shift and *N* is the total number of periods folded.
4. If *T* is the total observation time, then $N = T/P$ and the pulse total spread extent is *pT*, where, *p* is the search period change and is normally described in parts per million (ppm).
5. So with *p* ppm search period change the mean summed pulse width increases by *pT* and the pulse centre position changes to, $t_0 + pT/2$
6. Since the total integrated pulse power is constant, the resulting amplitude/period curve drops to one half when the observed pulse width, *W* doubles, or, $pT/W = 2$ (see Figure A.2.). So now we have a direct measure that confirms a pulsed signal is present for the record duration.
7. In practice the pulse extent and shape and amplitude change are affected by the pulsar scintillation amplitude along the record; at low signal-to-noise ratios it is also influenced by the underlying noise profile. Further variation occurs if reception is in drift-scan mode due to the receive antenna beam profile. To a first order however, this simple analysis describes the key properties observed in practice.

Assuming the pulsar pulse is similar to a Gaussian shaped pulse of equal half-height width *W*, the fold algorithm can be expressed as,

$$Fold(t) = \frac{1}{N}\sum_{n=1}^{N} A(n)\exp\left(-4\ln(2)\left[\frac{(t - t_0 + (n-1)pP)}{W}\right]^2\right) \qquad \text{(A.1)}$$

where, *t* is the time variable (bin) in a period

t_0 is the pulse position in a matched period

N is the total number of periods in the record, or *T* = *NP*.

n is the folded period number

P is the pulsar period

p is the period search factor

W is the pulsar pulse width

A(n) is the pulse amplitude in each period.

For modest signal-to-noise ratios this analysis provides measures useful for separating the pulsar pulse from large noise spikes or RFI by exploiting the characteristic amplitude, peak shift and shape around the search maximum.

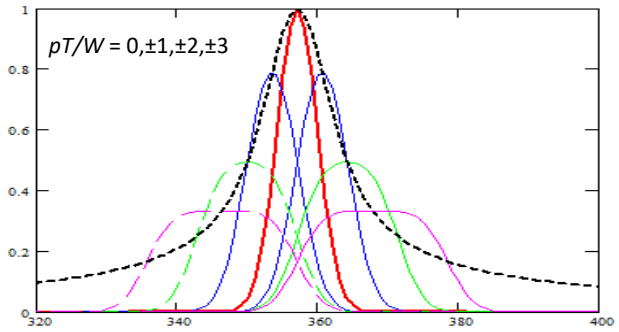

Figure A.2. Pulse Shift, Amplitude Shape and Width Change for, *pT/W* = 0,±1,±2,±3

Figure A.2 has been modelled assuming a Gaussian-shaped pulse; red, blue, green, magenta plot *pT/W* = 0,-1,-2,-3 (solid lines) and *pT/W* = 0,+1,+2,+3 (dotted lines) respectively. Figure A.2 shows (black dotted line) the peak amplitude profile and pulse peak shift as a function of period variation for the parameter, *pT/W*.

For example, the half height amplitude profile width (green plots) occurs when,

$$p = \pm 2W/T \qquad \text{(A.2)}$$

The half height width expected then is, $\Delta p = 4W/T$; dependant on the pulsar pulse width and record time. The response will however be modified by scintillation, antenna pattern in drift scan and the folded noise features and these should all be taken into The locus of the maxima shown in Figure A.2 (black dotted curve), is given by Equation A.1 when (t_0 - *t*) +(*n*-1)*pP* in the numerator is replaced by (t_0 - *t*)(1-*n/N*). account.

Appendix 2. Pulsar Matched-Filter Fold - MathCad Listing

MathCad program code, like pseudo code is easily translated into high level languages like Python or C.

B = number of bins, *M* = number of periods, *P* = test period, *Dat* = data file, *w* = pulse width, *Min*/*Max* = file min/max sample number.

$$\text{Fold}(B, M, P, Dat, Min, Max, w) :=$$

for $fs \in 0 .. M \cdot B - 1$

$\quad bdat_{fs} \leftarrow 0$

$\quad bcount_{fs} \leftarrow 0$

$\quad ffda_{fs} \leftarrow 0$

for $x \in Min .. Max - 1$

$\quad s \leftarrow \text{floor}\left[\left(\frac{x}{M \cdot P} - \text{floor}\left(\frac{x}{M \cdot P}\right)\right) \cdot M \cdot B\right]$

$\quad bdat_s \leftarrow bdat_s + Dat_x$

$\quad bcount_s \leftarrow bcount_s + 1$

for $b \in 0 .. M \cdot B - 1$

$\quad bindat_b \leftarrow \frac{bdat_b}{bcount_b}$

$\quad puls_b \leftarrow \exp\left[-4 \cdot \ln(2) \cdot \left(\frac{b - \frac{B \cdot M}{2}}{\frac{w}{1.25} \cdot \frac{B \cdot M}{P}}\right)^2\right]$

$fdat \leftarrow \text{cfft}(bindat)$

$fdat_0 \leftarrow 0$

$fpul \leftarrow \text{cfft}(puls)$

for $b \in 0 .. M \cdot B - 1$

$\quad mfdat_b \leftarrow fdat_b \cdot \left|\frac{fpul_b}{fpul_0 + 10^{-6}}\right|$

$tdat \leftarrow \text{icfft}(mfdat)$

$\text{Re}(tdat)$

Appendix 3. Data Compression/Fold Procedure (Method 2)

This second method sequence diagram is shown in Figure A.3.

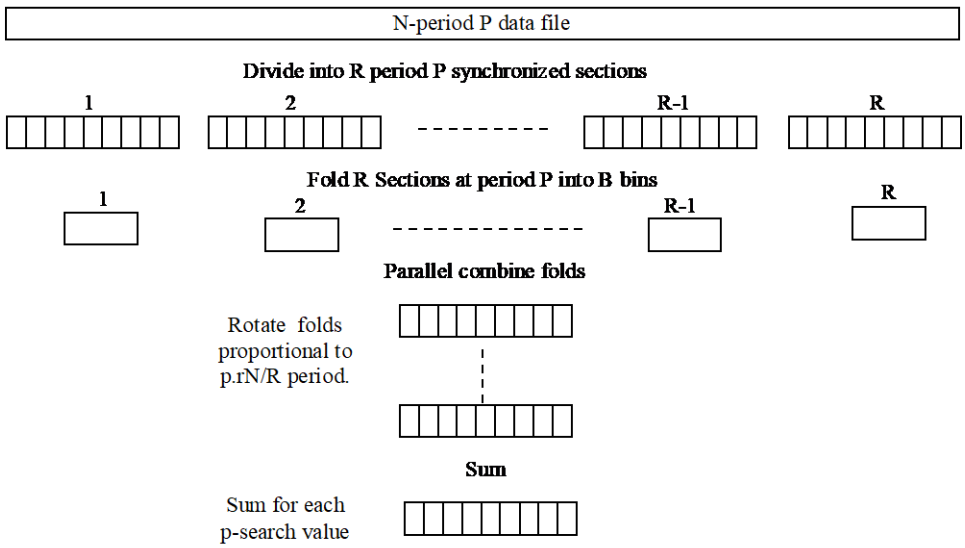

Figure A.3. Method 2 Sequence Diagram

The Method 2 processing sequence is,

1. Synchronously partition the data file into *R* sections as before. (*R* = *N*/*q*, where, *N* is the number of periods in the data file and *q* is calculated from Equation 1).
   As for Method 1, the batch Fold algorithm is applied.

$$Fb^{\langle r \rangle} := Fold\left[B, 1, P, Dat, r \cdot \frac{Mx}{R}, \frac{(r+1)\cdot Mx}{R}, pw\right] \qquad (A.3)$$

2. Define the section rotation function

$$Rot_r := \frac{N}{P} \cdot \frac{Mx}{2 \cdot R10^6} \cdot (1 + 2 \cdot r) \qquad (A.4)$$

3. Rotate section matrix terms and sum rotated sections to complete analysis.

$$Fp_{n,\,pp+PP} := \sum_{r=0}^{R-1} Fb_{mod(n+N+floor(pp \cdot Rot_r + .5),\,N),\,r} \qquad (A.5)$$

The final result is identical to that of Method 1 but may offer some computational advantages in some cases.

PW East September 2021

Peter East, *pe@y1pwe.co.uk* is retired from a Defense Electronics career in radar and electronic warfare system design. He has authored a book on Microwave System Design Tools, is a member of the British Astronomical Association since the early '70s and joined SARA in 2013. He has had a lifelong interest in radio astronomy; presently active in amateur detection of pulsars using SDRs, and researching low SNR pulsar recognition and analysis. He has recently written another book, 'Galactic Hydrogen and Pulsars - an Amateurs Radio Astronomy' describing his work in Radio Astronomy.
He maintains an active RA website at *http://www.y1pwe.co.uk*

Observation Reports

VHF Solar Radio Bursts Observed at Cohoe, Alaska on 26 August 2021

Whitham D. Reeve

A very strong Type V radio burst was observed at 2321 UTC on 26 August at Cohoe Radio Observatory (figure 1). A Type V solar radio burst is a short-lived continuum that is related to and follows some Type III radio sweeps. They do not occur in isolation and have no or weak polarization. An optical flare was observed concurrent with the Type V, and a Type II slow-drift burst followed a few minutes later at 2329. It is interesting that no coronal mass ejection was observed concurrent with the Type II burst. At the time of the Type V observations at Cohoe, the Sun was about 40° above the horizon and only a few degrees past transit at 187° True azimuth.

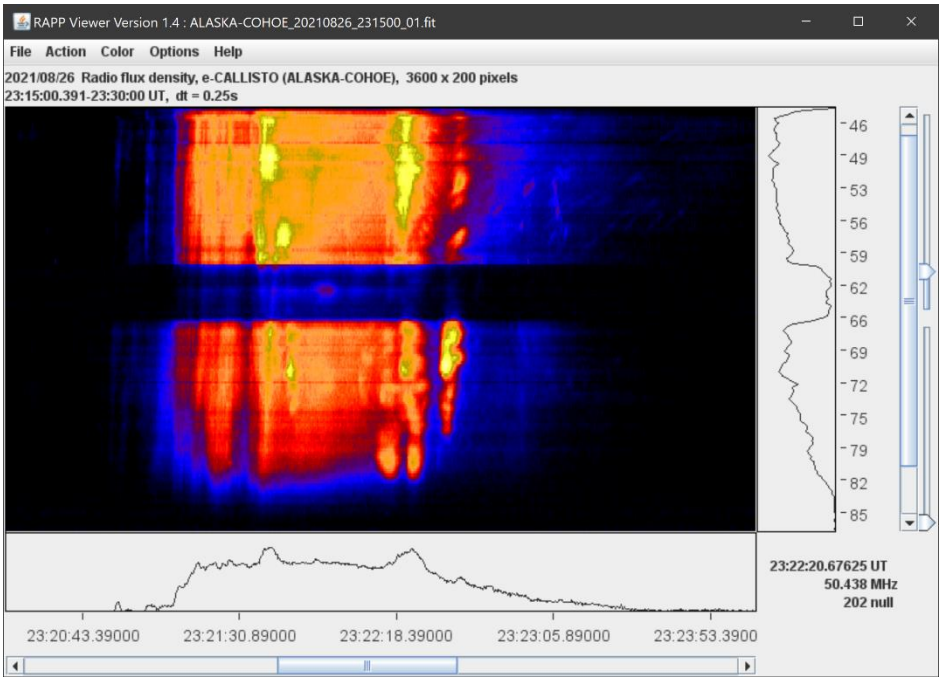

Figure 1 ~ Type V fast-drift radio bursts observed between 45 and 85 MHz. Frequency in MHz is shown on the right vertical scale and time in UTC is on the horizontal scale at the bottom. The colors indicate relative intensity with black-blue being lower and red-yellow being higher. The text in the lower-right corner indicates the time, frequency and relative intensity of the cursor location when the image was taken (the cursor is not visible in these images). The gap between 60 and 66 MHz is caused by intermodulation in the antenna active electronics from nearby FM broadcast transmitters.

According to the Space Weather Prediction Center's Events report {SWPC-EVNT}, the whole day was filled with solar radio activity including numerous Type III and Type VI radio sweeps and also radio bursts measured at discrete frequencies up to 8800 MHz. See {SOLAR} for information on the types and characteristics of other solar radio emissions.

Also of interest on 26 August was a series of Type III fast-drift radio bursts observed at 1816 UTC (figure 2), several hours earlier than the Type V burst described above. The almost equal time spacing between each burst is unusual but likely coincidental. At the time of these Type III observations at Cohoe, the Sun was about 25° above the horizon and 113° True azimuth. The Type III bursts actually were a part of a Type VI burst lasting from 1814 to 1830, but CRO did not observe the extended burstiing associated with a Type VI.

Instrumentation: An LWA crossed-dipole antenna and two Callisto spectrometers were used for these observations (figure 3). The Callistos have an instantaneous bandwidth of 300 kHz and an integration time of 1 ms. The Callisto software collects data as Flexible Image Transport System (FITS) files, which are stored locally. The files also are uploaded automatically to Fachhochschule Nordwestschweiz (FHNW) University of Applied Sciences & Arts website {FHNW} for permanent archiving.

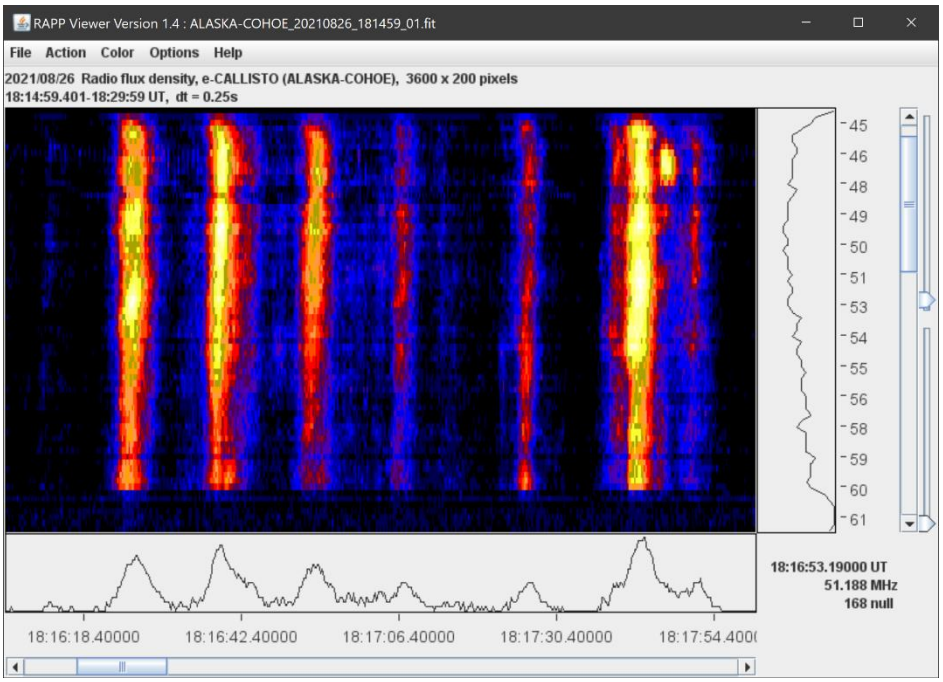

Figure 2 ~ Series of Type III radio sweeps. The first five bursts, starting with the weak indication on the far left, have remarkably equal spacing. The time spacings determined by visual analysis are 13.0, 13.0, 14.3, 13.3, 21.3, 14.3 and 8.8 seconds. The average spacing is 14.0 seconds and the standard deviation is 3.4 seconds. This and the previous image are screenshots of the RAPP Viewer software.

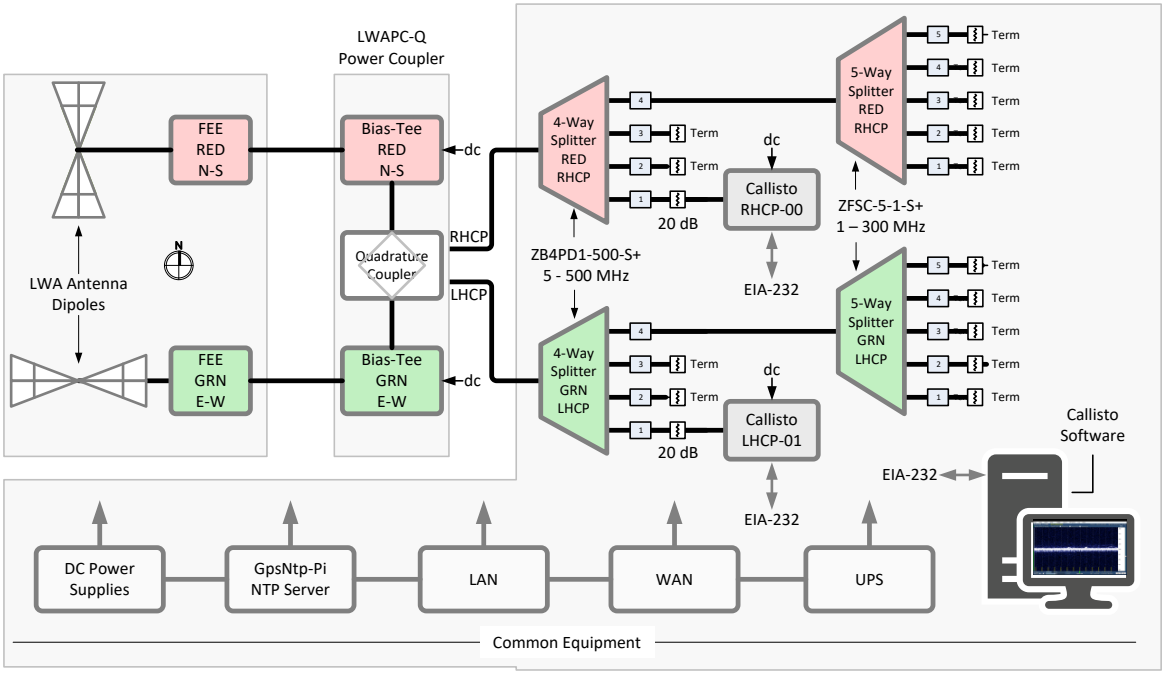

Figure 2 ~ System block diagram shows the components associated with the LWA Antenna and Callisto instruments and the common equipment shared across the observatory. Polarizations are color-coded: Red, RHCP; Green, LHCP. Image © 2021 W. Reeve

References & Weblinks:

{SWPC-EVNT} ftp://ftp.swpc.noaa.gov/pub/indices/events/

{SOLAR} http://www.reeve.com/Solar/Solar.htm

Geomagnetic Activity Observed at Anchorage, Alaska on 27 & 28 August 2021

Whitham D. Reeve

A geomagnetic transient was recorded by the Anchorage SAM-III magnetometer at 0115 UTC on 27 August, likely caused by the coronal mass ejection on 23 August (figure 1). The CME was from an eruptive filament that was observed off the Sun's northern limb by the SOHO/LASCO C2 spacecraft {SWPC}.

Even though the CME's embedded magnetic field had a significant southward component of –10 to –15 nT for several hours after arrival, the CME impact at Earth had little effect at first. However, about 8 hours later, the measured magnetic flux density at Anchorage rapidly decreased on all three magnetic axes. The dive started at solar midnight (1000 UTC, 2:00 am local), possibly indicating reconnection activity in the magnetotail. The negative deflection peaked at 1100 UTC. Disturbed conditions continued into the next day and finally settled down about mid-UTC day on 28 August (figure 2), corresponding to the early morning hours locally.

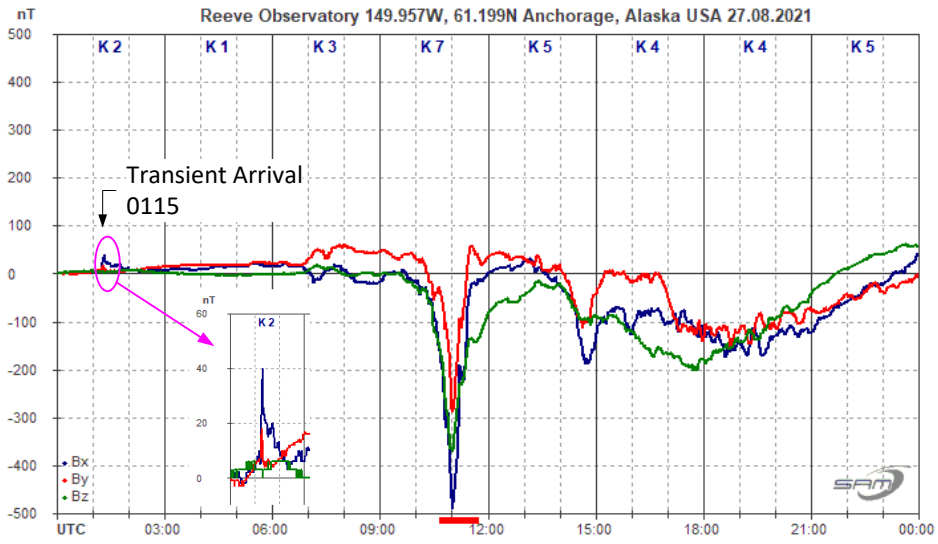

Figure 1 ~ Normalized magnetogram for 27 August 2021. An initial transient, similar to a sudden impulse, of +40 nT was recorded at 0115 UTC, likely caused by impact of the CME from 23 August. Geomagnetic storm conditions followed about 8 hours later with a rapid –500 nT change in magnetic flux density at 1100. Storm conditions continued until about 1500, when they temporarily abated until 2100 when they continued until the end of day.

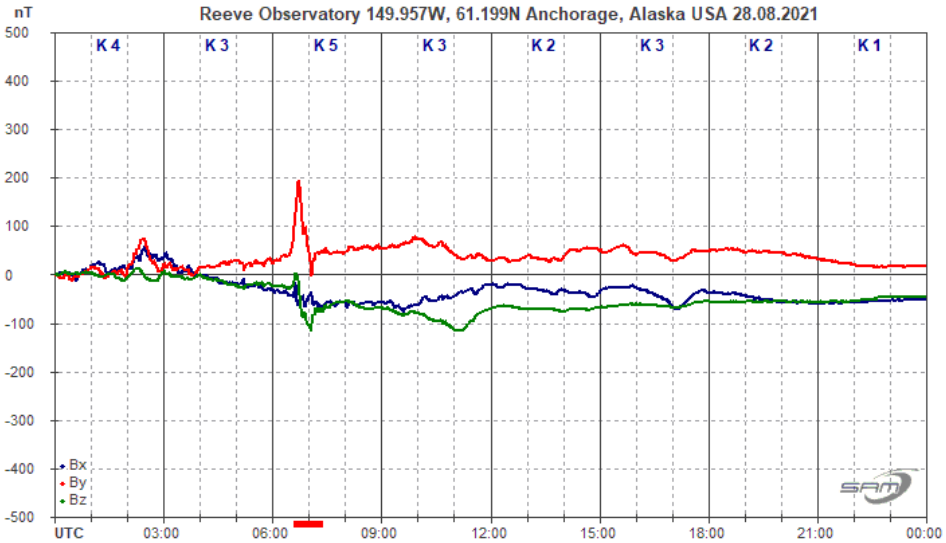

Figure 2 ~ Normalized magnetogram for 28 August 2021 set to the same scale as the previous figure. The disturbed conditions from the day before continued with a +200 nT deflection on the By (east-west) component just before 0700. Storm conditions, indicated by a K-index of 5, returned for the synoptic period 0600 to 0900 but the remainder of the day showed only relatively minor disturbances and background levels by end of day.

Instrumentation: Observations were made with a SAM-III magnetometer, which is configured for the geographic coordinate system: Bx (north-south), By (east-west) and Bz (vertical) {SAM-III}. The data was collected by the SAM_VIEW application software supplied with the magnetometer. The instrumentation block diagram is shown in figure 3.

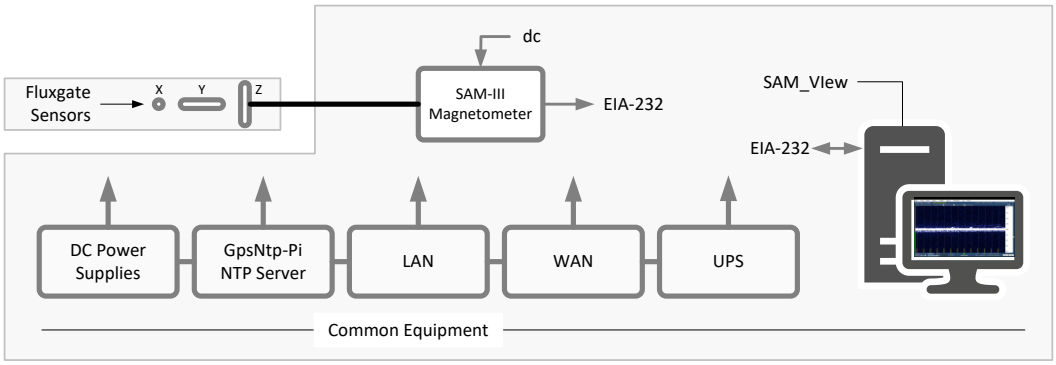

Figure 3 ~ System block diagram of the instruments used in the observations along with the common equipment shared across the observatory. The SAM-III sensors are buried about 1 m below ground to reduce temperature effects. Image © 2021 W. Reeve

Readers interested in geomagnetism may find the tutorial at {Reeve15} useful.

References & Weblinks:

{Reeve15} Reeve, W., Geomagnetism Tutorial, 2015, available at: http://www.reeve.com/Documents/SAM/GeomagnetismTutorial.pdf
{SAM-III} http://www.reeve.com/MagnetometerM3.htm
{SWPC} ftp://anonymous@ftp.swpc.noaa.gov/pub/forecasts/discussion/

Meteor Trail Reflections Observed at 25 MHz on 29 September 2021

Whitham D. Reeve

A series of short-duration meteor trail reflections (echoes) were observed at Anchorage, Alaska near the end of September (figures 1). The reflections were observed between about 1800 and 2100 UTC (8 am and 11 am local solar time) but the peak was between 1811 and 1911 UTC. The carrier frequencies 15 and 20 MHz (WWV and WWVH) and 25 MHz (WWV only) are continuously recorded, but only 25 MHz produced the meteor echoes shown here. WWV is about 3800 km east of Anchorage (figure 3).

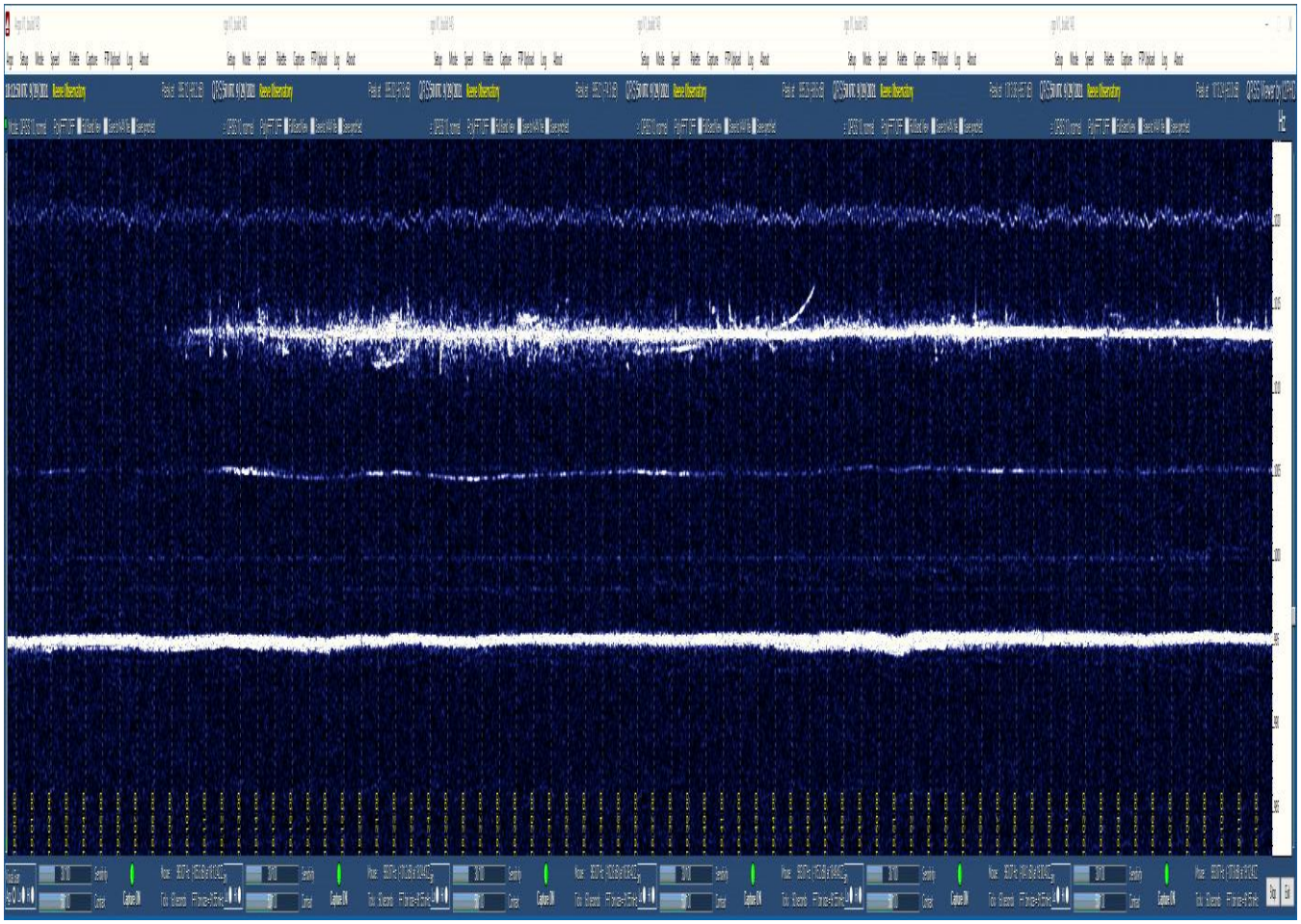

Figure 1 ~ Six spliced 12-minute Argo plots from 29 September 2021 beginning at 1800 and ending at 1912 UTC. The images have been stretched vertically to enhance the signal indications. The many blips and ticks on the upper trace are short-duration meteor trail reflections at 25 MHz. The intermittent trace in the middle is 20 MHz and the thick lower trace is 15 MHz. The long, curved indication at the center of the 25 MHz trace may be an airplane. Note that, although the 20 MHz signal is very weak, it started to appear at about the same time as the 25 MHz trace, indicating propagation conditions simultaneously supported or partially supported both frequencies at 1810 UTC, but only 25 MHz had the correct geometry for receiving meteor trail reflections.

Meteor echoes are received at Anchorage in the HF range only when propagation conditions provide suitable path geometry as explained in {Reeve21}. The radiant of the meteors in not known but the Orionids and Sextantids showers were predicted to be active {MetNws}. It is possible that sporadic meteors and not shower meteors were detected.

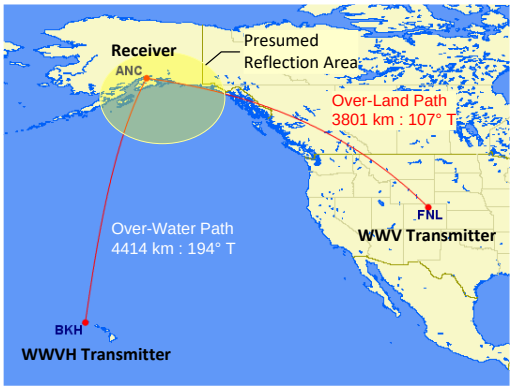

Figure 3 ~ Great circle path shown in red between WWV near Fort Collins, Colorado (FNL) and Anchorage (ANC). The presumed reflection area is shown by the yellow oval. The WWV path length is 3801 km and entirely over land. Also shown is the 4414 km long overwater path between WWVH near Kekaha, Kauai, Hawaii (BKH) and Anchorage. Both paths are long enough to require multi-hop propagation. Anchorage is at the southern edge of the auroral oval, which introduces additional complicating factors in HF propagation. Image from {GCMap}.

The echoes at 25 MHz were observed with an Icom R-8600 wideband receiver tuned to 25 001 014 Hz and set to LSB mode, thus producing a 1014 Hz beat note that is displayed by Argo software. Three receivers cover the previously mentioned carrier frequencies, and each uses a different frequency offset so that the signal traces are at different positions on the plot. The 15 and 25 MHz receivers are operated with the Preamp Off and the 20 MHz receiver (Icom R-75) has the Preamp On. The antenna is an 8-element log periodic dipole array with an 8-port receiver multicoupler. A block diagram shows the general setup (figure 4).

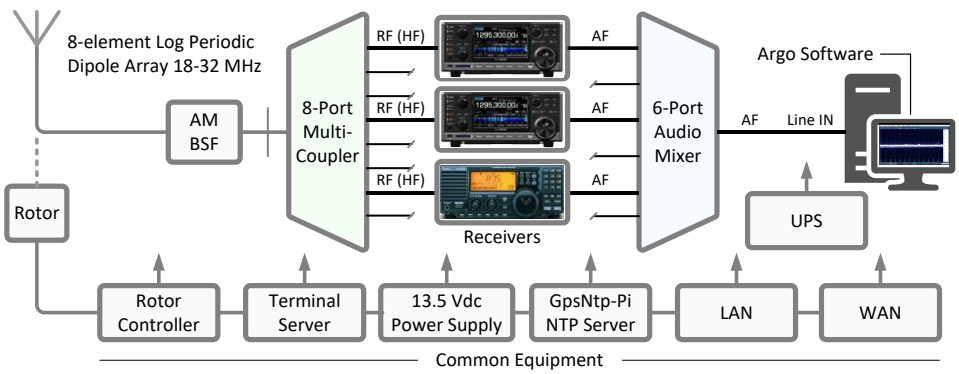

Figure 4 ~ Receiver and antenna system block diagram. PC timing is controlled by two GPS receiver-based network time servers. Common equipment includes infrastructure shared with other observatory equipment. The antenna usually is rotated to point at WWV on a true azimuth of 107°. Image ©2020 W. Reeve

Argo is setup for QRSS10 mode and adjusted to display a frequency span of 982 to 1025 Hz, which encompasses the receiver settings mentioned above. Near real-time Argo images may be found at the Reeve Meteor webpage at {Meteor}. The best time to observe meteor trail reflections at Anchorage is between about 1400 and 1900 UTC (0400 to 0900 local solar time).

Weblinks and references:

{GCMap} http://www.gcmap.com/mapui?P=FNL-anc-bkh
{Meteor} http://www.reeve.com/Meteor/Meteor_simple.html
{MetNws} https://www.meteornews.net/2021/09/24/meteor-activity-outlook-for-25-september-1-october-2021/
{Reeve21} Reeve, W., HF Meteor Trail Reflections Observed at Anchorage, Alaska USA, 2021, available at: https://www.reeve.com/Documents/Articles%20Papers/Reeve_MeteorRadioObsrv.pdf

Possible Observation of a FRB Using Radio Jove Technology

James Van Prooyen N8PQK

July 17, 2021

Summary: This is a report of a possible observation of a Fast Radio Burst (FRB) using the Radio Jove receiver and an add-on detector box. It appears that a FRB may have been detected. This report will give details.

Receiver and Detection Box: A detector box was created to allow the Radio Jove system to be used to observe events occurring over very short intervals of time. The "Detection box" feeds an A/D and a USB interface to a computer. A picture of the "Detection Box" is shown below.

The detector box has two options the 0.001 integration time options was used.
A/D: The A/D is a DATAQ DM-1100 and is pictured below:

Software: The software used for this observation was WINDAQ Version 3.09. Observations from the WINDAQ were plotted using MS Excel.

Observation Data: Data was taken at 1000 samples per second, with the output from the Radio Jove receiver routed through the Detection Box to the A/D and the computer. Radio Frequency was ~ 20.1 MHz. Date was June 19, 2021; time was between 12:30 AM ET (0430 GMT) and 2:30 AM ET (0630 GMT). A single Radio Jove dipole antenna was used. Shown below is plot of the full data set for the observation

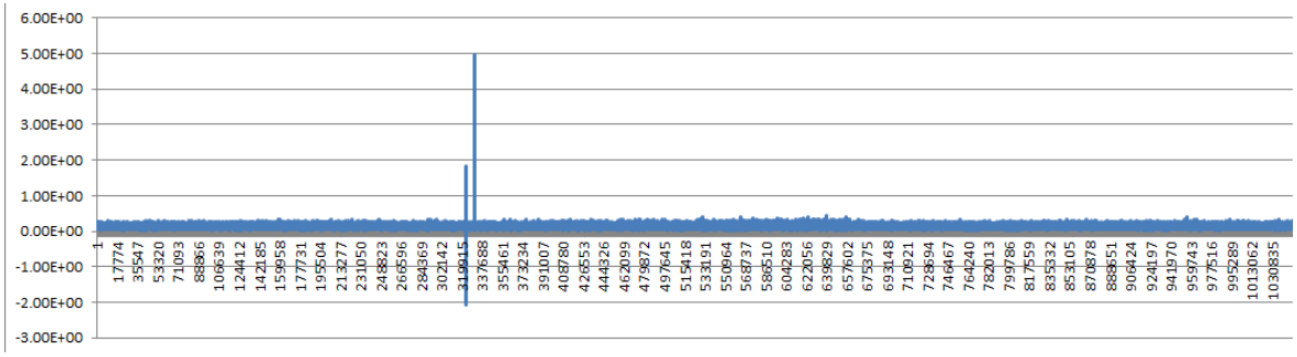

There were two events detected the first is an ionosonde and is well known. Here is a detailed plot of the 2nd event from the plot shown above:

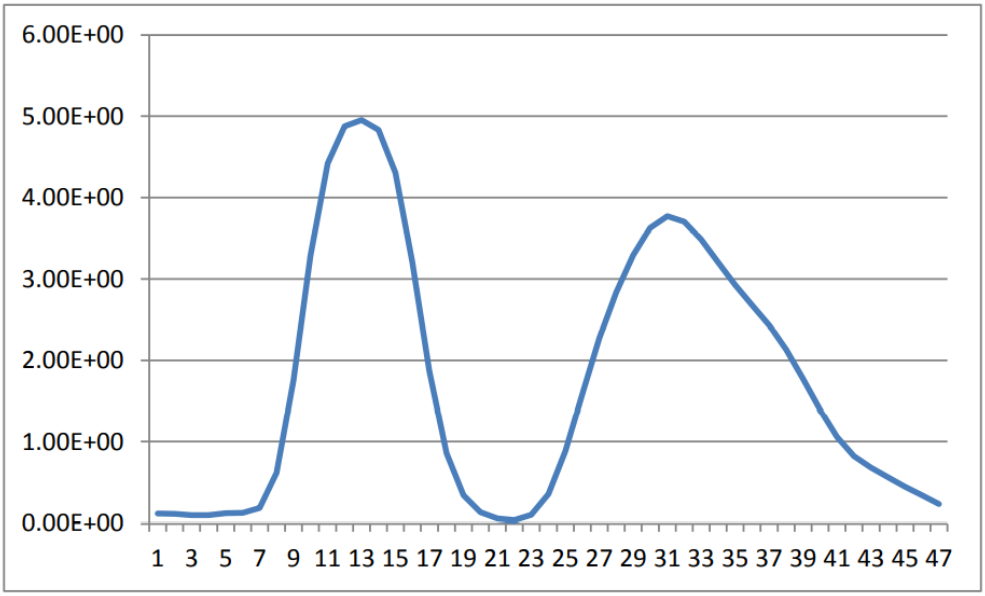

Several factors are pointing to the possibility that this could be FRB200428:
-The length of the event ~40 milliseconds.
-The fact that it was a double pulse, somewhat unique to this FRB.
-This is a known repeater with a period of ~16.4 days.
-It was high in the sky at the time of observation.
-It is thought to be located in our galaxy.
-It is full scale in the A/D; this FRB is the same when I look at 406 MHz (i.e. full scale on the A/D).
-Some FRB's are known to have very high flux values -We also have data from the CHIME radio telescope shown below

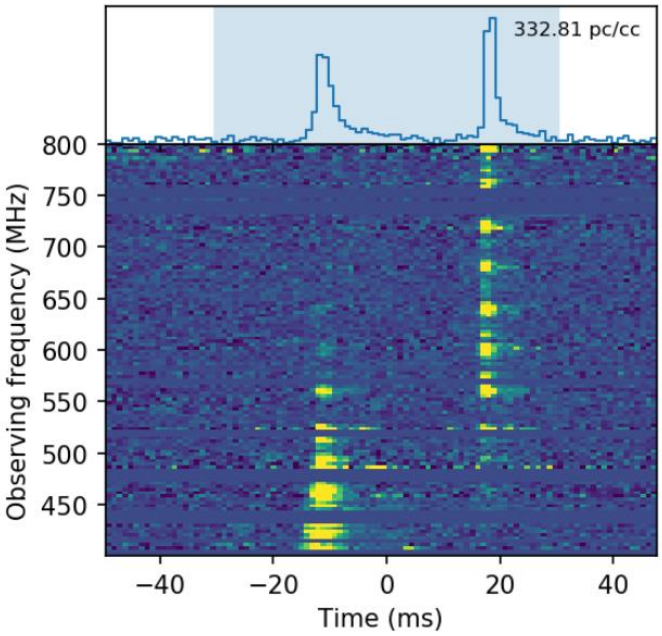

Reference: https://briankoberlein.com/blog/closer-to-home/
The above listed facts are not proof, but it is a very strong case of circumstantial evidence that this could be a FRB detection using Radio Jove system.
The only way to be sure if such an event is a FRB is to measure dispersion. We are in the process of building hardware and software to make this measurement in the future.
James Van Prooyen N8PQK
grro@sbcglobal.net

Membership

New Members

Please welcome our new or returning SARA members who have joined since the last journal. If your name is missing or misspelled, please send an email to treas@radio-astronomy.org. We will make sure it appears correctly in the next Journal issue.

First name	Last name	City	State	Country	Call Sign
Ellis	Lindsey	Indianapolis	IN	USA	KD9NOJ
Anthony	Fuller	Roswell	GA	USA	
John	MacDonald	Fort Myers	FL	USA	
Donald	Daughdrill	Troy	VA	USA	KN4JZW
Marcello	Montisci	Leini		Italy	
Leonard	Cacciatore	Hillsborough	NJ	USA	
Michael	Day	Florissant	MO	USA	
Randy	Hale	Murfreesboro	TN	USA	WA4UNH

Membership dues are $20.00 US per year and all dues expire in June. Student memberships are $5.00 US per year. Memberships must be renewed in June of each year. Or pay once and never worry about missing your dues again with the SARA Life Membership. SARA Life Memberships are now offered for a one-time payment of twenty times the basic annual membership fee (currently $400 US).

Journal Archives & Other Promotions

The rich and diverse legacy of member contributed content is available in the SARA Journal Archives. Table of contents for journals is available online at radio-astronomy.org/store.

The entire set of The Journal of The Society of Amateur Radio Astronomers is available on USB drive. It goes from the beginning of 1981 to the end of 2017 (over 6000 pages of SARA history!) Or you can choose one of the following USB drive's or DVD:* (Prices are US dollars and include postage.)

*All SARA journals and conference proceedings are available through the previous calendar year.

Prices, US dollars, including postage

Members	
Each USB drive	$15.00
USB drive + 1-year membership extension	$30.00
Non-members	
Each USB drive	$25.00
USB drive + 1-year membership	$30.00
Non-USA members	
Each USB drive	$20.00 (airmail)
USB drive+ 1-year members extension	$35.00

*Already a member and want any or all these USB drives or DVD's? Buy any one for $15.00 or get any three for $35.00.

SARA Store (radio-astronomy.org/store.)

SARA offers the above USB drives, DVDs, printed Proceedings and Proceedings on USB drive and other items at the SARA Store: http://www.radio-astronomy.org/e-store. Proceeds from sales go to support the student grant program. Members receive an additional 10% discount on orders over $50 US. Payments can be made by sending payment by PayPal to treas@radio-astronomy.org or by mailing a check or money order to SARA, c/o Brian O'Rourke, 337 Meadow Ridge Rd, Troy, VA 22974-3256

SARA Online Discussion Group
SARA members participate in the online forum at http://groups.google.com/group/sara-list. This is an invaluable resource for any amateur radio astronomer.

SARA Conferences
SARA organizes multiple conferences each year. Participants give talks, share ideas, attend seminars, and get hands-on experience. For more information, visit http://www.radio-astronomy.org/meetings.

Facebook
Like SARA on Facebook
http://www.facebook.com/pages/Society-of-Amateur-Radio-Astronomers/128085007262843

Twitter
Follow SARA on Twitter@RadioAstronomy1

What is Radio Astronomy?

This link is for a booklet explaining the basics of radio astronomy.
http://www.radio-astronomy.org/pdf/sara-beginner-booklet.pdf

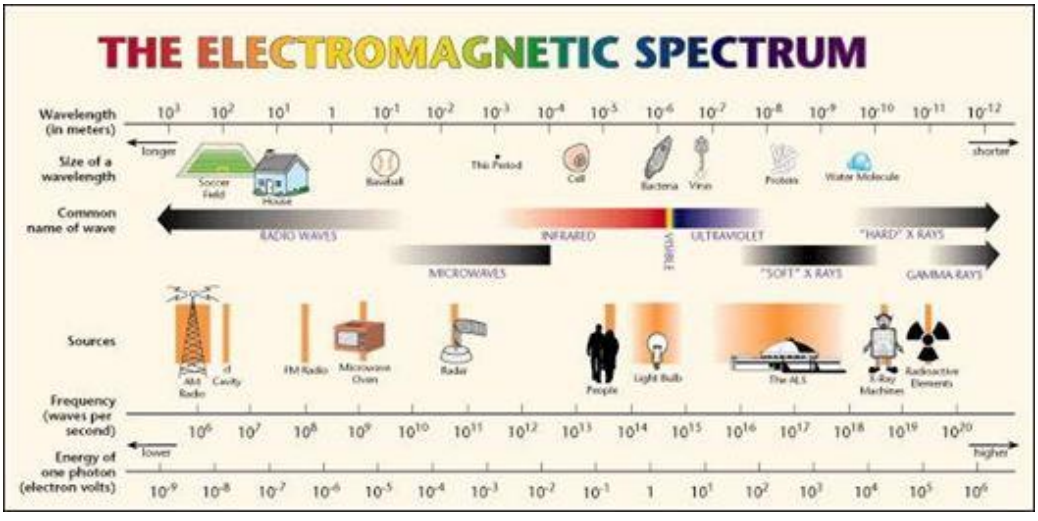

Administrative

Officers, directors, and additional SARA contacts

The Society of Amateur Radio Astronomers is an all-volunteer organization. The best way to reach people on this page is by email with SARA in the subject line SARA Officers.

President: Dennis Farr, WB4RJK, http://www.radio-astronomy.org/contact/President +1 813 833-3918
Vice President: Dr. Rich Russel, AC0UB http://www.radio-astronomy/contact/Vicepresident
Secretary: Bruce Randall, NT4RT, http://www.radio-astronomy/contact/Secretary +1 803-327-3325
Treasurer: Brian O'Rourke, K4UL, http://www.radio-astronomy/contact/Treasurer
Past President: Ken Redcap, tbd@radio-astronomy.org +1 319-591-1131
Founder Emeritus and Director: Jeffrey M. Lichtman, KI4GIY, jeff@radioastronomysupplies.com +1 954-554-3739

Board of Directors

Name	Term expires	Email
Ed Harfmann	2022	edharfmann@comcast.net
Dr. Wolfgang Herrmann	2023	messbetrieb@astropeiler.de
Tom Jacobs	2023	tdj0@bellsouth.net
Charles Osborne	2023	k4cso@charter.net
Keith Payea	2022	kbpayea@bryantlabs.net
Steve Tzikas	2022	Tzikas@alum.rpi.edu
Jon Wallace	2023	wallacefj@comcast.net
David Westman	2022	david.westman@engineeringretirees.org

Other SARA Contacts

All Officers	http://www.radio-astronomy.org/contact-sara	
All Directors and Officers	http://www.radio-astronomy.org/contact/All-Directors-and-Officers	
Eastern Conference Coordinator	http://www.radio-astronomy.org/contact/Annual-Meeting	
All Radio Astronomy Editors	http://www.radio-astronomy.org/contact/Newsletter-Editor	
Radio Astronomy Editors	Dr. Richard A. Russel	drrichrussel@netscape.net
Contributing Editor	Whitham D. Reeve	whitreeve@gmail.com
Educational Outreach	http://www.radio-astronomy.org/contact/Educational-Outreach	
Grant Committee	Tom Crowley	grants@radio-astronomy.org
Membership Chair	http://www.radio-astronomy.org/contact/Membership-Chair	
Technical Queries (David Westman)	http://www.radio-astronomy.org/contact/Technical-Queries	
Webmaster	Ciprian (Chip) Sufitchi, N2YO	webmaster@radio-astronomy.org

Resources

Great Projects to Get Started in Radio Astronomy

Radio Observing Program

The Astronomical League (AL) is starting a radio astronomy observing program. If you observe one category, you get a Bronze certificate. Silver pin is two categories with one being personally built. Gold pin level is at least four categories. (Silver and Gold level require AL membership which many clubs have membership. For the bronze level, you need not be a member of AL.)

Categories include
1) SID
2) Sun (aka IBT)
3) Jupiter (aka Radio Jove)
4) Meteor back-scatter
5) Galactic radio sources

This program is a collaboration between NRAO and AL. Steve Boerner is the Lead Coordinator and a SARA member.

For more information:
Steve Boerner
2017 Lake Clay Drive
Chesterfield, MO 63017
Email: sboerner@charter.net
Phone: 636-537-2495
http://www.astroleague.org/programs/radio-astronomy-observing-program

Radio Jove

The Radio Jove Project monitors the storms of Jupiter, solar activity and the galactic background. The radio telescope can be purchased as a kit or you can order it assembled. They have a terrific user group you can join.
http://radiojove.gsfc.nasa.gov/

INSPIRE Program

The INSPIRE program uses build-it-yourself radio telescope kits to measure and record VLF emissions such as tweeks, whistlers, sferics, and chorus along with man-made emissions. This is a very portable unit that can be easily transported to remote sites for observations.
http://theinspireproject.org/default.asp?contentID=27

SARA/Stanford SuperSID

Stanford Solar Center and the Society of Amateur Radio Astronomers have teamed up to produce and distribute the SuperSID (Sudden Ionospheric Disturbance) monitor. The monitor utilizes a simple pre-amp to magnify the VLF radio signals which are then fed into a high definition sound card. This design allows the user to monitor and record multiple frequencies simultaneously. The unit uses a compact 1-meter loop antenna that can be used indoors or outside. This is an ideal project for the radio astronomer that has limited space. To request a unit, send an e-mail to supersid@radio-astronomy.org

Radio Astronomy Online Resources

AJ4CO Observatory – Radio Astronomy Website: http://www.aj4co.org/	National Radio Astronomy Observatory http://www.nrao.edu
Radio Astronomy calculators http://www.aj4co.org/Calculators/Calculators.html	NRAO Essential Radio Astronomy Course http://www.cv.nrao.edu/course/astr534/ERA.shtml
Introduction to Amateur Radio Astronomy (presentation) http://www.aj4co.org/Publications/Intro%20to%20Amateur%20Radio%20Astronomy,%20Typinski%20(AAC,%202016)%20v2.pdf	Exotic Ions and Molecules in Interstellar Space -- ORION 2020 10 21. Dr. Bob Compton https://www.youtube.com/watch?v=r6cKhp23SUo&t=5s
RF Associates Richard Flagg, rf@hawaii.rr.com 1721-1 Young Street, Honolulu, HI 96826	The Radio JOVE Project & NASA Citizen Science – ORION 2020.6.17. Dr. Chuck Higgins https://www.youtube.com/watch?v=s6eWAxJywp8&t=5s
RFSpace, Inc. http://www.rfspace.com	UK Radio Astronomy Association http://www.ukraa.com/
CALLISTO Receiver & e-CALLISTO http://www.reeve.com/Solar/e-CALLISTO/e-callisto.htm	CALLISTO software and data archive: www.e-callisto.org
Deep Space Exploration Society http://DSES.science	Radio Astronomy Supplies http://www.radioastronomysupplies.com
Deep Space Object Astrophotography Part 1 -- ORION 2021 02 17. George Sradnov https://www.youtube.com/watch?v=Pm_Rs17KIyQ	Radio Jove Spectrograph Users Group http://www.radiojove.org/SUG/
European Radio Astronomy Club http://www.eracnet.org	Radio Sky Publishing http://radiosky.com
British Astronomical Association – Radio Astronomy Group http://www.britastro.org/baa/	The Arecibo Radio Telescope; It's History, Collapse, and Future - ORION 2020.12.16. Dr. Stan Kurtz, Dr. David Fields https://www.youtube.com/watch?v=rBZlPOLNX9E
Forum and Discussion Group http://groups.google.com/group/sara-list	Shirleys Bay Radio Astronomy Consortium marcus@propulsionpolymers.com
GNU Radio http://www.gnu.org/licenses/gpl.html	SARA Twitter feed https://twitter.com/RadioAstronomy1
SETI League http://www.setileague.org	SARA Web Site http://radio-astronomy.org
NRAO Essential Radio Astronomy Course http://www.cv.nrao.edu/course/astr534/ERA.shtml	SARA Facebook page https://www.facebook.com/pages/Society-of-Amateur-Radio-Astronomers/128085007262843
NASA Radio JOVE Project http://radiojove.gsfc.nasa.gov Archive: http://radiojove.org/archive.html	Simple Aurora Monitor: Magnetometer http://www.reeve.com/SAMDescription.htm
National Radio Astronomy Observatory http://www.nrao.edu	Stanford Solar Center http://solar-center.stanford.edu/SID/
A New Radio Telescope for Mexico - ORION 2021 01 20. Dr. Stan Kurtz https://www.youtube.com/watch?v=Q9aBWr1aBVc	

For Sale, Trade and Wanted

At the SARA online store: radio-astronomy.org/store.

SARA Polo Shirts

New SARA shirts have arrived.

We now have a good selection of X, XX, and XXX shirts available in all colors including white!

Shirts are $20 at the conference and $25 shipped.

Contact the treasurer at treas@radio-astronomy.org for availability and shipping.

Scope in a Box $295

radio-astronomy.org/store.

Kit of parts and software to build a working Radio Telescope to detect Hydrogen Line emissions. Available to USA addresses only at this time.

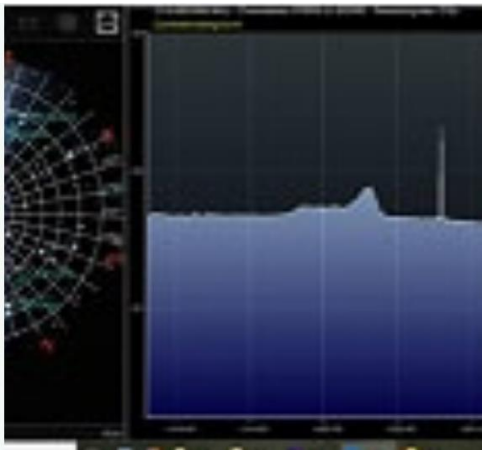

SuperSID Complete Kit ($112-$160 depending on options)
radio-astronomy.org/store.

SARA Publication, Journals and Conference Proceedings (various prices)
radio-astronomy.org/store.

SARA Journal USB Drive ($15-$35 depending on shipping option)
radio-astronomy.org/store.

The USB drive covers the society journal "Radio Astronomy" from the founding of the organization in 1981 thru 2020. Articles cover a wide range of topics including: cosmic radiation, pulsars, quasars, meteor detection, solar observing, Jupiter, Radio Jove, gamma ray bursts, the Itty Bitty Telescope (IBT), dark matter, black holes, the Jansky antenna, methanol masers, mapping at 408 MHz and more. This CD contains all of the above and more with over 4800 pages of articles on radio astronomy. Also included is a copy of Grote Reber's handwritten, 34 page document "Carriage and Mirror Detail" of his historic antenna now on display at the National Radio Astronomy Observatory (NRAO) in Green bank, WV. You also get an electronic copy of the 109 page "Basics of Radio Astronomy" from JPL Goldstone-Apple Valley Radio Telescope. Also included is the NRAO 40-foot radio telescope "Operators Manual", which by the way, you get to operate if you attend the Eastern SARA conference in July.

SARA Advertisements

There is no charge to place an ad in Radio Astronomy; but you must be a current SARA member. Ads must be pertinent to radio astronomy and are subject to the editor's approval and alteration for brevity. Please send your "For Sale," "Trade," or "Wanted" ads to edit@radio-astronomy.org. Please include email and/or telephone contact information. Please keep your ad text to a reasonable length. Ads run for one bimonthly issue unless you request otherwise.

Radio-Astro-Machine, zzblac@gmail.com
Elevation rotation adapter plate for Scope in a Box and custom machining. For further information visit https://radio-astro-machine.wixsite.com/my-site or send an email.

Typinski Radio Astronomy, Inc., info@typinski.com
Antenna systems and feed line components for HF radio astronomy

Jeff Kruth, WA3ZKR, kmec@aol.com
RF components from HF to MMW, various types including mixers, RF switches, amplifiers, oscillators, coaxial components, waveguide components, etc. I have a very large collection of stuff and the facilities to test and provide data. Please email with your needs and I will see if I have something for you. Have fun!

Stuart and Lorraine Rumley, sales@valontechnology.com
The Valon Technology 2100 Downconverter, when combined with our 5009 frequency synthesizer module, provides a high-performance, compact receiver downconverter system. Applications include hydrogen line studies at 1420MHz and radio astronomy in the protected 30MHz segment of the 21 cm band. For more information visit http://www.valontechnology.com/2100downconverter.html or send an email.

Radio2Space, filippo.bradaschia@primalucelab.com
SPIDER radio telescopes and turn-key-systems designed specifically for education.
https://www.radio2space.com
We developed our SPIDER radio telescopes as turn-key-system just to avoid the problem you perfectly highlighted in your website: "Purchasing a radio telescope isn't like buying an optical telescope. They are harder to find, and usually require assembly and software troubleshooting. In some cases, a radio telescope must be built from components." Our SPIDER radio telescopes are not designed for amateurs that prefer to build a radio telescope but to schools, universities, museums, and other science institutes that needs for a complete and ready-to-use system, just like the optical telescopes they can normally buy!

Radio Astronomy Supplies
http://www.radioastronomysupplies.com
jeff@radioastronomysupplies.com
Research and Educational Radio Telescopes and all associated equipment since 1994

Membership Information

Annual SARA dues Individual $20, Classroom $20, Student $5 (US funds) anywhere in the world. Membership includes a subscription to Radio Astronomy, the bimonthly Journal of The Society of Amateur Radio Astronomers, delivered electronically (via a secure web link, emailed to you as each new issue is posted). We regret that printing and postage costs prevent SARA from providing hardcopy subscriptions to our Journal.

We would appreciate the following information included with your check or money order, made payable to SARA:

Name: _____

Email Address : _____
(required for electronic Journal delivery)

Ham call sign: _____ (if applicable)

Address: _____

City: _____

State: _____

Zip: _____

Country: _____

Phone: _____

Please include a note of your interests. Send your application for membership, along with your remittance, to our Treasurer.

For further information, see our website at:
http://radio-astronomy.org/membership

How to get started?

SARA has a made a kit of software and parts to detect the Hydrogen line signal from space. This is an excellent method to get started in radio astronomy. It teaches the principles of antenna design, signal detection, and signal processing. Read more about this and other projects on our web site.

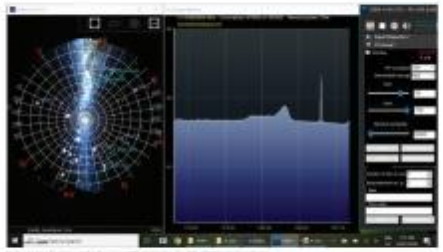

Society of Amateur Radio Astronomers, Inc.
Founded 1981

Membership supported, nonprofit [501(c) (3)]
Educational and Radio Astronomy Organization

Knowledge through Common Research, Education and Mentoring

SARA members have been privileged to use this forty foot diameter drift-scan hydrogen line radio telescope every year at their annual meeting in Green Bank.

http://radio-astronomy.org

Why Radio Astronomy?

Because about sixty five percent of our current knowledge of the universe has stemmed from radio astronomy alone. The discovery of quasars, pulsars, black holes, the 3K background from the "Big Bang" and the discovery of biochemical hydrogen/carbon molecules are all the result of professional radio astronomy.

The Society of Amateur Radio Astronomers

SARA was founded in 1981, with the purpose of educating those interested in pursuing amateur radio astronomy.

The society is open to all, wishing to participate with others, worldwide.

SARA members have many interests, some are as follows:

SARA Areas of Study and Research:

- Solar Radio Astronomy
- Galactic Radio Astronomy
- Meteor Detection
- Jupiter
- SETI
- Gamma Ray/High Energy Pulse
- Detection
- Antennas
- Design of Hardware / Software

The members of the society offer a friendly mentor atmosphere. All questions and inquiries are answered in a constructive manner. No question is silly!

SARA offers its members an electronic bi-monthly journal entitled Radio Astronomy. Within the journal, members report on their research and observations. In addition, members receive updates on the professional radio astronomy community and, society news.

Once a year SARA meets for a three-day conference at the Green Bank Observatory in Green Bank West Va.

There is also a spring conference held at various cities in the Western USA. Previous meeting have been at the VLA in Socorro, NM and at Stanford University.

How do I get started?

Just as a long journey begins with the first step, the project you elect must start with a clear idea of your objectives. Do you wish to study the sun? Jupiter? Make meteor counts? Do you wish to engage in imaging radio astronomy? What you decide will not only determine the type of equipment you will need, but also the local radio spectrum.

How do amateurs do radio astronomy?

Radio astronomy by amateurs is conducted using antennas of various shapes and sizes, from smaller parabolic dishes to simple wire antennas. These antennas are connected to receivers and most of these receivers are software defined radios these days. Data from the receivers are collected by computers, and the received signals will be displayed as charts, graphs or maybe even sky maps. As diverse as the observed objects, so is are the instruments and tools used. SARA members will always be supportive to find good solutions for what one wishes to observe.

Is amateur radio astronomy instrumentation expensive?

Technical information freely circulated in our monthly journal helps amateurs to obtain good low noise equipment from off the shelf assemblies, or to build their own units. The actual cash investment in radio astronomy equipment need not exceed that of any other hobby.

What are amateurs actually looking for in the received data?

The aim of the radio amateur is to find something new and unusual. Just as an amateur optical observer hopes to notice a supernova or a new comet, so does an amateur radio observer hope to notice a new radio source, or one whose radiation has changed appreciably.

The Reber Telescope at NRAO. Constructed by Grote Reber in 1937 in his back yard in Wheaton, Illinois

SARA Members discussing the IBT (Itty Bitty Telescope)